University of Crete

Physics Department

Master on Photonics and Nanoelectronics

Master Thesis

Parity- Time (PT) symmetry in coupled laser cavities

By

Andreas Choulakis

email: andrchoul@gmail.com

Supervisor Prof.: Konstantinos Makris

Contents

Abstract

In the context of non-Hermitian Photonics, we examine the effect of coupling to loss in multimode lasing systems. More specifically, we consider one-dimensional coupled ring and ridge cavities. Both cavities are intrinsically lossy and because of the partial pumping scheme the whole system's behavior resembles that of parity-time (PT)-symmetric systems. The nonlinear time dynamics is based on a modal expansion method (using as bi-orthogonal basis the constant-flux states) of Maxwell-Bloch semiclassical laser equations. A direct outcome of the underlying PT-symmetric behavior of the system is the suppression of higher order lasing modes. In particular, the coupled cavities operate in the single lasing regime for a considerable range of values of the pump, before the higher order modes start to lase. We investigate this range of pump values for two coupled ridge cavities for various design parameters. Two-mode, four and six mode lasing are computationally studied.

Acknowledgments

A very special gratitude goes to my supervisor Prof. Konstantinos Makris, for his guidance, patience and support, on both an educational and a personal level, during this thesis. I also feel grateful to him, for the many hours discussions we had about research. I have benefited enormously from his knowledge in his scientific field. His enthusiasm for physics, has inspired me and they will be invaluable for my further career.

Finally, I feel the need to thanks my family, for the devotion and trust they showed me throughout the duration of this journey.

Chapter 1 – Introduction

Laser Principles

The word LASER is an acronym for "**L**ight **A**mplification by **S**timulated **E**mission of **R**adiation". As this acronym says laser emits light through a process of optical amplification based on the stimulated emission of electromagnetic radiation and has many specific characteristics which differentiate it from other sources of light.

The laser has a far-reaching influence in various fields of science and technology, getting started from the spectroscopy and reaching until atmospheric physics, including medical applications.

A laser differs from other sources of light, in that it emits light coherently, spatially and temporally. This is a very important characteristic of laser light, because due to the spatial coherence it is possible to focus the emitted light to a tight spot, which gives rise to applications such as laser cutting and lithography. In addition, spatial coherence allows a laser beam to stay narrow, over great distances, which enables applications such as laser pointers. Regarding the temporal coherence, this allows to laser light to have a very narrow spectrum, i.e. the laser light is almost monochromatic. Temporal coherence enables the creation of ultrashort laser pulses, which reach the femtosecond scale.

Each laser system has two essential components: a laser cavity which traps light and supplies the needed optical feedback, and a gain medium that amplifies light in the presence of an external pump. The most common and primary laser cavities, are of Fabry-Perot type, (see fig. (1)). In these type of laser cavities, the light undergoes multiple reflections between two mirrors, which have reflectivity. One of them reaches the 100% and the other (from which light goes out of the cavity) is about 99%. Such laser cavities provide very good light confinement and for this reason we can neglect the openness of the cavity. These modes are known, as "cold cavity modes" and can be obtained by solving the Helmholtz equation (derived from Maxwell's equations),

$$\left[\boldsymbol{\nabla}^{\mathbf{2}} + \frac{\varepsilon_c(\boldsymbol{r})\omega^2}{c^2}\right]\varphi(\boldsymbol{r},\omega) = 0 \quad (1.1)$$

Where, ω is the lasing frequency of individual modes, c is the speed of light in vacuum and $\varepsilon_c(\boldsymbol{r})$ is the dielectric function of the passive cavity i.e. without taking into account the gain medium.

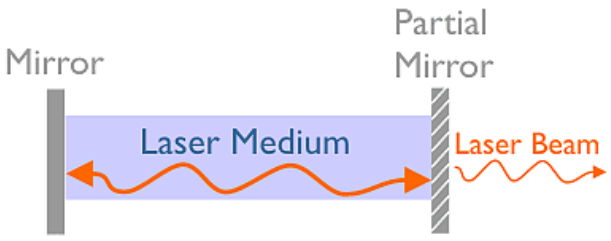

Figure 1- Representation of a Fabry-Perot laser cavity [4].

One of the theoretical challenges of modelling novel laser systems (micro-rings, micro-disk and micro sphere lasers) [5], [6], [7], [8] is the correct treatment of the openness of the cavity. There are several methods one can apply in order to describe the openness of a laser system. One way is to apply the concept of quasi-bound modes (QB) which can be defined in terms of the scattering matrix of the cavity. This scattering matrix relates incoming waves at a specific wavevector k, to all outgoing

channels [8], [9], [10]. Although QB modes have been extensively used in the standard open cavities analysis, they have two basic disadvantages. The first one is that the QB modes are not orthogonal to each other and the second one is that they don't conserve the photon flux outside the cavity. This difficulty has been recently overcome by the introduction of the Constant Flux (CF) states by T$\ddot{u}$reci, Stone et al [11]. Constant flux states, are the eigenfunctions, of the Helmholtz equation (eq. 1.1) with open boundary conditions, i.e. we make the specific hypothesis that modes outside the cavity region are plane waves with constant wavenumber. As the name suggests, the CF states conserve the photon flux outside the gain region, and it was shown that the CF state satisfy a bi-orthogonality relation with their adjoint eigenfunctions and they form a complete basis for the lasing modes, as we'll see in **Chapter 5**.

Light-matter interaction

Besides the correct treatment of the openness of the passive cavity, a successful laser theory also needs to take into our consideration the interaction between the light (radiation) and the active medium (matter). Each active medium is a collection of atoms (in a gas laser or in a semiconductor laser where the atoms exist in the heterostructure), of molecules (in dye lasers) etc. The common, lineament of the above laser systems, is that in order to have a laser action the gain medium needs to be inverted, meaning we should have more atoms in the excited state than in the ground state. The simplest and more widespread theory of laser is using the rate equations [1], [3]. In this approach the crucial quantities are the light intensity in the cavity (light rate equation) and the temporal change of inversion of the gain media (atomic rate equation). Under this approach it is possible to investigate the global properties of the laser such as modal intensities and lasing thresholds. Some of the important aspects such as the spatial variation of the electric field is not considered. Also, one assumes that each lasing mode corresponds to a cavity mode, which it isn't valid in general. As a result, coherent effects such as modal instabilities cannot be explained by the rate equations [12]. However, coherent transient effects are useful in studying the dynamic properties in any laser system. Most of the coherent transient phenomena, can be analyzed by using the density matrix formalism where the relaxation of the medium of two-level atoms is treated phenomenologically. In the treatment of coherent transient effects, it must be noted that both the electric field strength and the polarization of the active medium are rapidly changing functions, of both space and time. The spatial and temporal variation of the electric field **E,** in the presence of induced polarization **P**, must be expressed according to Maxwell's equation, while the polarization of the two-level medium induced by the electric field must be expressed via the equations of motion based on the density matrix. By combining these two different equations, we can obtain the electric field and the polarization at all instants of time and everywhere in space. The aforementioned combination, of Maxwell's classical equations of the light and the quantum mechanical equations of motion of the density matrix, are the so called semiclassical laser equations, which developed independently by Haken [1] and Lamb [14] in the 1960s. The basic equations of the semiclassical laser theory known as Maxwell-Bloch equations (MB), are coupled and nonlinear partial differential equations for the electric field, the induced polarization and population inversion in the gain medium. The derivation of these equations is shown in **Chapter 2** of the present letter.

It should be noted that spontaneous emission (SE) is not included in the semiclassical laser theory, and as a result the semiclassical laser theory predicts zero electric field and the polarization below the lasing threshold, and above it the lasing peaks are infinitely sharp (zero linewidth). The zero linewidth of lasing peaks it means that is not possible to calculate the linewidth of each spectra line from the semiclassical MB equations. We note here, the origin of the width in a spectral line is the quantum noise due to the spontaneous emission, which aren't included in these equations. If one wants to calculate the linewidth of a spectral line theoretically there are two different paths. The first one is to

include a classical noise in MB equations, due to the spontaneous emission [15], and the second is to solve the full quantum mechanical problem.

Semiclassical laser equations, can't be solved analytically due to the nonlinear coupling terms. The numerical solution of these equations, can be obtained with two different ways. The first approach is to directly study the steady state solutions [13] while the second approach is based on the expansion of the electric field and of the polarization on the cavity modes (closed or open). This thesis follows the second method.

Chapter 2 - Semiclassical laser theory

The purpose of this chapter is to derive the semiclassical laser equations, known as Maxwell-Bloch equations as also presented in [1] and [2]. We consider the interaction between a two-level atom and a coherent electromagnetic field. To describe this, we will begin by treating the atom quantum mechanically and the coherent electric field classically from Maxwell's equations. A diagram that gives the physical model of a laser system is given below:

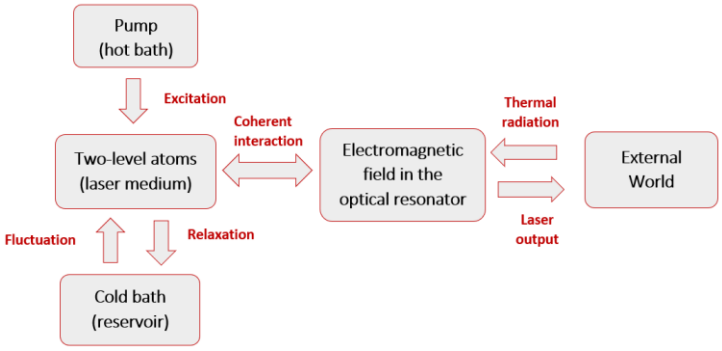

Figure 2- Model of a laser system [2].

2.1- Wave equation for the electric field strength

We start our analysis from Maxwell's equations, which are:

$$\nabla \times \boldsymbol{\mathcal{E}} = -\frac{\partial \boldsymbol{B}}{\partial t} \qquad (\mathbf{2.1.1})$$

$$\nabla \times \boldsymbol{H} = \boldsymbol{J} + \frac{\partial \boldsymbol{D}}{\partial t} \qquad (\mathbf{2.1.2})$$

$$\nabla \cdot \boldsymbol{\mathcal{E}} = 0 \qquad (\mathbf{2.1.3})$$

$$\nabla \cdot \boldsymbol{B} = 0 \qquad (\mathbf{2.1.4})$$

where, $\boldsymbol{\mathcal{E}}$ is the electric field, **B** is the magnetic field, **H** is the magnetized field, **J** is the current density which is expressed through Ohm's law, $\boldsymbol{J} = \sigma \cdot \boldsymbol{\mathcal{E}}$, with σ to be the electric conductivity and **D** is the dielectric displacement which depends on the electric field strength $\boldsymbol{\mathcal{E}}$ and from the induced polarization $\boldsymbol{\mathcal{P}}$ of the medium of two-level atoms. The expression which connects these observables is,

$$\boldsymbol{D} = \varepsilon \boldsymbol{\mathcal{E}} + \boldsymbol{\mathcal{P}} \qquad (\mathbf{2.1.5})$$

where **ε** is the dielectric function of the material. The first term in (2.1.5) describes the polarization due to the transitions between levels other than the two-levels in resonance with the electric field as well as the polarization in atoms with more than two levels, which may exist. We consider non-magnetic materials, $\boldsymbol{B} = \mu_0 \boldsymbol{H}$ and we assume that the electric field is transversal which is equivalent to the assumption, $\nabla \cdot \boldsymbol{\mathcal{E}} = 0$. Furthermore, we will consider only the electric field strength $\boldsymbol{\mathcal{E}}$, because it contains all the relevant information necessary for the laser theory.

We'll begin our derivation, with the differentiation of equation (2.1.2) with respect to time,

$$\nabla \times \frac{\partial \boldsymbol{H}}{\partial t} = \dot{\boldsymbol{J}} + \ddot{\boldsymbol{D}} \quad (\mathbf{2.1.6})$$

Equation (2.1.1) with $\boldsymbol{B} = \mu_0 \boldsymbol{H}$ becomes: $\nabla \times \boldsymbol{\mathcal{E}} = -\mu_0 \frac{\partial \boldsymbol{H}}{\partial t}$ and we take the "$\nabla \times$ " of the last equation,

$$\nabla \times (\nabla \times \boldsymbol{\mathcal{E}}) = -\mu_0 \nabla \times \left(\frac{\partial \boldsymbol{H}}{\partial t}\right) \quad (\mathbf{2.1.7})$$

By taking into account the identity, $\nabla \times (\nabla \times \boldsymbol{A}) = \nabla(\nabla \cdot \boldsymbol{A}) - \nabla^2 \boldsymbol{A}$, of a vector function **A** and with $\nabla \cdot \boldsymbol{A} = 0$, from (2.1.6) we take,

$$\frac{1}{\mu_0} \nabla^2 \boldsymbol{\mathcal{E}} = \sigma \dot{\boldsymbol{\mathcal{E}}} + \varepsilon \ddot{\boldsymbol{\mathcal{E}}} + \ddot{\boldsymbol{P}}$$

$$\Rightarrow \nabla^2 \boldsymbol{\mathcal{E}} - \mu_0 \varepsilon \ddot{\boldsymbol{\mathcal{E}}} - \mu_0 \sigma \dot{\boldsymbol{\mathcal{E}}} = \mu_0 \ddot{\boldsymbol{P}} \quad (\mathbf{2.1.8})$$

But $\varepsilon(\boldsymbol{r}) = n^2(\boldsymbol{r})\varepsilon_0$, where n(**r**) is the refractive index distribution inside the cavity. Because, $\varepsilon_0 \mu_0 = 1/c^2$ it follows that:

$$\varepsilon \mu_0 = n^2(\boldsymbol{r}) / c^2$$

Therefore, we have:

$$\nabla^2 \boldsymbol{\mathcal{E}} - \frac{n^2(\boldsymbol{r})}{c^2} \ddot{\boldsymbol{\mathcal{E}}} - \mu_0 \sigma \dot{\boldsymbol{\mathcal{E}}} = \mu_0 \ddot{\boldsymbol{P}} \quad (\mathbf{2.1.9})$$

2.2- Interaction Between a Two- Level Atom and a Coherent Field

We consider an atom that has only two eigenstates, which are described through the eigenfunctions: $\psi_1(\mathbf{r},t)$ and $\psi_2(\mathbf{r},t)$, with eigenenergies E_1 and E_2 ($>E_1$). Such an atom is described through an unperturbed Hamiltonian $\boldsymbol{H_0}$ and the time dependent Schrödinger equation is written as

$$i\hbar \frac{\partial \psi}{\partial t} = \boldsymbol{H_0} \psi \quad (\mathbf{2.2.1})$$

The solutions of (2.2.1) can be expressed as a product of a function that has only spatial dependence and a function which has only temporal dependence as,

$$\psi_n(\boldsymbol{r},t) = \varphi_n(\boldsymbol{r}) \cdot \exp\left(-i \frac{E_n}{\hbar} \cdot t\right), \; with\, n = 1 \; or \; 2 \quad (\mathbf{2.2.2})$$

Furthermore, we consider a linear polarized light along the z-axis, with electric dipole moment μ_z, and the Hamiltonian which describes the interaction between the two-level atom and the electric field in the frame of electric dipole approximation is,

$$H'(t) = -\boldsymbol{\mu_z} \cdot \boldsymbol{\mathcal{E}}(t) \quad (\mathbf{2.2.3})$$

It is, general possible to expand the wave function $\psi(\boldsymbol{r},t)$ of a certain atom in terms of the eigenfunctions $\psi_n(\boldsymbol{r},t)$, because they consist a complete basis,

$$\psi(\boldsymbol{r},t) = \sum_n a_n(t) \cdot \psi_n(\boldsymbol{r},t) \quad (\mathbf{2.2.4})$$

But in the case of our problem where we have only to eigenstates, this sum has only two terms, and the expansion coefficients, $a_1(t)$ and $a_2(t)$ represents the probability amplitudes of the eigenstates 1 and 2 respectively.

By writing the Schrödinger equation of the full Hamiltonian $H = H_0 + H'$ we obtain,

$$i\hbar\left(\frac{da_1}{dt}\psi_1 + \frac{d\psi_1}{dt}a_1 + \frac{da_2}{dt}\psi_2 + \frac{d\psi_2}{dt}a_2\right) = (H_0 + H')(a_1\psi_1 + a_2\psi_2) \quad (\mathbf{2.2.5})$$

$d$enoting that the stationary states have zero dipole moment, only the off-diagonal matrix elements of the H' have non-zero values, which are defined as $H'_{nm} = \int \varphi_n{}^* H' \varphi_m dr$. So, the perturbation part of the Hamiltonian is a two by two matrix of the form,

$$H' = \begin{bmatrix} 0 & H'_{12} \\ H'_{21} & 0 \end{bmatrix}.$$

Also, the eigenstates of the unperturbed Hamiltonian (H_0) $\psi_n(\boldsymbol{r}, t)$, are evolve over time via the exponential function $\sim e^{-iE_{1,2}t/\hbar}$. By multiplying successively with $\psi_1^* \, and \, \psi_2^*$ on (2.2.5) and integrating, by using the orthogonality of the eigenfunctions we get the relations

$$\dot{a}_1(t) = \frac{1}{i\hbar}a_2(t)H'_{12}e^{-i\omega_a t} \quad (\mathbf{2.2.6}\boldsymbol{a})$$

$$\dot{a}_2(t) = \frac{1}{i\hbar}a_1(t)H'_{21}e^{i\omega_a t} \quad (\mathbf{2.2.6}\boldsymbol{b})$$

where $\omega_a = \frac{E_2 - E_1}{\hbar}$, is the transition frequency of the two-level atom.

2.3- Induced Dipole Moment

As previously stated the stationary states of an unperturbed Hamiltonian for a two-level atom do not have dipole moment. Nevertheless, when the atom interacts with the light, a dipole moment is induced. Its expectation value is defined quantum-mechanically as,

$$p(t) = \int \psi^*(\boldsymbol{r}, t)\,(-e)z\psi(\boldsymbol{r}, t)dr \quad (\mathbf{2.3.1})$$

Therefore, for a two-level atom it becomes,

$$-p(t) = a_1 a_2^* \mu_{21} e^{i\omega_a t} + a_2 a_1^* \mu_{12} e^{-i\omega_a t} \quad (\mathbf{2.3.2})$$

μ_{21} and $\mu_{12}$are the off-diagonal elements of dipole matrix. The non-zero value of the induced dipole moment is responsible for the interaction between the light and the atoms of the active material in a laser system.

2.4- Density Matrix formalism

In order to make a complete description of the laser action we must take into our consideration the interaction between the light and an ensemble of atoms (or molecules). It is necessary to know the behavior of each atom and to find the ensemble average. Because of the difficulties of such calculation, we will use the density matrix formalism which simplifies the calculations.

Useful quantities for the description of the interaction between light and the ensemble of atoms are, the induced dipole moment, the transition probability, and the populations of the atoms. From, the expansion (2.2.4), we can remove the temporal dependence by rewriting (2.2.4) as

$$\psi(\boldsymbol{r},t)=\sum_n c_n(t)\cdot\varphi_n(\boldsymbol{r},t) \quad (\mathbf{2.4.1})$$

$$c_n(t)=a_n(t)e^{-i\left(\frac{E_n}{\hbar}\right)t} \quad (\mathbf{2.4.2})$$

The density matrix elements are given from,

$$\rho_{nm}=a_n a_m^* \exp\left(i\frac{E_m-E_n}{\hbar}t\right) \quad (\mathbf{2.4.3})$$

Therefore, for a two-level atom the density matrix is expressed as

$$\rho=\begin{bmatrix}|a_1|^2 & a_1a_2^*e^{i\omega_a t}\\ a_2a_1^*e^{-i\omega_a t} & |a_2|^2\end{bmatrix} \quad (\mathbf{2.4.4})$$

It is easy to see that the off-diagonal elements of the density matrix are connected with the dipole moment (equation 2.3.2), and the diagonal elements provide the population of the individual energy levels.

2.5- Equations of Motion of the Density Matrix

In this section, we describe the temporal dynamics of the density matrix which can be obtained from the time dependent Schrödinger equation. By substituting (2.4.1) into Schrödinger equation for the total Hamiltonian we have:

$$i\hbar\frac{\partial c_n(t)}{\partial t}=\sum_k c_k(t)H_{nk} \quad (\mathbf{2.5.1})$$

where H_{nk},is the matrix elements of the total Hamiltonian. From the definition of the density matrix elements, $\rho_{nm}=c_n c_m^*$ and by differentiation we get:

$$\frac{d\rho_{nm}}{dt}=\frac{dc_n}{dt}c_m^*+c_n\frac{dc_m^*}{dt} \quad (\mathbf{2.5.2})$$

Equation (2.5.2) due to (2.5.1) and (2.5.1) conjugate becomes,

$$i\hbar\frac{d\rho_{nm}}{dt}=\sum_k c_k H_{nk}c_m^*-c_n\sum_k c_k^*H_{km}=\sum_k(H_{nk}\rho_{km}-\rho_{nk}H_{km}) \quad (\mathbf{2.5.3})$$

where it is considered that $H_{nk}^*=H_{nk}$. At this point, due to commutation relation, $[H,\rho]=H\rho-\rho H$, the above equation takes the form,

$$i\hbar\frac{d\rho}{dt}=[H,\rho] \quad (\mathbf{2.5.4})$$

Equation (2.5.4) is the so-called equation of motion of the density matrix. If we call the eigenvalues of the energy, of the unperturbed Hamiltonian by E_n, the eq. (2.5.3) gives,

$$i\hbar\frac{d\rho_{nm}}{dt}=E_n\rho_{nm}-E_m\rho_{nm}+\sum_k(H'_{nk}\rho_{km}-\rho_{nk}H'_{km})$$

$$\Rightarrow \frac{d\rho_{nm}}{dt}=-i\omega_{nm}\rho_{nm}-\frac{i}{\hbar}\sum_k(H'_{nk}\rho_{km}-\rho_{nk}H'_{km}) \quad (\mathbf{2.5.5})$$

Eq. (2.5.5) for the density matrix elements, ρ_{11}, ρ_{21} gives:

$$\frac{d\rho_{11}}{dt} = \frac{i}{\hbar}(\rho_{12}H'_{21} - c.c) \quad (\mathbf{2.5.6}\boldsymbol{a})$$

$$\frac{d\rho_{21}}{dt} = -i\omega_a\rho_{21} + \frac{i}{\hbar}(\rho_{22} - \rho_{11})H'_{21} \quad (\mathbf{2.5.6}\boldsymbol{b})$$

The temporal derivative of matrix elements $\rho_{11}$and ρ_{21} is enough to describe the laser system via density matrix formalism. This is why, the other matrix elements are connected with $\rho_{11}$and ρ_{21}. The relations that make the connection are, $\rho_{21} = \rho_{12}^*$ and $\rho_{22} = 1 - \rho_{11}$ as shown in [2]. We recall that, the diagonal matrix elements, represents the populations of the individual levels of the atom, so we can define the population inversion as $d = \rho_{22} - \rho_{11}$. The off-diagonal matrix elements are connected with the dipole moment of the atom as we can see in the equation (2.3.2), and from this we'll obtain an equation for the temporal variation of the induced polarization in the active medium.

The importance of the density matrix, is that it can be used for the description of pure, as well as, mixed states. In many body problems the statistical average of the density matrix is known, although the wavefunctions of the individual atoms are unknown. In section (2.1) we examined the interaction between a coherent field and an atom without other perturbations. In general, in an ensemble of two-level atoms are present and incoherent perturbations like, interactions between other atoms of the active material and with the walls of the container as well as and the spontaneous emission which is also present in any quantum-mechanical system. In density matrix formalism it's possible to treat these effects phenomenologically by introduce relaxation constants. One of the most important relaxation constants which are included in the semiclassical laser equations is, the relaxation rate of the induced polarization, $\gamma_\perp$ (transverse relaxation rate). With that in mind, equation (2.5.6b) becomes,

$$\frac{d\rho_{21}}{dt} = (-i\omega_a - \gamma_\perp)\rho_{21} - \frac{i}{\hbar}\mu_{21}d \cdot \mathcal{E}(t) \quad (\mathbf{2.5.7})$$

As regards the population inversion we have: $\Delta N = (\rho_{22} - \rho_{11})N = N\Delta\rho$, where the temporal variation of the $\Delta\rho$ is obtained from (2.5.6a) and N is the number of atoms per unit volume ($N=n/V$) so we get,

$$\frac{d\Delta\rho}{dt} = -\frac{2i}{\hbar}(\rho_{12}H'_{21} - c.c) \quad (\mathbf{2.5.8})$$

This equation describes how the inversion changes due to the interaction of the electron and the electric field. When we wish to treat the laser processes we must not ignore the interaction of the atom with its surrounding as well as any incoherent perturbation which occur such as the non-radiative transitions. The pump process must also to taken into account. All these processes will lead to the relaxation of the inversion towards its stationary value which is denoted as $\Delta\rho^{(0)}$, with a relaxation rate, $\gamma_\parallel$ as described from the equation below:

$$\frac{d}{dt}\Delta\rho = \gamma_\parallel(\Delta\rho^{(0)} - \Delta\rho) + \frac{2i}{\hbar}\mathcal{E}(t) \cdot (\rho_{12}\mu_{21} - c.c.) \quad (\mathbf{2.5.9})$$

Do not forget that until now, we have derived expressions about the dipole moment and the population inversion of a single atom. But, we have to remind ourselves that we are not dealing with a single atom but with an ensemble of *N* atoms in the laser's active medium. Therefore, we have to examine how the macroscopic polarization is connected with the individual dipole moments. The expression which makes the connection is,

$$\mathcal{P}(\boldsymbol{r},t)=\sum_{\substack{ensemle\\atoms}}\delta(\boldsymbol{r}-\boldsymbol{r_a})p_a$$

where r_a and p_a is the position and the dipole moment of the individual atoms respectively and "δ" is the Dirac function. The dipole moment of the individual atoms can be expressed through the density matrix elements as, $-<p(t)>_{av}=\rho_{12}\mu_{21}+\rho_{21}\mu_{12}$. Also, for later purposes we introduce the abbreviations: $p^{(+)}=-\rho_{21}\mu_{12}$ and $p^{(-)}=-\rho_{12}\mu_{21}$, so that the dipole moment of the atoms can be represented in the form: $p=p^{(+)}+p^{(-)}$ where $p^{(+)}$ is the positive frequency part while $p^{(-)}$ is the negative frequency part as one can see in (2.3.2). If we decompose the polarization into a positive frequency part ($\mathcal{P}^{(+)}$) and a negative frequency part ($\mathcal{P}^{(-)}$) we have,

$$\mathcal{P}^{(+)}(\boldsymbol{r},t)=-\sum_{\substack{ensemle\\atoms}}\delta(\boldsymbol{r}-\boldsymbol{r_a})\mu_{12}\cdot\rho_{21}$$

and it is true that, $\mathcal{P}^{(+)^*}=\mathcal{P}^{(-)}$. Similarly, we can express the inversion density as,

$$\mathcal{D}(\boldsymbol{r},t)=\sum_{\substack{ensemle\\atoms}}\delta(\boldsymbol{r}-\boldsymbol{r}_a)d_a$$

where d_a are the inversion density of the individual atoms.

In order to derive an equation for the macroscopic quantity **P**, we multiply equation (2.5.7) on both sides by $\delta(\boldsymbol{r}-\boldsymbol{r_a})\mu_{12}$ and take the sum over all the ensemble of atoms. The term $\delta(\boldsymbol{r}-\boldsymbol{r_a})\mathcal{E}(\boldsymbol{r_a}$,t) which is appeared in the following derivation is equal to $\delta(\boldsymbol{r}-\boldsymbol{r_a})\mathcal{E}(\boldsymbol{r}$,t) so the final equation for the macroscopic quantity of the polarization is,

$$\frac{d\mathcal{P}^{(+)}(\boldsymbol{r},t)}{dt}=(-i\omega_a-\gamma_\perp)\mathcal{P}^{(+)}(\boldsymbol{r},t)-\frac{i\mu_{12}^2}{\hbar}\mathcal{E}\cdot\mathcal{D}(\boldsymbol{r},t)\qquad(\mathbf{2.5.10})$$

in a similar way we can obtain the differential equation which describes the change of $\mathcal{P}^{(-)}$. By proceeding in a similar way with equation (2.5.9) we obtain the following equation for the macroscopic quantity of the inversion density,

$$\frac{d\mathcal{D}(\boldsymbol{r},t)}{dt}=\gamma_\parallel(\mathcal{D}_0-\mathcal{D}(\boldsymbol{r},t))+\frac{2i}{\hbar}\mathcal{E}(\boldsymbol{r},t)\cdot[\,\mathcal{P}^{(+)}(\boldsymbol{r},t)^*-\mathcal{P}^{(+)}(\boldsymbol{r},t)]\quad(\mathbf{2.5.11})$$

In where, $\mathcal{D}_0$ is the inversion density if only pump and relaxation processes occur but not laser action. It is also called unsaturated inversion.

2.6- Equations of Semiclassical laser theory

In this section we summarize the basic equations we have derived in the preceding sections. The following three equations are the so-called Maxwell-Bloch equations of the Semiclassical laser theory.

The first equation is the differential equation of the electric field strength (2.1.9):

$$\nabla^2\boldsymbol{\mathcal{E}}-\frac{n^2(\boldsymbol{r})}{c^2}\ddot{\boldsymbol{\mathcal{E}}}-\mu_0\sigma\dot{\boldsymbol{\mathcal{E}}}=\mu_0\ddot{\mathcal{P}}\quad(\mathbf{2.6.1})$$

The second equation is the (2.5.10), for the positive frequency part of the polarization:

$$\dot{\mathcal{P}}^{(+)}(\boldsymbol{r},t) = (-i\omega_a - \gamma_\perp)\mathcal{P}^{(+)}(\boldsymbol{r},t) - \frac{i\mu_{12}^2}{\hbar}\mathcal{E}\cdot\mathcal{D}(\boldsymbol{r},t) \ (\mathbf{2.6.2})$$

And the last equation gives the inversion density (2.5.11):

$$\dot{\mathcal{D}}(\boldsymbol{r},t) = \gamma_\parallel(\mathcal{D}_0 - \mathcal{D}(\boldsymbol{r},t)) + \frac{2i}{\hbar}\mathcal{E}(\boldsymbol{r},t)\cdot[\,\mathcal{P}^{(+)}(\boldsymbol{r},t)^* - \mathcal{P}^{(+)}(\boldsymbol{r},t)] \quad (\mathbf{2.6.3})$$

2.7- Rotating wave approximation (RWA)

In the preceding section we decomposed the polarization into a positive and negative frequency part. The same decomposition can be applied to the electric field strength. We decompose the electric field as follows,

$$\mathcal{E}(t) = \mathcal{E}^{(+)}(t) + \mathcal{E}^{(-)}(t) \quad (\mathbf{2.7.1})$$

where, $\mathcal{E}^{(+)}(t) = A\cdot e^{-i\omega t}$ and $\mathcal{E}^{(-)}(t) = A^*\cdot e^{i\omega t}$, with A, A^* to be time dependent complex amplitudes which are referred as envelope functions of the electric field, and ω is the oscillation frequency of the individual modes of the laser. The time dependency of the envelope function *A* (or A*), is much slower from the exponential functions, which multiply them. We turn our attention to the temporal part of the right-hand side (r.h.s.) of the equation (2.6.3),

$$\mathcal{E}\left[\mathcal{P}^{(+)^*} - \mathcal{P}^{(+)}\right] \overset{(2.7.1)}{=} \mathcal{E}^{(+)}\mathcal{P}^{(-)} - \mathcal{E}^{(+)}\mathcal{P}^{(+)} + \mathcal{E}^{(-)}\mathcal{P}^{(-)} - \mathcal{E}^{(-)}\mathcal{P}^{(+)} \ (\mathbf{2.7.2})$$

Where, for reasons of brevity we neglect the notation of time dependency. Also, we note that the temporal variation of the polarization is of the form: $\mathcal{P}^{(+)}\sim e^{-i\omega_a t}$ $\mathcal{P}^{(-)}\sim e^{i\omega_a t}$, where ω_a is the transition frequency of the two-level atoms. The terms which arise are,

- $\mathcal{E}^{(+)}\mathcal{P}^{(-)}\sim e^{-i(\omega-\omega_a)t}$
- $\mathcal{E}^{(-)}\mathcal{P}^{(-)}\sim e^{i(\omega-\omega_a)t}$
- $\mathcal{E}^{(+)}\mathcal{P}^{(+)}\sim e^{-i(\omega+\omega_a)t}$
- $\mathcal{E}^{(-)}\mathcal{P}^{(-)}\sim e^{i(\omega+\omega_a)t}$

As one can see in the above expressions, there are terms that oscillate with frequency "$\omega-\omega_a$", and terms which oscillates with frequency "$\omega+\omega_a$". But in order to solve equation (2.6.3) we must integrate over the time, with the time interval to be long compared to the time of a single oscillation. So during the integration the contribution of the fast oscillating terms (with frequency "$\omega+\omega_a$") vanishes. As a consequence, we can ignore these terms and consider only the slowly oscillating terms (with frequency "$\omega-\omega_a$") which significantly contribute. We can write equation (2.6.3) as,

$$\frac{d\mathcal{D}(\boldsymbol{r},t)}{dt} = \gamma_\parallel(\mathcal{D}_0 - \mathcal{D}(\boldsymbol{r},t) + \frac{2i}{\hbar}[\,\mathcal{E}^{(+)}\mathcal{P}^{(+)^*} - \mathcal{E}^{(+)^*}\mathcal{P}^{(+)}] \quad (\mathbf{2.7.3})$$

We apply the same approximation for the polarization (2.6.2) [1] and we get,

$$\frac{d\mathcal{P}^{(+)}(\boldsymbol{r},t)}{dt} = (-i\omega_a - \gamma_\perp)\mathcal{P}^{(+)}(\boldsymbol{r},t) - \frac{i\mu_{12}^2}{\hbar}\mathcal{E}^{(+)}\cdot\mathcal{D}(\boldsymbol{r},t) \quad (\mathbf{2.7.4})$$

So, from the above equations we can see that only the positive frequency part of the electric field is needed, therefore we can write the differential equation (2.6.1) for $E^{(+)}$,

$$\nabla^2\mathcal{E}^{(+)} - \frac{n^2(\boldsymbol{r})}{c^2}\ddot{\mathcal{E}}^{(+)} - \mu_0\sigma\dot{\mathcal{E}}^{(+)} = \mu_0\ddot{\mathcal{P}}^{(+)} \quad (\mathbf{2.7.5})$$

2.8- Modal expansion method

In this section we will begin from equations presenting above, namely (2.7.3)-(2.7.5), in order to obtain the simpler form which will be suitable for computational analysis. We will begin by expanding the electric field $\mathcal{E}(\mathbf{r},\mathrm{t})$ and the polarization $\mathcal{P}(\mathbf{r},\mathrm{t})$ of a laser medium in a complete basis which consists of the eigenstates (modes) of a closed resonator or of an open resonator [1]. These modes are the solutions of the Helmholtz differential equation,

$$\boldsymbol{\nabla^2}\varphi_m(\boldsymbol{r}) + \frac{\omega_m^2}{c^2}n^2(\boldsymbol{r})\varphi_m(\boldsymbol{r}) = 0 \quad (\mathbf{2.8.1})$$

Where, $\varphi_m(\boldsymbol{r})$ is the m-eigenfunction of the closed (or open) resonator, ω_m is the frequency of the mth-mode of the resonator, c is the speed of the light in vacuum and n(**r**) is the refractive index of the laser material and its be in general a complex function of the position. In the present thesis we will consider one dimensional cavity, because we are interested only about the longitudinal modes of the resonator. So, the Laplacian operator has only the term represents the derivative of the x-coordinate. This implies that (2.8.1) will be,

$$\varphi_m''(x) + \frac{\omega_m^2}{c^2}n^2(x)\varphi_m(x) = 0 \quad (\mathbf{2.8.2})$$

Equation (2.8.2) is solved with appropriate boundary conditions (open, closed or periodic). The aforementioned expansions into the complete basis are,

$$\mathcal{E}^{(+)}(x,t) = \sum_m e_m(t)\varphi_m(x) \quad (\mathbf{2.8.3})$$

$$\mathcal{P}^{(+)}(x,t) = \sum_m p_m(t)\varphi_m(x) \quad (\mathbf{2.8.4})$$

If we replace the above expansions in equation (2.7.5),

$$\nabla^2\mathcal{E}^{(+)} - \frac{n^2(x)}{c^2}\ddot{\mathcal{E}}^{(+)} - \mu_0\sigma\dot{\mathcal{E}}^{(+)} = \mu_0\ddot{\mathcal{P}}^{(+)}$$

we take,

$$-\sum_m \frac{\omega_m^2}{c^2}e_m(t)n^2(x)\varphi_m(x) - \frac{n^2(x)}{c^2}\sum_m \varphi_m(x)\,\ddot{e}_m(t) - \mu_0\sigma\sum_m \varphi_m(x)\,\dot{e}_m(t) = \mu_0\sum_n \varphi_n(x)\ddot{p}_n(t) \quad (\mathbf{2.8.5})$$

we multiply with $\varphi_q(x)$ and integrating over the cavity length both parts of (2.8.5),

$$-\sum_m \frac{\omega_m^2}{c^2} e_m(t) \int_{-l}^{l} n^2(x)\varphi_m(x)\varphi_q(x) - \frac{1}{c^2}\sum_m \int_{-l}^{l} n^2(x)\varphi_m(x)\varphi_q(x)\,dx\,\ddot{e}_m(t)$$
$$-\mu_0\sigma\sum_m \int_{-l}^{l} \varphi_m(x)\varphi_q(x)dx\,\dot{e}_m(t) = \mu_0\sum_n \int_{-l}^{l} \varphi_n(x)\varphi_q(x)dx\,\ddot{p}_n(t)$$

Making use of the biorthogonality condition: $\int_{-l}^{l} \varepsilon(x)\varphi_n(x)\varphi_m(x)dx = 0$, which is valid for both sets of boundary conditions (Appendix [A]) lead us to:

$$-\frac{\omega_m^2}{c^2} e_m(t) - \frac{1}{c^2}\ddot{e}_m(t) - \mu_0\sigma\sum_m \int_{-l}^{l} \varphi_m(x)\varphi_q(x)dx\,\dot{e}_m(t)$$
$$= \mu_0\sum_n \int_{-l}^{l} \varphi_n(x)\varphi_q(x)dx\,\ddot{p}_n(t) \quad (\mathbf{2.8.6})$$

We define:

$$B_{mn} = \int_{-l}^{l} \varphi_m(x)\varphi_q(x)dx$$

Also, we can to pull out from the functions, $e_m(t)\ and\ p_m(t)$ the fast oscillating term $\sim e^{-i\omega_a t}$, i.e. $e_m(t) = e_{m,0}(t)e^{-i\omega_a t}$ and $p_m(t) = p_{m,0}(t)e^{-i\omega_a t}$.

$$(2.8.6)\Rightarrow -\frac{\omega_m^2}{c^2} e_{m,0}(t)e^{-i\omega_a t} - \frac{1}{c^2}\{\ddot{e}_{m,0}(t) - 2i\omega_a\dot{e}_{m,0}(t) - \omega_a^2 e_{m,0}(t)\}e^{-i\omega_a t} -$$
$$\mu_0\sigma\sum_m B_{mn}(\dot{e}_{m,0}(t) - i\omega_a e_{m,0}(t))e^{-i\omega_a t} = \mu_0\sum_n B_{mn}\{\ddot{p}_{n,0}(t) - 2i\omega_a\dot{p}_{n,0}(t) -$$
$$\omega_a^2 p_{n,0}(t)\}e^{-i\omega_a t} \qquad (\mathbf{2.8.7})$$

To simplify the above equation, we use the slowly varying envelope approximation **(SVEA)** [2]. This means that we can ignore the term of the second derivative of the electric field and polarization, as well as the first derivative of the polarization. In addition, in the first summation to the r.h.s. the first derivative of the electric field strength (envelope function) is much less than the magnitude of the second term in the same summation. So, we can ignore, the first one compared with the last one:

$$(2.8.7) \Rightarrow \dot{e}_{m,0}(t) = \frac{i}{2\omega_a}[\omega_a^2 - \omega_m^2] - \frac{\sigma}{2\varepsilon_0}\sum_m B_{mn}e_{m,0}(t) + \frac{i\omega_a}{2\varepsilon_0}\sum_n B_{mn}e_{n,0}(t)$$

With the definition of, $K_m = \frac{\sigma}{2\varepsilon_0}\sum_m B_{mn}$, the above equation becomes:

$$\dot{e}_{m,0}(t) = \frac{i}{2\omega_0}[\omega_a^2 - \omega_m^2] - K_m e_{m,0}(t) + \frac{i\omega_a}{2\varepsilon_0}\sum_n B_{mn}e_{n,0}(t) \qquad (\mathbf{2.8.8})$$

Regarding the polarization of the laser material, we have to begin from equation (2.7.4):

$$\frac{d\mathcal{P}^{(+)}(x,t)}{dt} = (-i\omega_a - \gamma_\perp)\mathcal{P}^{(+)}(x,t) - \frac{i\mu_{12}^2}{\hbar}\mathcal{E}^{(+)}\cdot\mathcal{D}(x,t)$$

By the substitution of the expansions (2.8.3) and (2.8.4) in the above equation,

$$\sum_n \dot{p}_{n,0}(t)\,\varphi_n(x) = -\gamma_\perp\sum_n p_{n,0}(t)\,\varphi_n(x) - \frac{i\mu_{12}^2}{\hbar}\sum_q e_{q,0}(t)\,\mathcal{D}(x,t)\varphi_q(x)$$

Then by multiplying both parts of the above equation with $\varepsilon(x)\varphi_m(x)$ and integrating along the cavity,

$$\sum_n \dot{p}_{n,0}(t)\int_{-l}^{l}\varepsilon(x)\varphi_m(x)\varphi_n(x)\,dx = -\gamma_\perp\sum_n p_{n,0}(t)\int_{-l}^{l}\varepsilon(x)\varphi_m(x)\varphi_n(x)\,dx - \frac{i\mu_{12}^2}{\hbar}\sum_q e_{q,0}(t)\int_{-l}^{l}\varepsilon(x)\mathcal{D}(x,t)\varphi_q(x)\varphi_m(x)\,dx$$

$$\Rightarrow \quad \dot{p}_{m,0}(t) = -\gamma_\perp p_{m,0}(t) - \frac{i\mu_{12}^2}{\hbar}\sum_n e_{n,0}(t)\mathcal{D}_{mn}(x,t), \text{ where,}$$

$$\mathcal{D}_{mn}(x,t) = \int_{-l}^{l}\varepsilon(x)\mathcal{D}(x,t)\varphi_q(x)\varphi_m(x)\,dx$$

$$\boxed{\dot{p}_{m,0}(t) = -\gamma_\perp p_{m,0}(t) - \frac{i\mu_{12}^2}{\hbar}\sum_n e_{n,0}(t)\mathcal{D}_{mn}(x,t) \quad (\mathbf{2.8.9})}$$

As a final step of our analysis we begin from the equation (2.7.3), describes the inversion density as presented below,

$$\frac{d\mathcal{D}(x,t)}{dt} = \gamma_\parallel(\mathcal{D}_0 - \mathcal{D}(x,t) + \frac{2i}{\hbar}[\mathcal{E}^{(+)}\mathcal{P}^{(+)^*} - \mathcal{E}^{(+)^*}\mathcal{P}^{(+)}]$$

As we done before, we use the above expansions (2.8.3) and (2.8.4), and we get,

$$\dot{\mathcal{D}}(x,t) = \gamma_\parallel\big(\mathcal{D}_0 - \mathcal{D}(x,t)\big) + \frac{2i}{\hbar}\sum_r\sum_q[e_{r,0}(t)\varphi_r(x)\,p_{q,0}^*(t)\varphi_q^*(x) - p_{q,0}(t)\varphi_q(x)e_{r,0}^*(t)\varphi_r^*(x)]$$

Then we multiply both parts of the above equation, with $\varepsilon(x)\varphi_n(x)\varphi_m(x)$ and take the integral along the cavity length,

$$\frac{d}{dt}\int_{-l}^{l}\varepsilon(x)\varphi_m(x)\varphi_n\mathcal{D}(x,t)dx = \gamma_\parallel\left(\int_{-l}^{l}\varepsilon(x)\varphi_m(x)\varphi_n\mathcal{D}_0(x)dx - \int_{-l}^{l}\varepsilon(x)\varphi_m(x)\varphi_n\mathcal{D}(x,t)dx\right) + \frac{2i}{\hbar}\sum_r\sum_q[e_{r,0}(t)\,p_{q,0}^*(t)\int_{-l}^{l}\varepsilon(x)\varphi_m(x)\varphi_n\varphi_r(x)\varphi_q^*(x)dx - p_{q,0}(t)e_{r,0}^*(t)\int_{-l}^{l}\varepsilon(x)\varphi_m(x)\varphi_n\varphi_r^*(x)\varphi_q(x)dx]$$

By setting, $\mathcal{D}_{0,mn} = \int_{-l}^{l}\varepsilon(x)\varphi_m(x)\varphi_n\mathcal{D}_0(x)dx$, $\mathcal{D}_{mn} = \int_{-l}^{l}\varepsilon(x)\varphi_m(x)\varphi_n\mathcal{D}(x,t)dx$, $A_{mn,rq} = \int_{-l}^{l}\varepsilon(x)\varphi_m(x)\varphi_n\varphi_r(x)\varphi_q^*(x)dx$, $A'_{mn,rq} = \int_{-l}^{l}\varepsilon(x)\varphi_m(x)\varphi_n\varphi_r^*(x)\varphi_q(x)dx$ we take,

$$\boxed{\dot{\mathcal{D}}_{mn} = \gamma_\parallel\big(\mathcal{D}_{0,mn} - \mathcal{D}_{mn}\big) + \frac{2i}{\hbar}\sum_{r,q}[e_{r,0}(t)p_{q,0}^*(t)A_{mn,rq} - e_{r,0}^*(t)p_{q,0}(t)A'_{mn,rq}] \quad (\mathbf{2.8.10})}$$

2.9- Normalized Equations

For computational reasons we have to normalize our equations. We'll begin with the normalization of Helmholtz equation, by introducing the dimensionless distance $\bar{x} = x/L$, where x is the distance in physical units and **L (=2l+d)**, is the total system's length.

$$\frac{\partial^2 \varphi(\bar{x})}{L^2 \partial \bar{x}^2} + \varepsilon(\bar{x}) k_m^2 \varphi(\bar{x}) = 0$$

$$\Rightarrow \frac{\partial^2 \varphi(\bar{x})}{\partial \bar{x}^2} + \varepsilon(\bar{x}) L^2 k_m^2 \varphi(\bar{x}) = 0$$

So, the dimensionless eigenvalues of the Helmholtz equation are, $\boldsymbol{\bar{k}_m^2 = L^2 k_m^2}$. As regards the eigenfrequencies of the cold resonator, arises that: $\bar{k}_m = k_m L = \frac{\omega_m}{c/n} L = \left(\frac{nL}{c}\right) \omega_m \equiv t_{RT} \omega_m \equiv \bar{\omega}_m$, where we have normalized the time and the frequency as respect to roundtrip time t_{RT}, inside the cavity, as shown below.

All the variables, presented above, are rendered dimensionless through, $E_m = e_{m,0}/E_c$, $P_m = p_{m,0}/E_c$, $D_{mn} = \mathcal{D}_{mn}/D_c$, $\bar{\omega}_m = \omega_m t_{RT}$, $\bar{\omega}_a = \omega_a t_{RT}$, $\bar{K} = K t_{RT}$ and $\bar{\gamma}_{\perp,\parallel} = \gamma_{\perp,\parallel} t_{RT}$ as it arises from the aforementioned change of variables where, $E_c = \frac{\hbar \sqrt{\gamma_\perp \gamma_\parallel L}}{2\mu_{12}}$, $P_c = \frac{E_c}{\mu_0 c^2}$, $D_c = \frac{\gamma_\perp \hbar}{\mu_0 c^2 \mu_{12}^2}$, $t_{RT} = \frac{nL}{c}$. Therefore, the final normalized equations are:

$$\dot{E}_m = \frac{i}{2\bar{\omega}_a}[\bar{\omega}_a^2 - \bar{\omega}_m^2] E_m - \bar{K} E_m + \frac{i\bar{\omega}_a}{2} \sum_n B_{mn} E_n \quad (\mathbf{2.9.1})$$

$$\dot{P}_m = -\bar{\gamma}_\perp P_m - i\bar{\gamma}_\perp \sum_n D_{mn} E_n \quad (\mathbf{2.9.2})$$

$$\dot{D}_{mn} = \bar{\gamma}_\parallel \left[D_{0,mn} - D_{mn}\right] + \frac{i\bar{\gamma}_\parallel}{2} \sum_{r,q} \left[E_r P_q^* \tilde{A}_{mn,rq} - E_r^* P_q \tilde{A}'_{mn,rq} \right] \quad (\mathbf{2.9.3})$$

This step produces the following dimensionless complex-valued parameters appearing in the above equations: $B_{mn} = \int_{-l}^{l} \varphi_m(x) \varphi_q(x) dx$, $D_{0,mn} = \int_{-l}^{l} \varepsilon(x) \varphi_m(x) \varphi_n \bar{d}_0(x) dx$,

$\tilde{A}_{mn,rq} = L \int_{-l}^{l} \varepsilon(x) \varphi_m(x) \varphi_n \varphi_r(x) \varphi_q^*(x) dx$, $\tilde{A}'_{mn,rq} = L \int_{-l}^{l} \varepsilon(x) \varphi_m(x) \varphi_n \varphi_r^*(x) \varphi_q(x) dx$ which are in general complex valued and they are calculated prior to numerically solving the time dependent equations.

2.10- Physical units

The physical units of the parameter values used in our numerical simulations are obtained starting from the transverse relaxation rate $\gamma_\perp \sim 10^{13} s^{-1}$ as referred in [36]. From the normalization $\bar{\gamma}_\perp = \gamma_\perp t_{RT}$ and for $\bar{\gamma}_\perp = 1$ we get that $t_{RT} \sim 10^{-13} s$, also arises that for $\bar{\gamma}_\parallel = 10^{-3}$, $\gamma_\parallel = \bar{\gamma}_\parallel / t_{RT} \sim 10^{10} s^{-1}$. But, $t_{RT} = \frac{n_{av} L}{c}$ and as an average refractive index we set, $n_{av} \sim 3$ so we get the total system's length, $L \sim 10 \mu m$. As regards the resonant frequencies of our resonator we have that, $\bar{\omega}_m \approx 20$ (normalized units) therefore in physical units we get $\omega_m = \bar{\omega}_m / t_{RT} \sim 10^{14} s^{-1}$ and the corresponding wavelengths are, $\lambda_m \sim 1\ \mu m$.

Regarding the electric fields, the induced polarizations and the density of inversion of populations we have the following expressions: $E_c = \frac{\hbar\sqrt{\gamma_\perp \gamma_\parallel}}{2\mu_{12}}$, $P_c = \frac{E_c}{\mu_0 c^2}$, $D_c = \frac{\gamma_\perp \hbar}{\mu_0 c^2 \mu_{12}^2}$. Their physical units are, $[E] = V/m$, $[P] = Cb/m^2$, $[D] = \#atoms/m^3$. Therefore, the critical parameters through which we make the normalization of Maxwell-Bloch equations have the following values: $E_c \sim 10^8\ V/m$, $P_c \sim 10^{-3} Cb/m^2$ and $D_c \sim 10^{28} m^{-3} \sim 10^{46} \mu m^{-3}$, for $\mu_{12} \sim 10^{-30} Cm \sim 1\ Debye$.

2.11- Single mode Class A laser

When both relaxation rates, $\bar{\gamma}_\perp$ and $\bar{\gamma}_\parallel$ are much larger than the outcoupling decay of the electric field, we can assume that the induced polarization $\bar{p}_{m,0}$ and the matrix elements $\bar{d}_{mn}$ have reached the steady state and therefore do not depend on time. In this case we consider the derivatives of equations (2.9.2) and (2.9.3) equal to zero. For the derivation purposes we consider real and constant dielectric function in the cavity region a single mode resonator. The semiclassical equations (2.9.1)-(2.9.3) can be written as,

$$\dot{E} = \frac{i}{2\bar{\omega}_a}[\bar{\omega}_a^2 - \bar{\omega}^2]E - \bar{\gamma}E + \frac{i\bar{\omega}_a}{2} B_{11} P \qquad (\mathbf{2.10.1})$$

$$\dot{P} = -\bar{\gamma}_\perp P - i\bar{\gamma}_\perp D \cdot E \qquad (\mathbf{2.10.2})$$

$$\dot{D} = \bar{\gamma}_\parallel [D_0 - D] + \frac{i\bar{\gamma}_\parallel}{2} \tilde{A}_{11,11}[E \cdot P^* - E^* \cdot P] \qquad (\mathbf{2.10.3})$$

By taking $\dot{P} = 0$ we get,

$$(2) \Rightarrow -\bar{\gamma}_\perp P - i\bar{\gamma}_\perp D \cdot E = 0 \Rightarrow$$

$$\boldsymbol{P = -iD \cdot E} \quad (\mathbf{2.10.4})$$

Also, for $\dot{D} = 0$,

$(2.10.3) \Rightarrow D = D_0 + \frac{i}{2}\tilde{A}_{11,11}[E \cdot P^* - E^* \cdot P]$, which by using (2.10.4) takes the form,

$$\boldsymbol{D = \frac{D_0}{1 + \tilde{A}_{11,11}|E|^2}} \quad (\mathbf{2.10.5})$$

By substituting into the above expressions, the polarization and inversion, in (2.10.1), we obtain the final equation (which is a nonlinear Schrödinger equation with saturable nonlinearity):

$$\boldsymbol{\dot{E} = \frac{i}{2\bar{\omega}_a}\left[\bar{\omega}_a^2 - \bar{\omega}^2\right]E - \bar{\gamma}E + \frac{\bar{\omega}_a B_{11}}{2}\frac{D_0}{1 + \tilde{A}_{11,11}|E|^2}E} \quad (\mathbf{2.10.6})$$

As we can see in equation (2.10.6), the final term in the right-hand side, represents the gain saturation.

Chapter 3 -Parity-Time (PT) symmetry

In 1998 Bender and Boettcher [16] showed that quantum systems of non-Hermitian Hamiltonians may have a real spectrum if they commute with the $\hat{P}\hat{T}$ operator, i.e. when they exhibit PT-symmetry. The experimental verification of the predictions of PT symmetry in quantum mechanical systems, has posed serious challenges due to decoherence effects, many body interactions and the difficulty of implementing non-Hermiticity in a PT-symmetry fashion [17]. A decade later, the experimental verification, of the predictions arises from the PT-symmetric Hamiltonians, came from an entirely unexpected brunch of physics, namely optics and photonics [18, 19, 20, 21, 22, 23, 24, 25] and which is presented in a section below.

Subsequently we'll discuss the quantum mechanical properties of spatial inversion and time reversal operators $\hat{P}$ and $\hat{T}$ respectively, and the necessary and sufficient conditions which must be fulfilled in order to be a system PT-symmetric, i.e. the existence of real eigenvalues (spectra) of a non-Hermitian Hamiltonian.

3.1- PT symmetry-Basic concepts and definitions

In 1998, Bender and Boettcher [16] showed that quantum systems of non-Hermitian Hamiltonians can have a real spectrum (i.e. a real set of eigenvalues) if they commute with the $\hat{P}\hat{T}$ operator. This counterintuitive result goes against the commonly held view that real eigenvalues are only associated with Hermitian observables. The necessary (but not sufficient) condition for a system to be PT-symmetric is that the complex potential involved should satisfy the condition $V(\vec{r}) = V^*(-\vec{r})$ [26] as one can understand from the action of the $\hat{P}\hat{T}$ operator on a Hamiltonian of a complex potential $V(\vec{r})$.

The action of the Parity operator $\hat{P}$, amounts to the spatial reflection, namely: $\vec{r} \to -\vec{r}$ and $\vec{p} \to -\vec{p}$, where $\vec{p}$ is the momentum. The action of this operator on each quantum state described as,

$$\hat{P}\psi(\vec{r},t) = \psi(-\vec{r},t) \quad (\mathbf{3.1.1})$$

while the action of the time reversal operator $\hat{T}$ means the change $t \to -t$ [27] and its action has as a following the changes, $\vec{p} \to -\vec{p}$, $\vec{r} \to \vec{r}$ and $i \to -i$. So, the action of the $\hat{T}$ operator on the above mentioned, quantum state is described:

$$\hat{T}\psi(\vec{r},t) = \psi^*(\vec{r},-t) \quad (\mathbf{3.1.2})$$

The symbol "*" means the complex conjugate, of the wavefunction, and arises from the fact that $\hat{T}$, is an antilinear and antiunitary operator [27]. Because the classical momentum and coordinate change their signs under spatial inversion, the operators which describe these observables are transformed under spatial inversion as,

$$\hat{P}^+\hat{r}\hat{P} = -\hat{r} \quad (\mathbf{3.1.3})$$

$$\hat{P}^+\hat{p}\hat{P} = -\hat{p} \quad (\mathbf{3.1.4})$$

Furthermore, the coordinate and the momentum are transformed under time reversal as,

$$\hat{T}^+\hat{r}\hat{T} = \hat{r} \quad (\mathbf{3.1.5})$$

$$\hat{T}^{+}\hat{p}\hat{T} = -\hat{p} \quad (\mathbf{3.1.6})$$

If the Hamiltonian of a system can be represented in the form of the polynomial in momentum and coordinate operators, $\hat{H} = \hat{H}(\hat{p}, \hat{r}, t)$, then the action of the above two operators on the Hamiltonian is described as follows. For the $\hat{P}$ operator,

$$\hat{P}^{+}\hat{H}\hat{P} = \hat{H}\left(\hat{P}^{+}\hat{p}\hat{P}, \hat{P}^{+}\hat{r}\hat{P}, t\right) = \hat{H}(-\hat{p}, -\hat{r}, t) \qquad (\mathbf{3.1.7})$$

and the system is $\hat{P}$- invariant if its Hamiltonian does not change after the inversion of coordinates, i.e.,

$$\hat{H}(\hat{p}, \hat{r}, t) = \hat{H}(-\hat{p}, -\hat{r}, t) \qquad (\mathbf{3.1.8})$$

Respectively for $\hat{T}$operator,

$$T^{+}\hat{H}\hat{T} = \hat{H}^{*}\left(\hat{T}^{+}\hat{p}\hat{T}, \hat{T}^{+}\hat{r}\hat{T}, t\right) = \hat{H}^{*}(-\hat{p}, \hat{r}, -t) \quad (\mathbf{3.1.9})$$

And a system is $\hat{T}$- invariant if its Hamiltonian does not change under time reversal, i.e. [27],

$$\hat{H}(\hat{p}, \hat{r}, t) = \hat{H}(-\hat{p}, \hat{r}, -t) \qquad (\mathbf{3.1.10})$$

By combining the expressions (3.1.8) and (3.1.10), we can obtain the transformation of the Hamiltonian under the action of the $\hat{P}\hat{T}$ operator,

$$\hat{P}^{+}\hat{T}^{+}\hat{H}(\hat{p}, \hat{r}, t)\hat{P}\hat{T} = \hat{H}\left(\hat{P}^{+}T^{+}\hat{p}\hat{P}\hat{T}, \hat{P}^{+}T^{+}\hat{r}\hat{P}\hat{T}\,, t\right) = \hat{H}^{*}(\hat{p}, -\hat{r}\,, -t) \quad (\mathbf{3.1.11})$$

If we consider a Hamiltonian of the form $\hat{H} = \frac{\hat{\boldsymbol{p}}^2}{2m} + V(\vec{r})$, where m is the mass and V is the complex potential function of a particle, and it's of the form, $V(\vec{r}) = V_R(\vec{r}) + iV_I(\vec{r})$, the system is PT-symmetric if $V(\vec{r}) = V^{*}(-\vec{r})$ which gives $V_R(\vec{r}) = V_R(-\vec{r})$ and $V_I(\vec{r}) = -V_I(-\vec{r})$. Namely, the real part of the potential is an even function of $\vec{r}$, and the imaginary part is an odd function of $\vec{r}$.

Necessary and sufficient condition for real eigenvalues of a PT- symmetric Hamiltonian, is that the eigenvectors to be PT- symmetric [27].

3.2- Phase transition in PT- symmetric systems

We consider a Hamiltonian of the form, $\hat{H} = \hat{H}(\hat{p}, \hat{r}, t, \mu)$, where μ, is a critical parameter that defines the phase of the system i.e. if it's in PT- symmetric phase (real spectrum) or in a broken PT- phase (partially complex spectrum).

We will begin with the description of a two-level system, which described by the two by two Hamiltonian,

$$\hat{H} = \begin{bmatrix} i\gamma & \kappa \\ \kappa & -i\gamma \end{bmatrix} \quad (\mathbf{3.2.1})$$

This Hamiltonian is PT-symmetric since it has the general form, of a PT matrix which is, $A = \begin{bmatrix} x & y \\ y^{*} & x^{*} \end{bmatrix}$ [28], with star (*) symbol we mean the complex conjugate. The diagonalization of (3.2.1) gives the eigenvalues and the corresponding eigenvectors of this system,

$$E_{1,2} = \pm\sqrt{\kappa^2 - \gamma^2}\,, \qquad \psi_{1,2} = \left(\frac{i\gamma}{\kappa} \pm \sqrt{1 - \frac{\gamma^2}{\kappa^2}} \quad 1\right)^{T} \quad (\mathbf{3.2.2})$$

As one can see from expressions (3.2.2) the PT-symmetry is unbroken, so it has an entire real spectrum if, $\kappa \geq \gamma$. Otherwise, if $\kappa <$γ, the spectrum becomes complex, with both eigenvalues to form a complex conjugate pair. At the point κ=γ in the parameter space, PT-symmetry is spontaneously broken, the two eigenvalues coalesce and the eigenvectors becomes linearly dependent. These are, the so-called exceptional points (EP), which arises in non-Hermitian physics [29].

Finally, it's crucial to make a distinction between the eigenvalue coalescence and the well known degeneracy. At the EP, both eigenvalues and eigenvectors are the same. In contrary, in the degeneracy case two eigenvalues are the same but the eigenvectors remain linearly independent.

3.3- Parity-time symmetry in Optics and Photonics

Despite the distinct physical origins of the Schrödinger equations for electrons and Maxwell's theory of light, it can be shown that, under certain conditions they exhibit a similar mathematical form, as we present below. Due to this analogy, it is possible to investigate PT symmetry in optics and photonics, where the many body interactions, which is present in quantum mechanical systems, are equivalent to nonlinear optical interactions. Thereby, its attainable the correspondence of these distinct branches of physics [17]. For making insight in the correspondence of quantum mechanics and photonics, we'll begin by consider the one-dimensional (1D) Schrödinger equation of a single particle of mass m,

$$i\hbar\frac{\partial\psi}{\partial t} = \hat{H}\psi, \qquad \hat{H} = -\frac{\hbar^2}{2m}\frac{\partial^2}{\partial x^2} + V(x) \quad (\mathbf{3.3.1})$$

where ψ, in the wavefunction, $\hbar$ is the reduced Planck's constant and V(x) is the potential. For an isolated system potential V(x) is a real function and is related with the conservative force acting on a particle. However, open quantum systems are described through non-Hermitian Hamiltonians which accounts the coupling between system and its environment. In such cases, the potential becomes a complex function and the system follows to described through Schrödinger equation, and the orthogonality relations, must then be modified. On the other side, the paraxial equation of electromagnetic wave propagation under the slowly varying envelope approximation is [17],

$$i\frac{\partial E(x,z)}{\partial z} = \left[-\frac{1}{2k_0 n_0}\frac{\partial^2}{\partial x^2} + V(x)\right]E(x,z) \equiv \hat{H}E(x,z) \quad (\mathbf{3.3.2})$$

where the propagation distance z along the optical axis, plays the role of time, in Schrödinger equation. In the above equation, k_0 is the free space wavevector, n_0 is the refractive index of the background space and $V(x) = k_0[n_R(x) + in_I(x)]$ is the complex optical potential, in which is due the non Hermiticity. $n_R(x)$, and $n_I(x)$ are the spatial distribution of the real and imaginary part of the refractive index respectively. It is now clear the way which the quantum mechanics is related with optics, the refractive index profile plays the role of the complex potential. This is how the non-Hermiticity is realized in Photonics structures by the complex value of dielectric permittivity. Following this correspondence, and keeping in mind that the PT quantum mechanical formalism dictates that $V(r) = V^*(-r)$, we can define as Parity-Time (PT) symmetry in optical systems the condition $\varepsilon(r) = \varepsilon^*(-r)$, where $\varepsilon(r)$ is the permittivity of the medium, which is related to the material refractive index, by the relation: $\varepsilon^2(r) = n(r)$, when we are dealing with non-magnetic materials.

Chapter 4 - Single mode coupled ring cavities (class A lasers)

The purpose of this chapter is to examine a system of two coupled micro-ring cavities (photonic molecule) with balanced gain and loss that exhibit single mode lasing operation at pump powers well above threshold. It's is of our interest to study the behavior of this system around its exceptional point, in two different ways. The first one, is linear in order to verify the existence of exceptional points by making analytical computations. In the second approach we'll consider, the nonlinear interactions, and we'll assume class A laser, which means that, radiation loss is much smaller than the transverse and longitudinal relaxation rates. This system is described by equation (2.10.6) and the coupling strength between two resonators, is introducing phenomenologically, in the equations of modal fields in the two cavities.

In our analysis, we assume dual micro-ring resonators as it shown in fig. (3), and for demonstration purposes we assume that each cavity supports only one transverse mode, due to their very small width. Notice also, that we consider here the cold modes of the cavity and not the ones described by the CF-states.

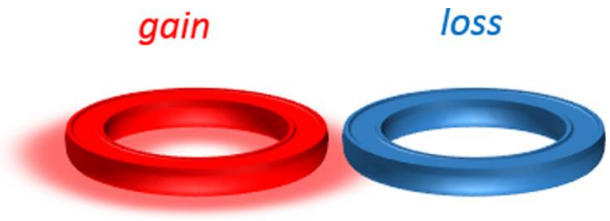

Figure 3- PT symmetric arrangement of two coupled micro-ring cavities [30].

For convenience we rewrite, the differential equation of the electric field, equation (2.10.6), for both resonators where one has a net gain while the other has loss. In the case of a single mode laser and by taking into account the coupling between the envelopes of the electric fields we get [30]:

$$\dot{E}_1 = \frac{i}{2\bar{\omega}_a}\left[\bar{\omega}_a^2 - \bar{\omega}^2\right]E_1 - \bar{\gamma}E_1 + \frac{\bar{\omega}_a B_{11}}{2}\frac{D_0}{1+\tilde{A}_{11,11}|E_1|^2}E_1 + i\kappa E_2 \quad (4.1)$$

$$\dot{E}_2 = \frac{i}{2\bar{\omega}_a}\left[\bar{\omega}_a^2 - \bar{\omega}^2\right]E_2 - \bar{\gamma}E_2 - \frac{\bar{\omega}_a B_{11}}{2}\frac{f_0}{1+\tilde{A}_{11,11}|E_2|^2}E_2 + i\kappa E_1 \quad (4.2)$$

where, $\bar{\gamma}$ is the linear loss which is present in both cavities, D_0 is the unsaturated gain in the active cavity, and f_0 is the unsaturated loss in the passive cavity. The last term in both equations describes the temporal coupling between two modes (one in each cavity), with coupling strength κ. Also, it is assumed that in each cavity the mode frequency ($\bar{\omega}$) is the same since they are identical.

4.1- Linear Analysis

In order to analyze the response of this system under linear conditions, we assume that the modal field amplitudes are small, i.e. $|E_1|,|E_2|\sim 0$ [30]. This assumption, allow us to write the above equations in the linear form,

$$\dot{\boldsymbol{E}}_{\boldsymbol{1}} = -\tilde{\boldsymbol{\gamma}}\boldsymbol{E}_{\boldsymbol{1}} + \widetilde{\boldsymbol{D}}_{\boldsymbol{0}}\boldsymbol{E}_{\boldsymbol{1}} + \boldsymbol{i\kappa}\boldsymbol{E}_{\boldsymbol{2}} \qquad \textbf{(4.1.3)}$$

$$\dot{\boldsymbol{E}}_{\boldsymbol{2}} = -\tilde{\boldsymbol{\gamma}}\boldsymbol{E}_{\boldsymbol{2}} - \tilde{\boldsymbol{f}}_{\boldsymbol{0}}\boldsymbol{E}_{\boldsymbol{2}} + \boldsymbol{i\kappa}\boldsymbol{E}_{\boldsymbol{1}} \qquad \textbf{(4.1.4)}$$

where we set $-\tilde{\gamma} = \frac{i}{2\bar{\omega}_a}\left[\bar{\omega}_a^2 - \bar{\omega}^2\right] - \bar{\gamma}$, $\widetilde{D}_0 = \frac{\bar{\omega}_a B_{11}}{2} D_0$ and $\tilde{f}_0 = \frac{\bar{\omega}_a B_{11}}{2} f_0$.

The eigenvalues of this system can be directly obtained, by assuming the form:

$$(E_1\ E_2)^T = (e_{01}\ e_{02})^T e^{-i\lambda t}$$

by the symbol T we mean the transpose eigenvector, λ is the eigenvalues of this system and e_{01} , e_{02} are the modal amplitudes of the modes in the active and passive cavity respectively and they are complex constants. So, the linear system of equation (4.1.3), (4.1.4) in matrix form is,

$$\frac{d}{dt}\begin{pmatrix} E_1 \\ E_2 \end{pmatrix} = \begin{pmatrix} -\tilde{\gamma} + \widetilde{D}_0 & i\kappa \\ i\kappa & -\tilde{\gamma} - \tilde{f}_0 \end{pmatrix}\begin{pmatrix} E_1 \\ E_2 \end{pmatrix}$$

$$\Rightarrow \quad -i\lambda e^{-i\lambda t}\begin{pmatrix} e_{01} \\ e_{02} \end{pmatrix} = \begin{pmatrix} -\tilde{\gamma} + \widetilde{D}_0 & i\kappa \\ i\kappa & -\tilde{\gamma} - \tilde{f}_0 \end{pmatrix}\begin{pmatrix} e_{01} \\ e_{02} \end{pmatrix} e^{-i\lambda t}$$

$$\Rightarrow \quad \begin{pmatrix} -\tilde{\gamma} + \widetilde{D}_0 + \lambda i & i\kappa \\ i\kappa & -\tilde{\gamma} - \tilde{f}_0 + \lambda i \end{pmatrix}\begin{pmatrix} e_{01} \\ e_{02} \end{pmatrix} = \begin{pmatrix} 0 \\ 0 \end{pmatrix} \qquad (\mathbf{4.1.5})$$

The solution of this eigenvalue problem, is possible if we set the determinant of the matrix in the left-hand side equal to zero. By making this, we find the eigenvalues to be,

$$\lambda_{1,2} = \frac{-i(2\tilde{\gamma} + \tilde{f}_0 - \widetilde{D}_0) \pm \sqrt{4\kappa^2 - (\tilde{f}_0 + \widetilde{D}_0)^2}}{2} \qquad (\mathbf{4.1.6})$$

From eq. (4.1.6) we can see that the two eigenvalues coalesce when $\left(\tilde{f}_0 + \widetilde{D}_0\right) = \pm 2\kappa$. In addition, we can make a distinction of two cases. The first case is when $\left(\tilde{f}_0 + \widetilde{D}_0\right) < 2\kappa$ and the second one when $\left(\tilde{f}_0 + \widetilde{D}_0\right) > 2\kappa$.

I. Unbroken phase: $\left(\tilde{\boldsymbol{f}}_{\boldsymbol{0}} + \widetilde{\boldsymbol{D}}_{\boldsymbol{0}}\right) < \boldsymbol{2\kappa}$

In this first case, the eigenvalues of the system are,

$$\lambda_{1,2} = \frac{-i(2\tilde{\gamma} + \tilde{f}_0 - \widetilde{D}_0)}{2} \pm \sqrt{\kappa^2 - \left(\frac{\tilde{f}_0 + \widetilde{D}_0}{2}\right)^2} \qquad (\mathbf{4.1.7})$$

we set $cos\theta = \sqrt{\kappa^2 - (\frac{\tilde{f}_0+\tilde{D}_0}{2})^2}$, and we substitute the eigenvalues (eq. (4.1.7)) in (4.1.5), in order to find the corresponding eigenvalues,

$$\begin{pmatrix} -\tilde{\gamma} + \tilde{D}_0 + i(\frac{-i(2\tilde{\gamma} + \tilde{f}_0 - \tilde{D}_0)}{2} \pm cos\theta) & i\kappa \\ i\kappa & -\tilde{\gamma} - \tilde{f}_0 + i(\frac{-i(2\tilde{\gamma} + \tilde{f}_0 - \tilde{D}_0)}{2} \pm cos\theta) \end{pmatrix} \begin{pmatrix} e_{01} \\ e_{02} \end{pmatrix} = \begin{pmatrix} 0 \\ 0 \end{pmatrix}$$

which for e_{01}=1, gives $e_{02} = isin\theta \pm cos\theta = \pm e^{\pm i\theta}$. Finally, the eigenvectors are,

$$\begin{pmatrix} E_1 \\ E_2 \end{pmatrix} = \begin{pmatrix} 1 \\ \pm e^{\pm i\theta} \end{pmatrix} e^{(\frac{\tilde{D}_0 - \tilde{f}_0}{2} - \tilde{\gamma})t} e^{\pm icos\theta \cdot t} \quad (\mathbf{4.1.8})$$

As one can see the two eigenvectors are nonorthogonal with a phase factor θ, depends on coupling, and on the gain-loss contrast and a PT-like bifurcation is present for cosθ=0.

II. Broken phase: $\left(\tilde{\boldsymbol{f}}_{\mathbf{0}} + \tilde{\boldsymbol{D}}_{\mathbf{0}}\right) > 2\boldsymbol{\kappa}$

In this case, the eigenvalues of the system are,

$$\lambda_{1,2} = \frac{-i(2\tilde{\gamma} + \tilde{f}_0 - \tilde{D}_0)}{2} \pm i\sqrt{(\frac{\tilde{f}_0 + \tilde{D}_0}{2})^2 - \kappa^2} \quad (\mathbf{4.1.9})$$

By the definition $sinh\theta$=$\sqrt{(\frac{\tilde{f}_0+\tilde{D}_0}{2})^2 - \kappa^2}$, the eigenvalue problem gives,

$$\begin{pmatrix} -\tilde{\gamma} + \mathrm{D}_0 + i(\frac{-i(2\tilde{\gamma} + \tilde{f}_0 - \tilde{D}_0)}{2} \pm isinh\theta) & i\kappa \\ i\kappa & -\tilde{\gamma} - f_0 + i(\frac{-i(2\tilde{\gamma} + \tilde{f}_0 - \tilde{D}_0)}{2} \pm isinh\theta) \end{pmatrix} \begin{pmatrix} e_{01} \\ e_{02} \end{pmatrix} = \begin{pmatrix} 0 \\ 0 \end{pmatrix}$$

As in the first case, so here we set e_{01}=1 and for the second component of the eigenvector arises that, $e_{02} = i[cosh\theta \mp sinh\theta] = ie^{\pm\theta}$. Consequently, the corresponding eigenvectors are,

$$\begin{pmatrix} E_1 \\ E_2 \end{pmatrix} = \begin{pmatrix} 1 \\ ie^{\pm\theta} \end{pmatrix} e^{(\frac{\tilde{D}_0 - \tilde{f}_0}{2} - \tilde{\gamma})t} e^{\mp sinh\theta \cdot t} \quad (\mathbf{4.1.10})$$

From equation (4.1.10) it's clear that the phase difference between the modal field amplitudes is $\Delta\varphi = \pi/2$ and moreover, they are unequal.

4.1-1 Weak coupling coefficient: Linear analysis

The parameter values which were used in our simulation are, $\bar{\omega}_\alpha = 20$, $\bar{\omega} = 20.919$, $\bar{\gamma} = 0.02$ ($\tilde{\gamma} = 0.02 + 0.94i$) and κ=0.17 ($\frac{\kappa}{Re\{\tilde{\gamma}\}} = 8.5$). We'll examine the regimes, of lasing in the PT-symmetric phase or in the broken PT-phase as mentioned in the above section.

- **Lasing in the unbroken phase**

For the loss in the passive cavity to has the value, $\tilde{f}_0 = 0.1$ we take the behavior presented in fig. (4), where exists an Exceptional Point at pump value, $\tilde{D}_0^{(EP)} = 0.24$ and the system is lasing in the PT-phase, where the threshold value of the gain is, $\tilde{D}_0^{(th,PT)} = 0.14$.

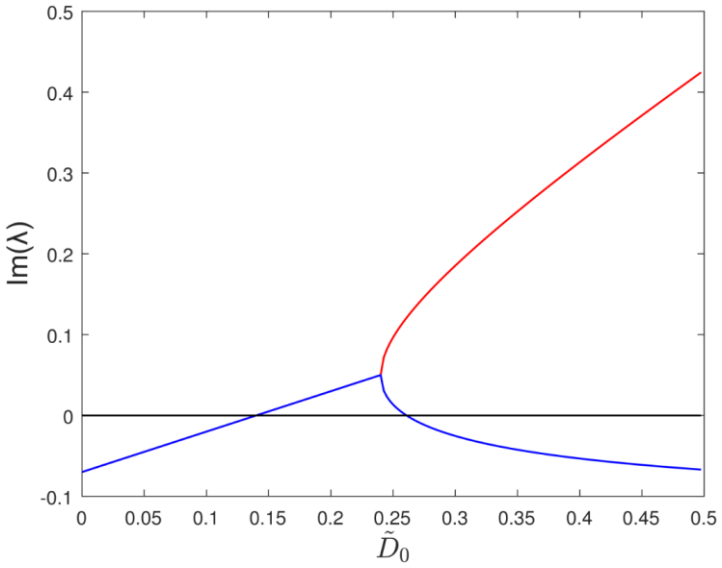

Figure 4 - Imaginary part of the eigenvalues as a function of the applied gain. The two eigenvalues of the system are shown with blue and red. Amplification occurs if Im{λ}>0, so the system lases in the PT-phase.

- **Lasing in the broken phase**

When the loss in the passive cavity has the value, $\tilde{f}_0 = 0.3$ we have similar behavior with that presented in fig. (4), where exists an Exceptional Point at the pump value, $\tilde{D}_0^{(EP)} = 0.04$. This system lases in the broken PT-phase where the threshold value is, $\tilde{D}_0^{(th,BPT)} = 0.11$.

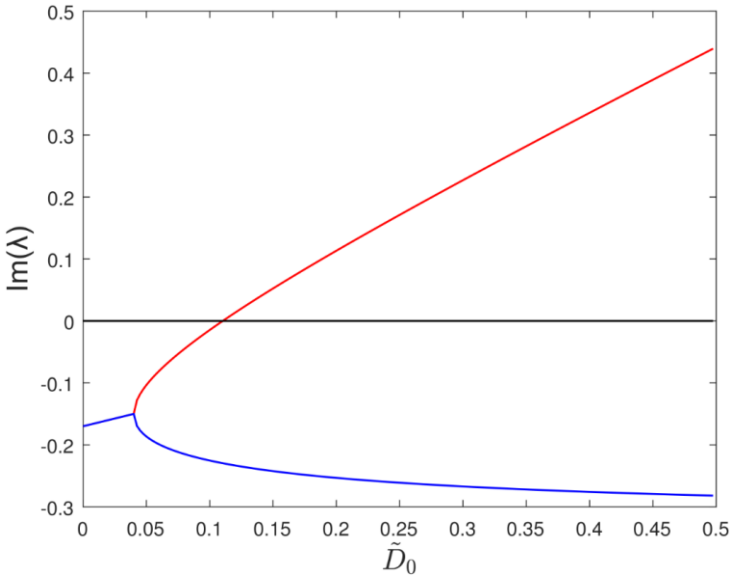

Figure 5- Imaginary part of the eigenvalues as a function of the applied gain. The two eigenvalues of the system are shown with blue and red. Amplification occurs if Im{λ}>0, so the system lases in the broken PT-phase.

In figs. (4,5) we observe that the existence of an Exceptional Point (EP) when a bifurcation occurs, signifies the lasing in the PT and in the broken-PT phase, respectively. We can define the $Im\{\lambda\}$ as modal gain, which is negative for gain values below the threshold, zero on the threshold and positive for pump values greater than the lasing threshold.

If the system is operating in the first regime (PT-phase), the fields experience linear amplification as long as the gain is greater than the total loss of the system. The net gain/loss of the system is described from the factor, $\frac{\tilde{D}_0-\tilde{f}_0}{2}-Re\{\tilde{\gamma}\}$. When $\frac{\tilde{D}_0-\tilde{f}_0}{2}-Re\{\tilde{\gamma}\}>0$ the modal fields exhibit linear amplification, so the threshold value of the gain in the unbroken phase is, $\tilde{D}_{th}^{(U)}=\tilde{f}_0+2Re\{\tilde{\gamma}\}$.

On the other hand, if the system operates in the second regime (Broken PT-phase), the net gain/loss in the system, is $\frac{\tilde{D}_0-\tilde{f}_0}{2}-Re\{\tilde{\gamma}\}+\sqrt{(\frac{\tilde{f}_0+\tilde{D}_0}{2})^2-\kappa^2}$. Growth will occur if $\frac{\tilde{D}_0-\tilde{f}_0}{2}-Re\{\tilde{\gamma}\}+\sqrt{\left(\frac{\tilde{f}_0+\tilde{D}_0}{2}\right)^2-\kappa^2}>0$ which gives the threshold value of the gain in the broken PT-phase, $\tilde{D}_{th}^{(B)}=\frac{Re\{\tilde{\gamma}\}^2+\tilde{f}_0Re\{\tilde{\gamma}\}+\kappa^2}{Re\{\tilde{\gamma}\}+\tilde{f}_0}$.

From the above results, we see that the thresholds are uniquely determined from the parameters $\tilde{\gamma},\tilde{f}_0,\kappa$. We can summarize the two lasing thresholds by the following inequality,

$$\tilde{D}_0>\min[\frac{Re\{\tilde{\gamma}\}^2+\tilde{f}_0Re\{\tilde{\gamma}\}+\kappa^2}{Re\{\tilde{\gamma}\}+\tilde{f}_0},\tilde{f}_0+2Re\{\tilde{\gamma}\}].$$

which indicates that the pump value in the active cavity must be higher than one of the above thresholds in order to have lase either in the Broken PT-phase or in the PT-phase.

4.1-2 Strong coupling coefficient: Linear analysis

In this section we consider the case of strong coupling between the modes of two cavities. The coupling strength is increased from κ=0.17 (section 4.1.1) to κ=0.4 $\boldsymbol{(\frac{\kappa}{Re\{\tilde{\gamma}\}}=20)}$ with the loss value to be the same with that of the above section ($\tilde{f}_0=0.3$)[1]. Notice that a PT-like bifurcation (EP) doesn't happen here and the system is frozen in the PT-symmetric regime, as described from fig. (6).

[1]For greater values of the loss f_0 the system undergoes a transition from a PT phase to a broken PT phase. But we are interested in what happened when we hold all other parameters the same and changing only the coupling between two cavities.

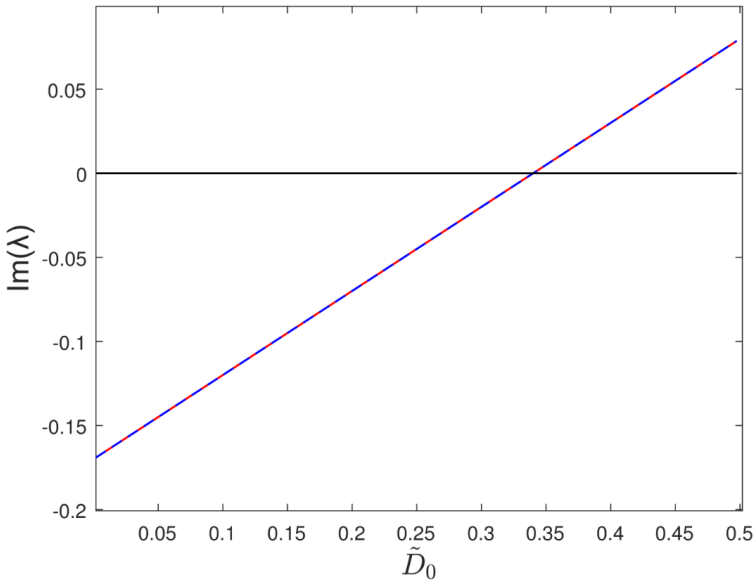

Figure 6- Both eigenvalues follow the same trajectory as the applied gain increases. With red are represented the values of the 1st eigenvalue and with dashed blue the values of the 2nd eigenvalue, as a function of the applied gain.

As one can see both modes lase simultaneously (for the same value of pump), as verified from the crossing between eigenvalues trajectories and the zero line, which represents the threshold modal gain.

4.2- Non-linear dynamical analysis

As the field in the PT-coupled cavity configuration starts to lase, nonlinear effects make their appearance. To analyze the response of the system under non-linear conditions we'll solve the full system of equations **(4.1)**, **(4.2)**. The parameters values where used in the simulation are presented in table 1, and they are the same for the parameters used in the above section for the linear analysis.

Table 1- Parameter values

$\tilde{f}_0$(loss in passive cavity)	κ (coupling)	$\bar{\omega}_\alpha$(center frequency)	$\bar{\omega}$ (mode's frequency)	n (refractive index)	K (radiation loss)	$\tilde{\gamma}$	$\bar{\gamma}_\perp$ (transverse relaxation rate)	$\bar{\gamma}_\parallel$ (longitudinal relaxation rate)
0.1 or 0.3	0.17 or 0.4	20	20.919	3	0.02	$0.02 + 0.94i$	10	1

In the non-linear regime, we obtain the numerical solution of coupled differential equations (4.1) and (4.2) by applying a fourth order Runge-Kutta integration algorithm. The spatial profile of the mode, in each cold cavity is depicted in fig. (7):

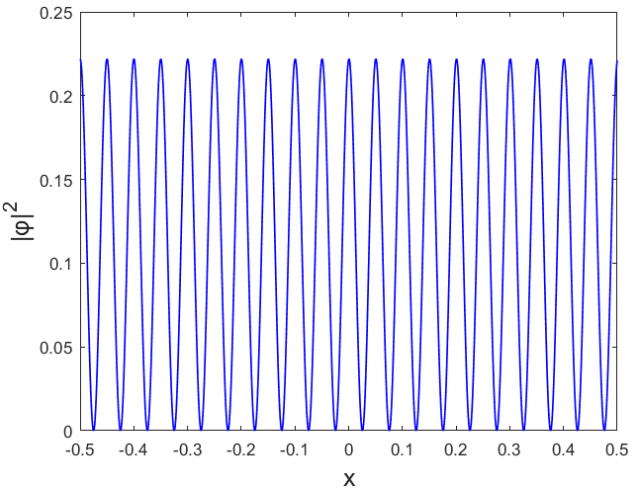

Figure 7- Mode profile in the cold resonator, for periodic boundary conditions, with refractive index n=3.

4.2-1 Weak coupling coefficient

- Lasing in the PT-phase

For the parameter values presented in table 1 (for $\tilde{f}_0 = 0.1$), we obtain the modal intensity in each ring as well as the intensity ratio $\boldsymbol{\rho} = {|\boldsymbol{E_2}|^2}/{|\boldsymbol{E_1}|^2}$ as a function of the applied gain as shown in fig. (8.a,b) respectively. Both modes (in each cavity) lase on the threshold pump value, $\widetilde{\boldsymbol{D}}_{\boldsymbol{0}}^{(\boldsymbol{th})} = \boldsymbol{0.14}$ (which is equal to the threshold pump value which was obtained in the linear analysis of the previous section) and the system lases in the PT-symmetric phase as one can understand from the fact that ρ=1 for each pump value.

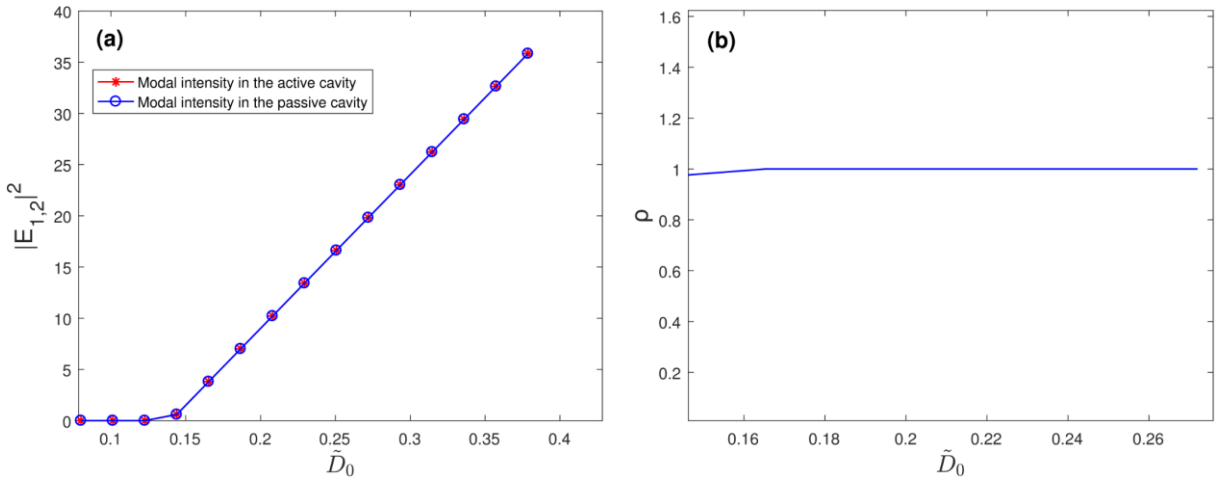

Figure 8- (a) Modal intensities as a function of the applied gain in the active cavity. (b) Intensities ratio as a function of the applied gain in one cavity. The system appears to be frozen in the PT-phase.

Therefore, for the parameter values we use, we don't observe the existence of an exceptional point. The time dynamics of the modal intensities, for the pump value $\widetilde{D}_0 = 0.378$ is shown in fig. (9):

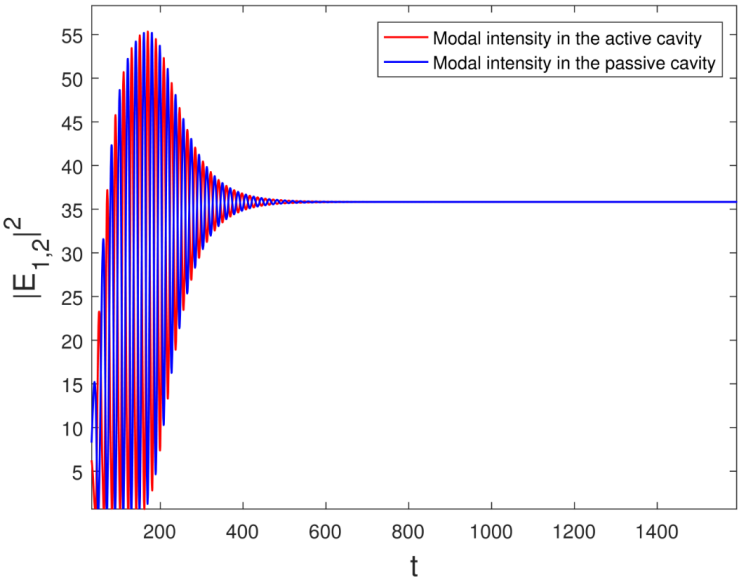

Figure 9- Time dynamics of modal intensities for the pump value, $\widetilde{D}_0 = 0.378$.

- Lasing in the broken PT-phase

For the parameter values presented in table 1 (for $\tilde{f}_0 = 0.3$), we obtain the modal intensity in each ring as a function of the applied gain as one can see in fig. (10.a). Both modes (in each cavity) lase on the threshold pump value, $\widetilde{\boldsymbol{D}}_{\boldsymbol{0}}^{(\boldsymbol{th})} = \boldsymbol{0.11}$ (which is equal to the threshold pump value which was obtained in the linear analysis of the previous section). A PT-bifurcation takes place, for $\widetilde{\boldsymbol{D}}_{\boldsymbol{0}} = \widetilde{\boldsymbol{D}}_{\boldsymbol{0}}^{(\boldsymbol{EP})} = \boldsymbol{0.397}$, and the system undergoes a transition from a broken-PT into PT-symmetric phase. Regarding the modal intensities, they are unequal and their difference is decreased as the gain value approaches the EP. If we continue to increase the applied gain the modal intensities become equal. This behavior is depicted in fig. (10).

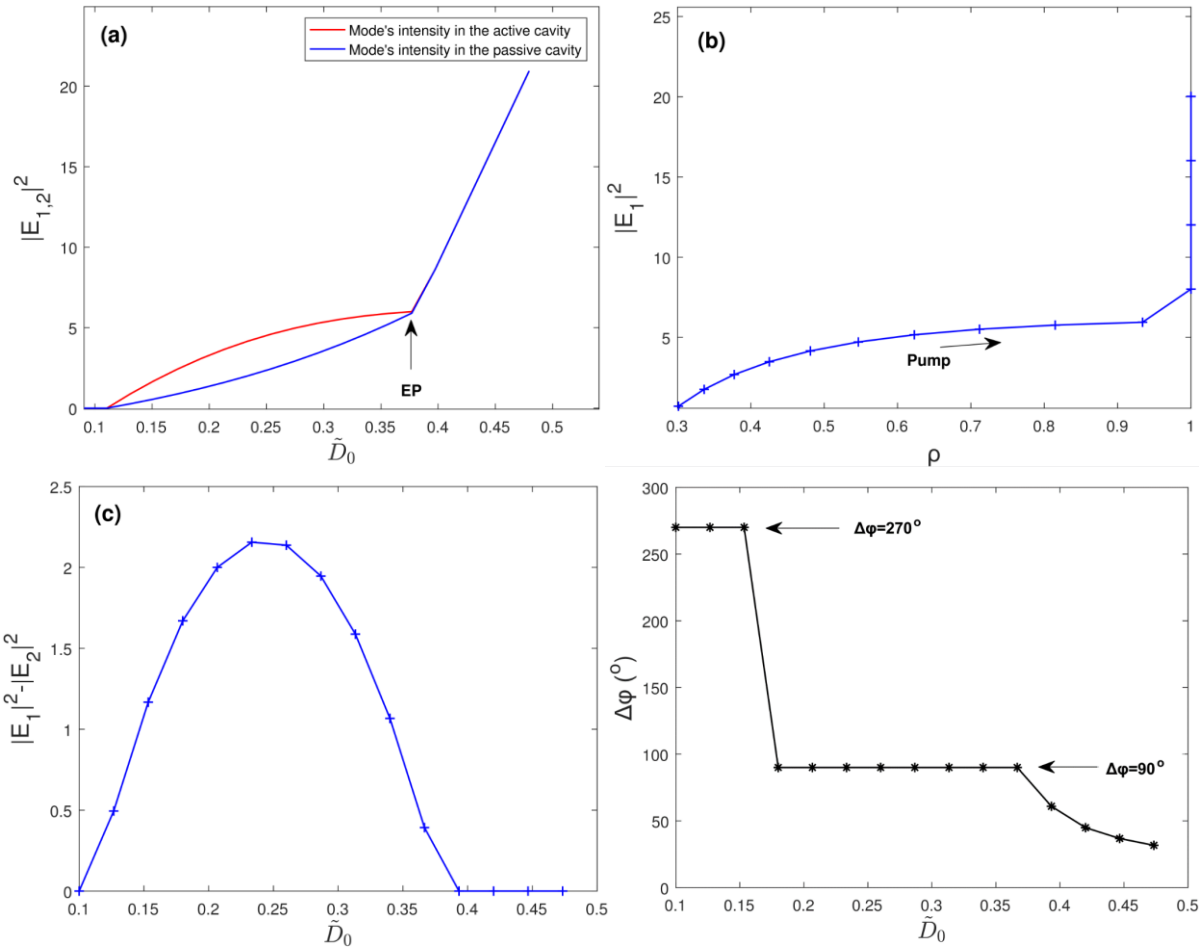

Figure 10-Its shown, in (a) the intensity of each mode in (b) mode's intensity in the active cavity and the intensity ratio $\rho = |E_2|^2/|E_1|^2$ *in (c)difference of modal intensities and (d) phase difference between modal fields, as a function of the applied gain. κ= 0.17, the radiation loss is* $\bar{\gamma}$*=0.02 and the phenomenological loss in passive cavity is* $\tilde{f}_0$ *=0.3.*

In fig. (10.b), its shown that mode's intensity in the active cavity, as well as, the intensity ratio $\boldsymbol{\rho = |E_2|^2/|E_1|^2}$, are increased with the increase of the applied gain in the active cavity. Up to the pump value $\widetilde{D}_0^{(EP)} = 0.397$, the intensity ratio becomes unity, which identifies the equal distribution of the energy in to cavities. In the above section it's shown that in the broken-PT phase the two fields have a phase difference $\Delta\varphi = 90°$ (eq. (4.1.10)), as is verified from fig. (8.d). Until a certain value of $\widetilde{D}_0$ the phase difference is $\Delta\varphi = \varphi_2 - \varphi_1 = 270° = -90°$ and then its locked in $+90°$ until the EP. The above results are similar with that of [30].

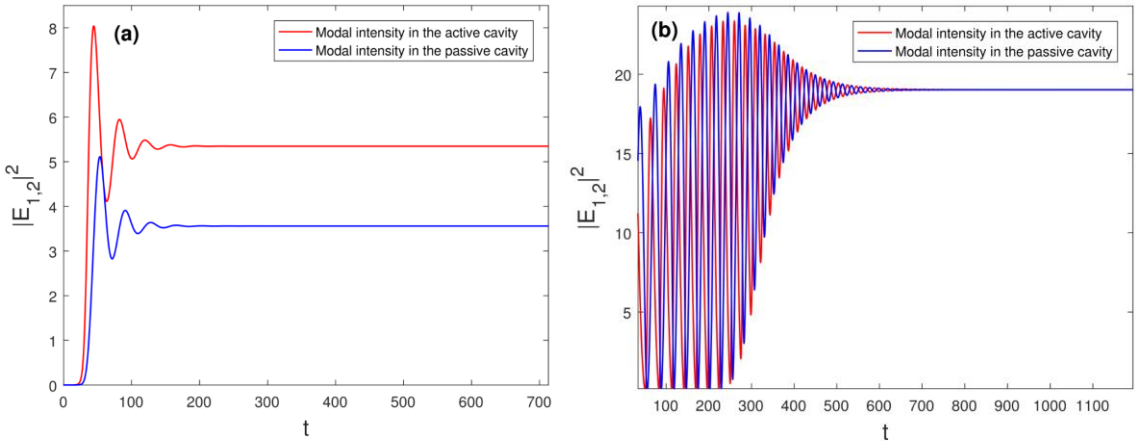

Figure 11- (a) Modal intensities for $\widetilde{D}_0$=0.3, the system is in the broken PT-phase (b) Modal intensities for $\widetilde{D}_0$=0.46, the system is in the PT-phase. In both cases the coupling strength is κ= 0.17, the radiation loss is $\overline{\gamma}$=0.02 and the phenomenological loss in the passive cavity is $\tilde{f}_0$ =0.3.

The time dynamics of modal intensities in the broken PT-phase (fig. 11.a) and in the PT-phase (fig. 11.b) are shown for pump values $\widetilde{D}_0 = 0.3$ and $\widetilde{D}_0 = 0.46$ respectively. In the first case the modal intensities have different steady state values, while in the second case they coalesce.

4.2-2 Strong coupling regime

In this section we consider a strong coupling between the two cavities. The coupling strength is increased from κ=0.17 (section 4.2.1) to κ=0.4 and the loss in the passive cavity is $\tilde{f}_0 = 0.3$.

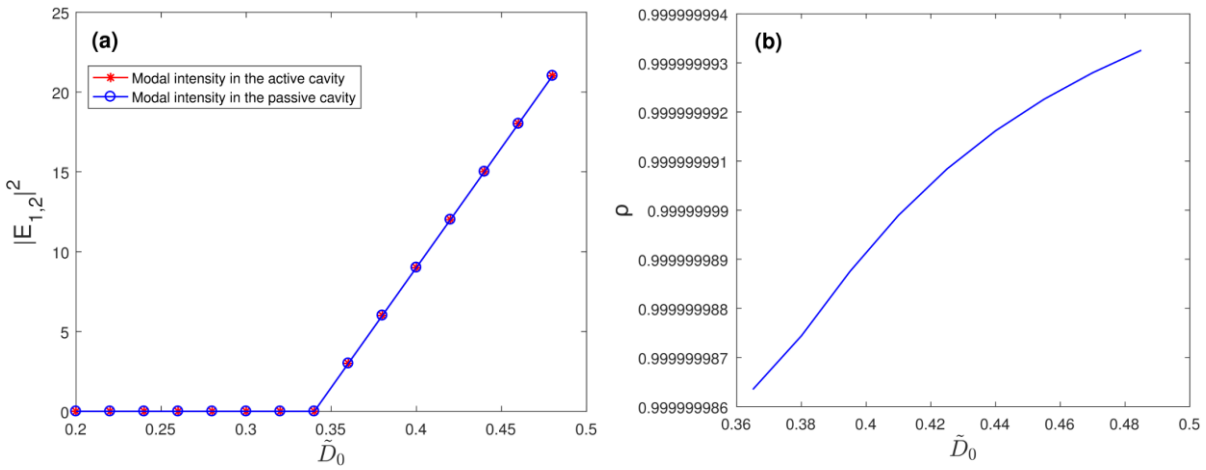

Figure 12- (α) Modal intensities as a function of the applied gain in one cavity. With red crosses is represented the intensity in the active cavity while with blue circles represent the intensity in the passive cavity. (b) Intensities ratio, as defined in the text as a function of the applied gain. In both figures it's confirmed that the system is frozen in the PT symmetric phase.

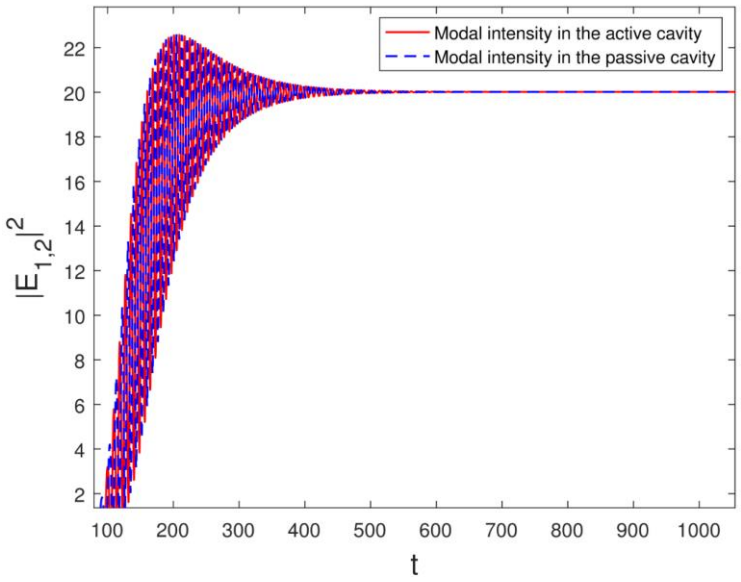

Figure 13- Modal intensities as a function of time for $\widetilde{D}_0$=0.47. Both modes have equal steady state values, and identify the PT-symmetric phase of the system.

As shown in the above figures the system is frozen in the PT-symmetric phase, and in this case we didn't observe an EP. This is due to the fact that the two coupled cavities, strongly interact and for each value of the applied gain they follow each other.

Chapter 5 –Steady State ab initio Laser theory (SALT)

One of the main goals of this chapter is to treat the openness of the laser system with the Constant Flux (CF) states [11], which are the eigenstates of Helmholtz equation (1.1) with open boundary conditions. The laser system we are interested to examine, consists of two cavities which are at distance d, from each other. So, the eigenfunctions which we are going to find are eigenfunctions of the composite system. Then, we continue with the approximate calculation of lasing thresholds, for several modes from the linearized SALT analysis (Steady State Ab-initio Laser Theory) [13]. Finally, we present the relation between the time domain solutions of MB equations with CF-boundary conditions (Constant-Flux Time Domain solutions (CFTD)) and the SALT solutions for the same boundary conditions.

5.1- Computation of Constant-Flux states

The standard modal approach for time dynamics, expands the electric field and the polarization into a superposition of the modes of the closed resonator. That way the "modes" of the cavity form an orthogonal basis and the decay (optical losses) due to the openness of the problem are added to the final equations phenomenologically. This means that the open nature of any laser system is not treated properly and such an approach lead to serious problems particularly in the bad cavity limit (random lasers). In order to avoid the aforementioned problems, we will expand the electric field and the polarization into a series of the proper "open modes" of the problem. These are the so-called constant flux states (CF-states). These modes (CF) correspond to the eigenstates of the passive scattering problem with radiating boundary conditions that conserve the flux outside the cavity, because outside the cavity the lasing frequency is real. In addition, we mention that CF-states are parametric eigenmodes of the Helmholtz equation, and the related parameter is the laser frequency k, (real number). Below is presented the generalized eigenvalue problem, which gives the eigenmodes and the eigenfrequencies of the system,

$$\varphi_n'' + k_n^2 \varepsilon_c(x)\varphi_n = 0 \quad (\mathbf{5.1.1})$$

$$\varphi_n'(\pm l) = \pm ik\varphi_n(\pm l) \quad (\mathbf{5.1.2})$$

The non-hermiticity of the φ_n eigenmodes is a direct outcome of the non-Hermitian open boundary conditions (CF boundary conditions) at the endpoints of the system of two coupled cavities ($-l = L + \frac{d}{2}$ and $l = L + \frac{d}{2}$). In fig. (14), one can see the representation of our system,

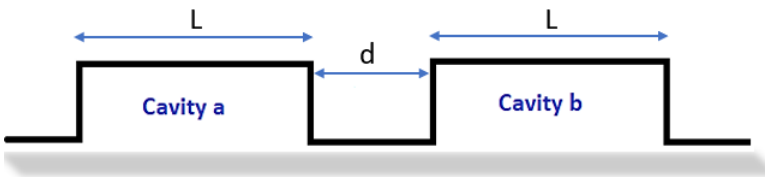

Figure 14- Representation of the system composites of two ridge cavities.

The $\varphi_n(x,k)$ eigenmodes constitute a basis with the following biorthogonality condition, $\int_{-l}^{l} \varepsilon_c(x)\varphi_n(x,k)\varphi_m(x,k)\,dx = \delta_{n,m}$, as we prove in appendix [A].

In our analysis we follow the ansatz, which proposed in [31] and assumes that we can choose as parameter k, in the CF- states calculation, the atomic frequency center, which we refer as ω_α (c=1). The numerical calculation of the CF-states is achieved by making space discretization and by using the finite difference method for the solution of the generalized Helmholtz differential equation, as presented in appendix [B]. The Helmholtz equation at the grid point p_n, is written as:

$$\frac{\varphi_{n+1}+\varphi_{n-1}-2\varphi_n}{\Delta^2} = -n_n^2 k_m^2 \varphi_n \quad (\mathbf{5.1.3})$$

where Δ is the distance between two successive grid points and n_n^2 is the dielectric permittivity is each position on the x-axis, characterized by the n-index. At point p_1 with the outgoing boundary condition, $\frac{\varphi_1-\varphi_0}{\Delta} = -\frac{in_l k(\varphi_1+\varphi_0)}{2}$ we obtain an expression for φ_0,

$$\varphi_0 = \frac{2+in_l k\Delta}{2-in_l k\Delta}\varphi_1 \equiv \beta_l \varphi_1 \quad (\mathbf{5.1.4})$$

using this expression together with the Helmholtz equation yields,

$$\frac{\beta_l - 2}{\Delta^2}\varphi_1 + \frac{1}{\Delta^2}\varphi_2 = -n_1^2 k_m^2 \varphi_1 \quad (\mathbf{5.1.5})$$

Similar expression can be obtained analogously for the right side of the cavity,

$$\frac{\beta_r - 2}{\Delta^2}\varphi_N + \frac{1}{\Delta^2}\varphi_{N-1} = -n_N^2 k_m^2 \varphi_N,$$

where $\beta_r = \frac{2+in_l k\Delta}{2-in_l k\Delta}$, while n_l and n_r are the refractive indices out of the cavity region, on the left and the right side respectively and we have considered that they are equal to unity. By combining the equations for all grid points we take the matrix form for the generalized eigenvalue problem,

$$\begin{pmatrix} \frac{\beta_l-2}{\Delta^2} & 1/\Delta^2 & 0 & \cdots & 0 \\ 1/\Delta^2 & -2/\Delta^2 & 1/\Delta^2 & 0 & \cdots \\ \cdots & \cdots & \cdots & \cdots & \cdots \\ 0 & \cdots & 1/\Delta^2 & -2/\Delta^2 & 1/\Delta^2 \\ 0 & \ldots & 0 & 1/\Delta^2 & \frac{\beta_r-2}{\Delta^2} \end{pmatrix} \begin{pmatrix} \varphi_1 \\ \varphi_2 \\ \cdots \\ \varphi_{N-1} \\ \varphi_N \end{pmatrix} = -k_m^2 \begin{pmatrix} n_1^2 & & & & \\ & n_2^2 & & \cdots & \\ & & & n_{N-1}^2 & \\ & & & & n_N^2 \end{pmatrix} \begin{pmatrix} \varphi_1 \\ \varphi_2 \\ \cdots \\ \varphi_{N-1} \\ \varphi_N \end{pmatrix} \quad (\mathbf{5.1.6})$$

The solution of this eigenvalue problem (5.1.6) gives us the open cavity frequencies and the corresponding eigenvectors.

5.2- Linear calculation of lasing thresholds

Based on what we mentioned in chapter 2, the fundamental equations of semiclassical laser theory, known as Maxwell-Bloch equations, are coupled nonlinear equations of the electric field **E**, the polarization **P**, and the inversion **D**. In this section we will talk about the steady-state ab-initio laser theory (SALT), which gives a set of self-consistent time-independent equations for the steady state solutions of the Maxwell-Bloch equations. The fundamental equation of SALT as it's presented in [11] is,

$$\left[\boldsymbol{\nabla}^2 + \left(\varepsilon_c(\boldsymbol{r}) + \frac{\gamma_\perp}{(\omega_\mu - \omega_\alpha) + i\gamma_\perp}\frac{D_0(\boldsymbol{r})}{1 + \sum_n \Gamma_n |\Psi_n(\boldsymbol{r})|^2}\right) k_\mu^2\right] \Psi_\mu(\boldsymbol{r}) = 0 \quad (\mathbf{5.2.1})$$

where $\varepsilon_c(\boldsymbol{r})$ is the dielectric function of the active medium, $\gamma_\perp$ is the transverse relaxation constant, ω_α is the center frequency of the Lorentzian gain curve, $D_0(\boldsymbol{r})$ is the pump parameter (expressed as inversion of populations), ω_μ and k_μ are the eigenfrequencies and the corresponding wavenumbers, $\Psi_\mu(\boldsymbol{r})$ are the eigenfunctions which corresponds to ω_μ, and $\Gamma_n(\omega_n) = {\gamma_\perp}^2/({\gamma_\perp}^2 + (\omega_n - \omega_a)^2))$, is the homogeneous broadened Lorentzian gain curve.

In the equation (5.2.1) the effect of the gain medium is incorporated in the term,

$$\varepsilon_g(\boldsymbol{r}, \omega) = \frac{\gamma_\perp}{(\omega - \omega_\alpha) + i\gamma_\perp}\frac{D_0(\boldsymbol{r})}{1 + \sum_n \Gamma_n |\Psi_n(\boldsymbol{r})|^2} \quad (\mathbf{5.2.2})$$

The additional dielectric function $\varepsilon_g(\boldsymbol{r}, \omega)$ is in general complex; its imaginary part is negative (amplifying) when the gain medium is inverted and its value depends on the pump strength. At lasing threshold value of $D_0(\boldsymbol{r})$, the gain compensates the outcoupling loss as well as any cavity loss from the cavity dielectric function. For lasing to occur to the i-th mode, D_0 must overcome the corresponding threshold value $D_0^{(i)}$ for this mode. A new mode appears once, D_0 surpasses its threshold. When D_0, reaches the threshold value for each lasing mode, it interacts with itself through the nonlinear term in denominator of (5.2.2), which express the spatial hole burning effect. At the same time, the lasing modes interacts with other modes. In addition, another factor which also determines the order of the lasing mode is the position of this under the homogeneously broadened gain curve Γ(ω). We consider a Lorentzian shape of Γ(ω), and modes in the vicinity of ω_α usually overcomes first their threshold value, so they make lase first.

Despite the crucial role playing by nonlinear modal interactions, we can solve the linear eigenvalue problem and find the threshold lasing modes and the corresponding lasing frequencies. Subsequently, we will present the way in which we find the aforementioned parameters. We are interested about the one-dimensional problem, and we ignore the nonlinear term in (5.2.1),

$$\left[\frac{d^2}{dx} + \left(\varepsilon_c(x) + \frac{\gamma_\perp D_0(x)}{(\omega - \omega_\alpha) + i\gamma_\perp}\right)\omega^2\right]\Psi(x) = 0 \quad (\mathbf{5.2.3})$$

The solution of (5.2.3) is obtained by consider the non-Hermitian CF boundary conditions, as we show in the above section. We can rewrite the above eigenvalue problem as an eigenvalue problem where the eigenvalue is the pump value D_0,

$$\hat{L}(\omega)\Psi(x) = -D_0(x)\Psi(x) \quad (\mathbf{5.2.4})$$

where,

$$\hat{L}(\omega) = \frac{(\omega - \omega_\alpha) + i\gamma_\perp}{\gamma_\perp \omega^2}\left(\frac{d^2}{dx} + \varepsilon_c(x)\omega^2\right) \quad (\mathbf{5.2.5})$$

By scanning the free normalized parameter $\bar{\omega}$ (unknown lasing frequency in normalized units) to the physically relevant interval $\bar{\omega} = [\bar{\omega}_\alpha - 3, \bar{\omega}_\alpha + 3]$ and keep tracking the path of the eigenvalues of the non-Hermitian operator $\hat{L}(\omega)$ in the complex plane, we can easily find the value of $\bar{\omega}$, for which the eigenvalues of $\hat{L}$, becomes real. That way we can find the lasing frequencies (in ascending order) and the linear lasing thresholds. The solution of the linear problem provides an estimate for the nonlinear.

For the case of two coupled ridge cavities at a distance d/L=0.025 with dielectric permittivity in both cavities $\varepsilon_c = (3 + 0.001i)^2$, and with $\varepsilon_c = 1.2^2$ in the space between them, the linear threshold calculation for $\bar{\gamma}_\perp = 1$ $\bar{\omega}_\alpha = 20$ (the bar means that the parameters are in normalized units), gives the eigenvalues trajectories presented in fig. (15. a, b) for the cases of uniform and non-uniform pump distribution respectively:

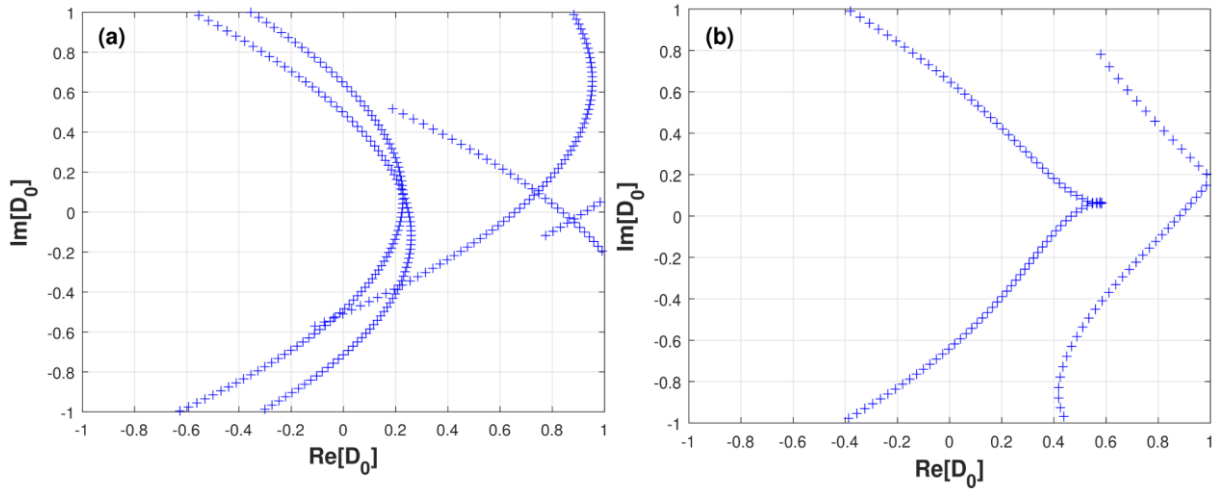

Figure 15- Eigenvalues trajectories in the complex plane for $\bar{\gamma}_\perp = 1$ and for the regimes of: (a) Uniform pump (b) nonuniform pump. The lasing frequencies arises from the claim that, $Im\{D_0\} = 0$.

The corresponding figures are presented in fig. (16. a, b), for the case of $\bar{\gamma}_\perp = 10$:

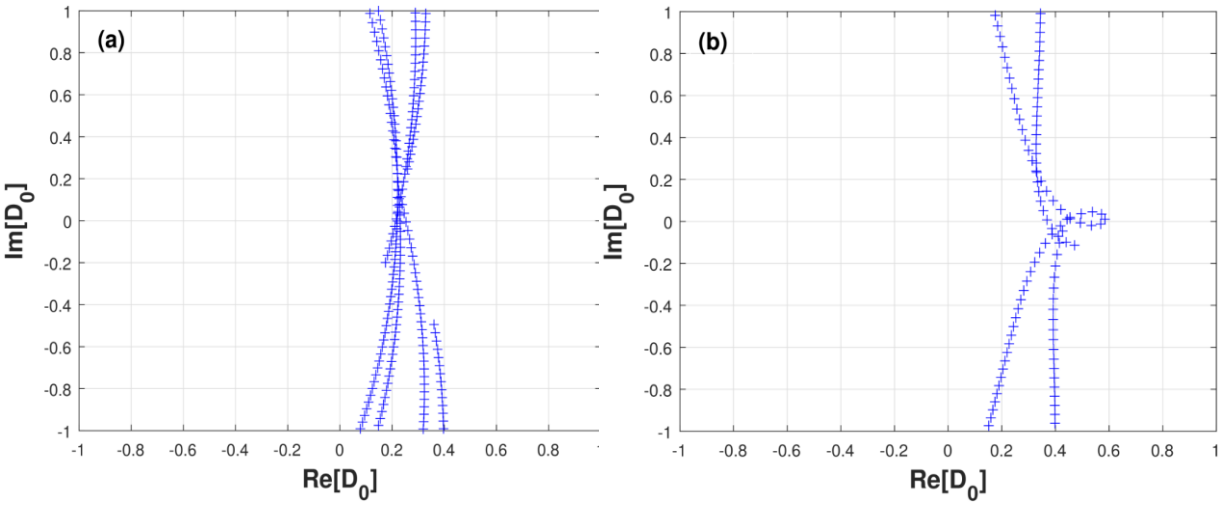

Figure 16 -Eigenvalues trajectories in the complex plane for $\bar{\gamma}_\perp = 10$ and for the regimes of: (a) Uniform pump (b) nonuniform pump. The lasing frequencies arises from the claim, $Im\{D_0\} = 0$.

Similar results are obtained for the case of $\bar{\gamma}_\perp = 1$, with the only differences to be the intracavity distance which is four time greater i.e. it becomes d/L=0.1, and the permittivity of both cavities which becomes $\varepsilon_c = (3 + 0.008i)^2$. The corresponding results are presented below:

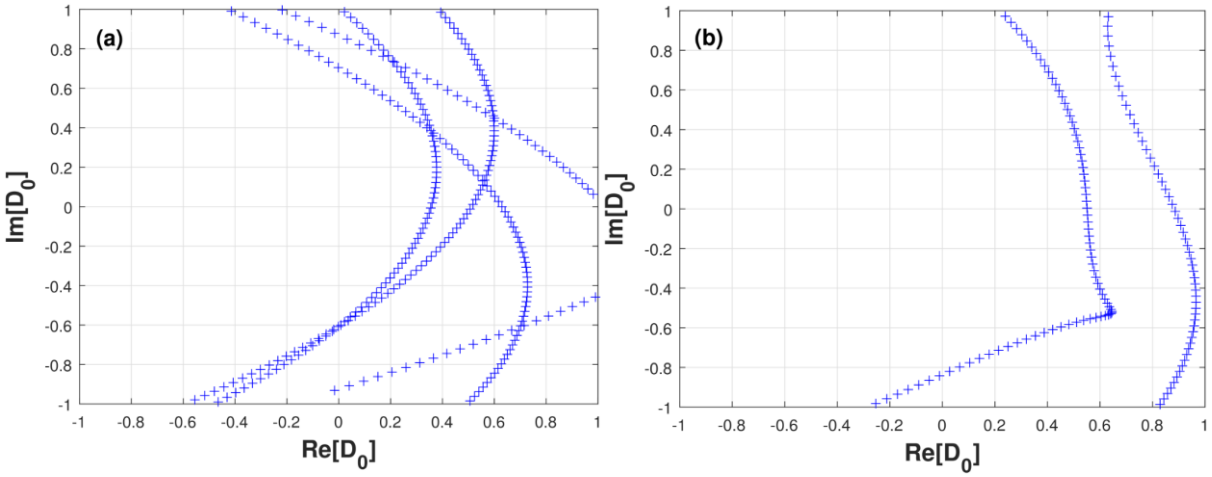

Figure 17- Eigenvalues trajectories in the complex plane for $\bar{\gamma}_\perp = 1$ and for the regimes of: (a) Uniform pump (b) nonuniform pump. The lasing frequencies arises from the claim, $Im\{D_0\} = 0$.

As one can see from the linear threshold analysis, fig. (15), (16), (17) the modes which makes lasing and the corresponding lasing thresholds are different for the cases of uniform and non-uniform pumping. This fact is also verified from the solution of the full nonlinear problem through Maxwell-Bloch equations (Chapters 6, 7, 8).

In this thesis, we'll refer three different cases which are:

1. **$\bar{\gamma}_\perp = 1$, distance between cavities d/L=0.025 and the cavities refractive index to be $n = 3 + 0.001i$: Case Ia**
2. **$\bar{\gamma}_\perp = 10$, distance between cavities d/L=0.025 and the cavities refractive index to be $n = 3 + 0.001i$: Case Ib.**
3. **$\bar{\gamma}_\perp = 1$, distance between cavities d/L=0.1 and the cavities refractive index to be $n = 3 + 0.008i$: Case II.**

5.3- Lasing modes for different gain curves

The homogeneous broadened gain curves, $\Gamma_n(\omega_n) = \bar{\gamma}_\perp{}^2/(\bar{\gamma}_\perp{}^2 + (\bar{\omega}_n - \bar{\omega}_a)^2))$, and the cold cavity modes as arising from the Helmholtz equation for CF-boundary conditions are presented in fig. (18) for the case of cavities with, $\varepsilon_c = (3 + 0.001i)^2$ which are at distance d/L=0.025 (case I). In fig. (19) we present the corresponding gain curve, for the case of cavities with, $\varepsilon_c = (3 + 0.008i)^2$ which are at distance d/L=0.1 (case II).

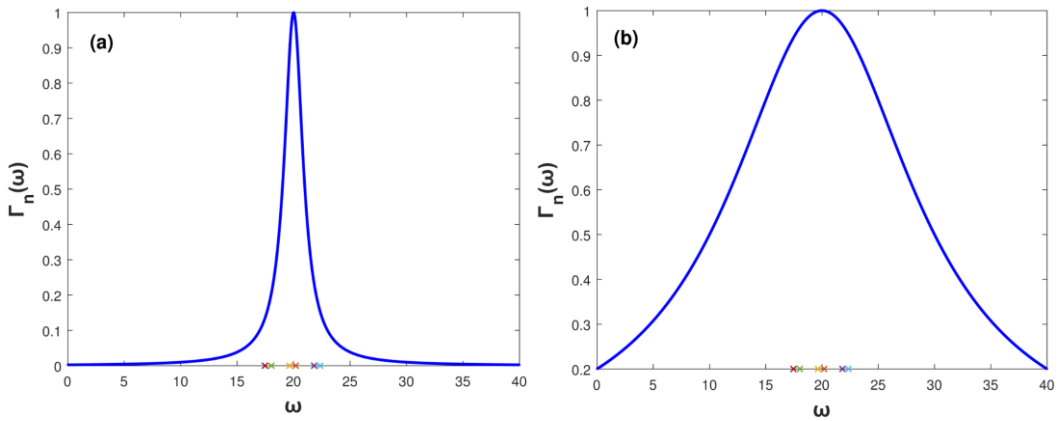

Figure 18 - Homogeneous broadened gain curves: Case I, for $\overline{\gamma}_\perp = 1$ in (a) and $\overline{\gamma}_\perp = 10$ in (b).

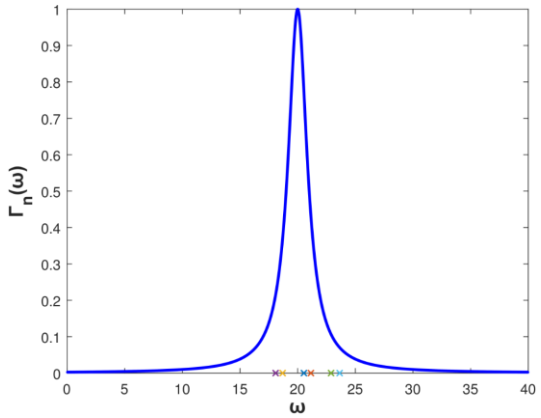

Figure 19- Homogeneous broadened gain curve, Case II, for $\overline{\gamma}_\perp = 1$.

The CF-eigenvalues, are depicted in the complex plane in fig. (20) for both cases mentioned above.

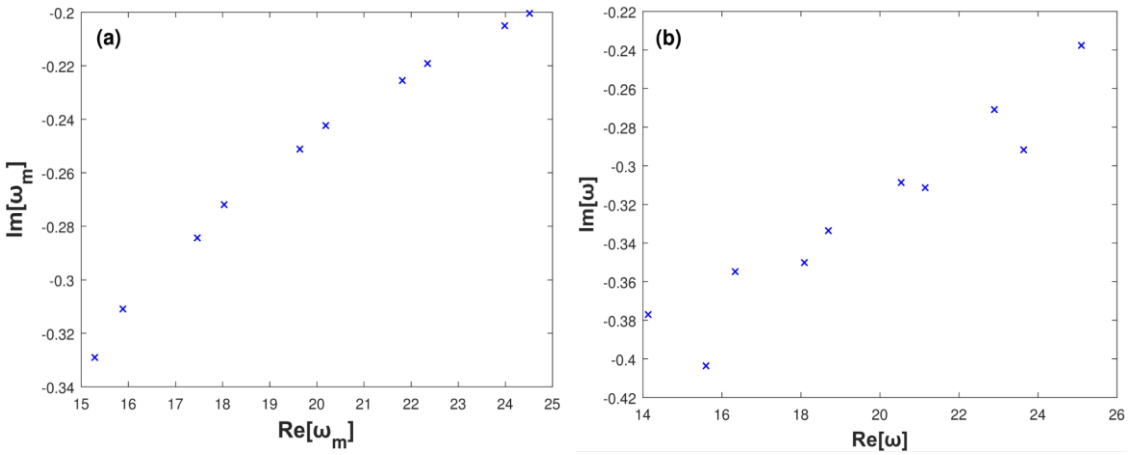

Figure 20- CF- eigenvalues in the complex plane for (a) Case I (b) Case II.

Tables 2, 3 show the first six CF-frequencies of the open resonator, which lases as well as their Q-factors for both cases I, II respectively, while in tables 4,5 are presented the corresponding linear lasing thresholds for the regimes of uniform and nonuniform pumps.

The quality factor (Q-factor) of a resonator is a measure of the outcoupling losses. Different cavity modes have different Q-factors, because each mode has its own relaxation rate. In this thesis we will adopt the definition as given in [34],

$$Q_m = \frac{Re\{\omega_m\}}{2Im\{\omega_m\}} \quad (\mathbf{5.2.1})$$

where ω_m are the frequencies of the open resonator, which are complex due to the outcoupling losses[2].

Table 2- CF- frequencies and the corresponding Q-factors for cavities at distance d/L=0.025

CF-frequencies	d/L=0.025	Q_m
1	20.188-0.242i	41.649
2	19.639-0.251i	39.094
3	21.814- 0.225i	48.366
4	18.033-0.272i	33.159
5	22.349-0.219i	50.992
6	17.463-0.284i	30.707

Table 3 - CF- frequencies and the corresponding Q-factors for cavities at distance d/L=0.1

CF-frequencies	d/L=0.1	Q_m
1	20.537-0.309i	33.270
2	21.145-0.311i	33.959
3	18.694-0.334i	28.0195
4	18.088-0.350i	25.829
5	22.896-0.271i	42.262
6	23.638-0.292i	40.518

Table 4- Linear lasing thresholds for the regimes of uniform and non-uniform applied pump for the cases Ia and Ib.

CF-frequencies	Linear thresholds uniform pump $\overline{\gamma}_\perp = 1$	Linear thresholds non-uniform pump $\overline{\gamma}_\perp = 1$	Linear thresholds uniform pump $\overline{\gamma}_\perp = 10$	Linear thresholds non-uniform pump $\overline{\gamma}_\perp = 10$
1	0.225	0.456	0.219	0.444
2	0.245	-	0.230	0.495
3	0.665	0.884	0.216	0.368
4	0.845	-	0.253	0.443
5	-	-	0.210	-
6	-	-	0.275	-

[2] As one can see, the cavity's modes has very small Q-factors, as compared with the laser cavities presented in [35]. This approach was made intentionally, for computational reasons. High Q-cavities means that the radiation losses are small enough, so the system needs a long time to reach its steady state, which demands very long computational time. Nevertheless, system's behavior does not change.

Table 5 -Linear lasing thresholds for the regimes of uniform and non-uniform applied gain for the case II.

CF-frequencies	Linear thresholds uniform pump $\overline{\gamma}_{\perp} = 1$	Linear thresholds non-uniform pump $\overline{\gamma}_{\perp} = 1$
1	**0.357**	**0.550**
2	**0.629**	**-**
3	**0.510**	**0.880**
4	**-**	**-**
5	**-**	**-**
6	**-**	**-**

The spatial profiles of CF-modes are shown in fig. (21) for the case I and in fig. (22) for the case II.

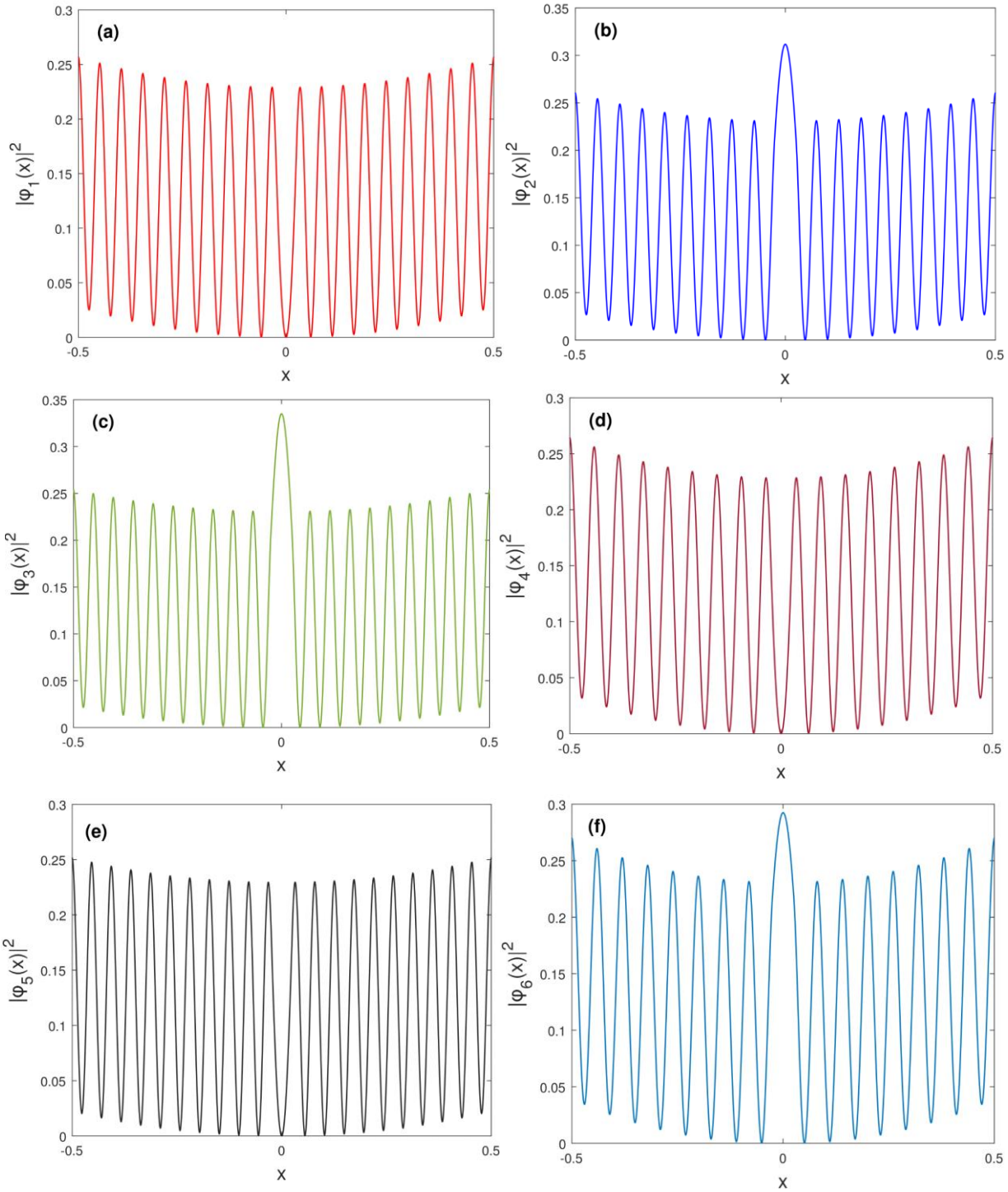

Figure 21- Spatial profiles of the first six open (CF) cavity modes (a), (b), (c), (d), (e), (f) respectively.

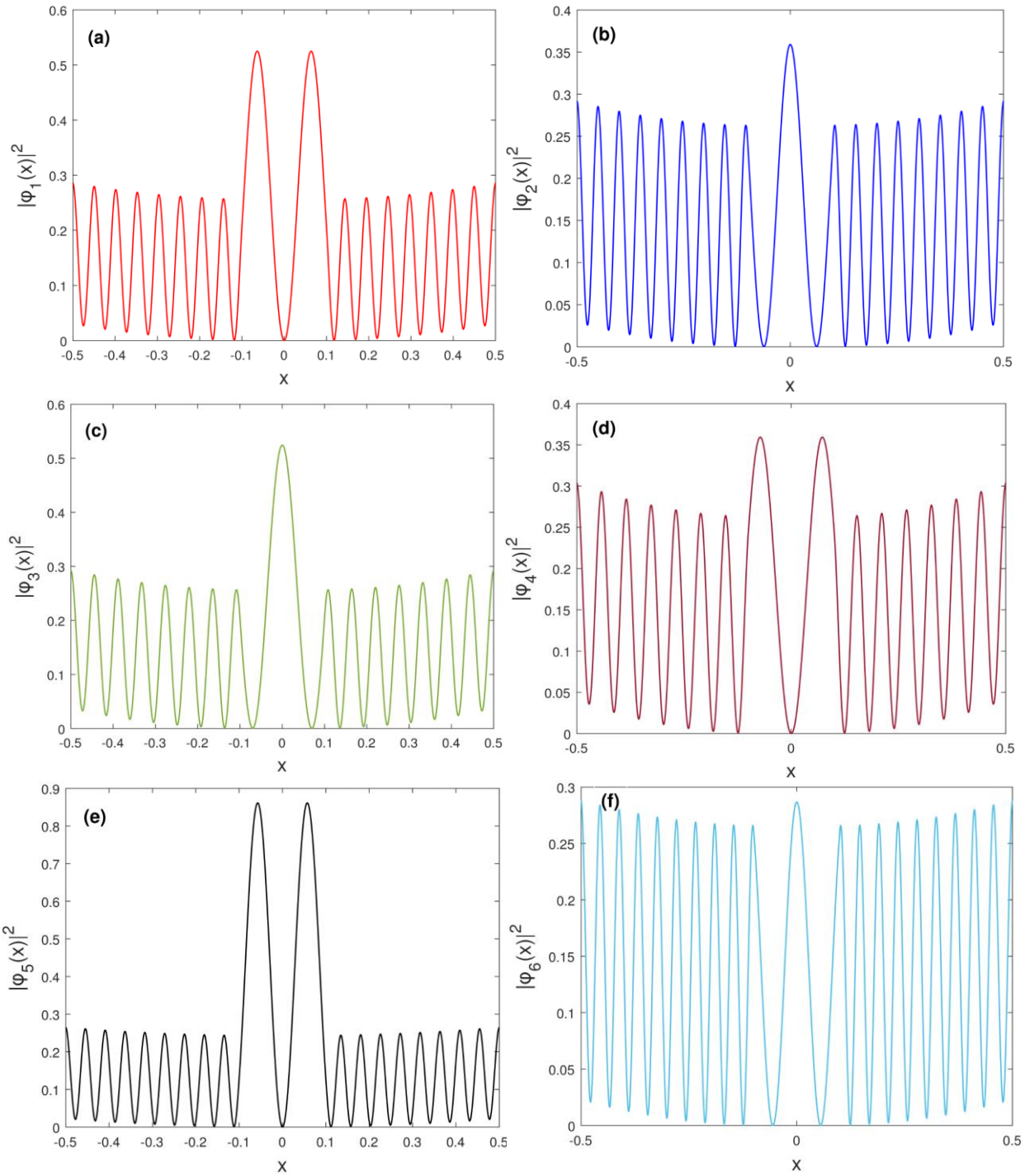

Figure 22- Spatial profiles of the first six open (CF) cavity modes (a), (b), (c), (d), (e), (f) respectively.

5.4- Expansion in the constant flux (CF) basis

In the last section of chapter 2, we referred to the basic equations that constitute the semiclassical laser theory. For consistency reasons we repeat them here,

$$\dot{E}_m = \frac{i}{2\bar{\omega}_0}[\bar{\omega}_a^2 - \bar{\omega}_m^2]E_m + \frac{i\bar{\omega}_a}{2}\sum_n B_{mn}\,P_n \qquad (\mathbf{5.4.1})$$

$$\dot{P}_m = -\bar{\gamma}_\perp P_m - i\bar{\gamma}_\perp \sum_n D_{mn} E_n \qquad (\mathbf{5.4.2})$$

$$\dot{D}_{mn} = \bar{\gamma}_\parallel \left[D_{0,mn} - D_{mn}\right] + \frac{i\bar{\gamma}_\parallel}{2} \sum_{r,q} \left[E_r P_q^* \tilde{A}_{mn,rq} - E_r^* P_q \tilde{A}'_{mn,rq} \right] \qquad (\mathbf{5.4.3})$$

with the only difference that we don't have the outcoupling loss terms anymore, because they are incorporated in the complex frequency $\bar{\omega}_m$. We extend the approach making in chapter 2, by expanding the electric field and the polarization, in terms of CF-states. As we refer in section 5.1, is in general good approximation to consider that $\varphi_m(x,k) \approx \varphi_m(x,\bar{\omega}_a)$. Therefore, we have the following:

$$\mathcal{E}^{(+)}(x,t) = \sum_m e_{m,0}(t) e^{-i\omega_a t} \varphi_m(x,\omega_a) \qquad (\mathbf{5.4.4})$$

$$\mathcal{P}^{(+)}(x,t) = \sum_m p_{m,0}(t) e^{-i\omega_a t} \varphi_m(x,\omega_a) \qquad (\mathbf{5.4.5})$$

as we suppose in the derivation made in chapter 2, before we make the normalization.

For the SALT analysis, we can make the more specific assumption [31] that the total electric field is a linear combination of the components of each individual mode, with the corresponding lasing frequencies arises from SALT analysis,

$$\mathcal{E}^{(+)}(x,t) = \sum_m \Psi_m(r) e^{-i\omega_m t} \qquad (\mathbf{5.4.6})$$

where $\Psi_m(r)$ are the modes arises by solving SALT equation (5.2.1) for a specific D_0, and $\bar{\omega}_m$ are the corresponding lasing frequencies. Then each lasing mode is expanded into a complete basis of CF states as shown in [31],

$$\Psi_m(r) = \sum_n a_n^{(\mu)} \varphi_n(x,\omega_a) \qquad (\mathbf{5.4.7})$$

By the substitution of (5.4.7) in (5.4.6) we take the total field as predicted from SALT and we equate this with the total electric field as we consider in our time domain analysis, (5.4.4). This way we obtain the correspondence between time domain solutions and SALT in normalized units,

$$E_m(t) = e^{i\bar{\omega}_a t} \sum_\mu a_n^{(\mu)} e^{-i\bar{\omega}_\mu t} \qquad (\mathbf{5.4.8})$$

where $\bar{\omega}_\mu$ are lasing frequencies. From (5.4.8) is clear that each lasing mode is in general a linear combination of all CF states, as it is verified from the results presented in chapter 6, mainly when the cavity is exposed in the nonuniform pump.

Chapter 6 – Two mode lasing in ridge cavities

The aim of this chapter is to understand the effect of inhomogeneous pump distribution, on the number of lasing frequencies which appear in the Fourier spectrum of the electric field, for a system of two coupled cavities at a distance **d/L=0.025**, as shown in fig. (14). We'll examine two different cases of the Lorentzian gain curve's width, the first one is for $\bar{\gamma}_{\perp} = \mathbf{1}$ **(case Ia)** while the second one is for $\bar{\gamma}_{\perp} = \mathbf{10}$ **(case Ib)**. Here we present the simulation results related to a two-mode laser in a system of two coupled cavities for two different regimes. The first one refers to the homogeneous pump in both cavities while the second one refers to the case of pumping only one cavity, as shown in fig. (23):

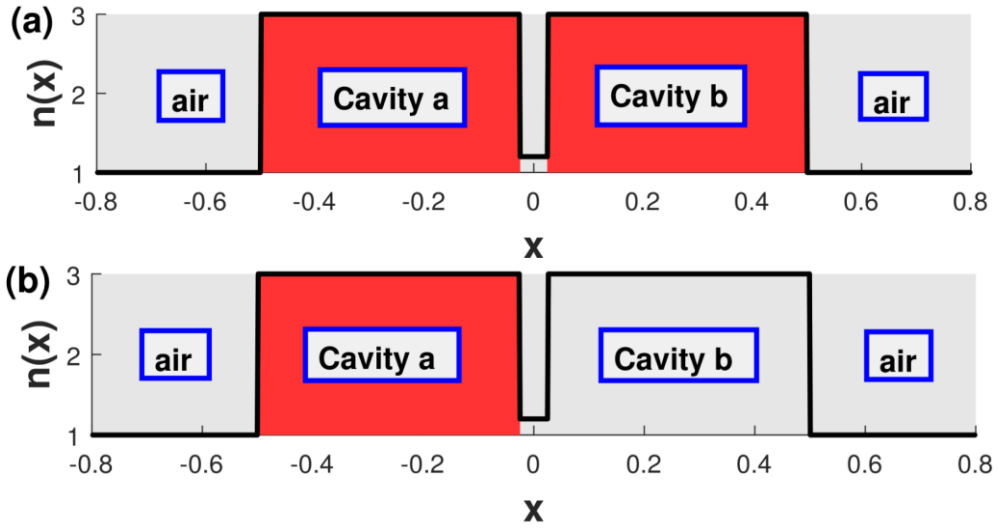

Figure 23- Two different pumping regimes: (a) Pump is applied uniformly (b) Pump is applied nonuniformly.

6.1- Two mode lasing (Case Ia)

The parameter values where used for the numerical solution of Maxwell-Bloch equations, are shown in table 6:

Table 6- Parameter values used in the numerical simulation

$\bar{\gamma}_{\perp}$	$\bar{\gamma}_{\parallel}$	$\bar{\omega}_a$	Cavities refractive index	Intracavity refractive index
1	10^{-3}	20	3+0.001i	1.2

From the linear SALT analysis described in section 5.2, for the case of uniform and non-uniform pump distribution in both cavities, arises the modes with the lowest linear lasing threshold. Their corresponding spatial profile of these modes are shown in fig. (21. a,b).

6.1-1. Uniform pump

When gain is applied uniformly in both cavities, the first two CF-states which lase are these with open cavity frequencies, $\boldsymbol{\omega_1 = 20.188 - 0.242i}$ and $\boldsymbol{\omega_2 = 19.639 - 0.251i}$, as shown in section 5.3. The time dynamics of the square magnitude of electric field coefficients, the induced polarization coefficients and the inversion matrix coefficients for the pump value $D_0 = 0.337$, as arises from the numerical solution of the Maxwell-Bloch equations are shown in fig. (24):

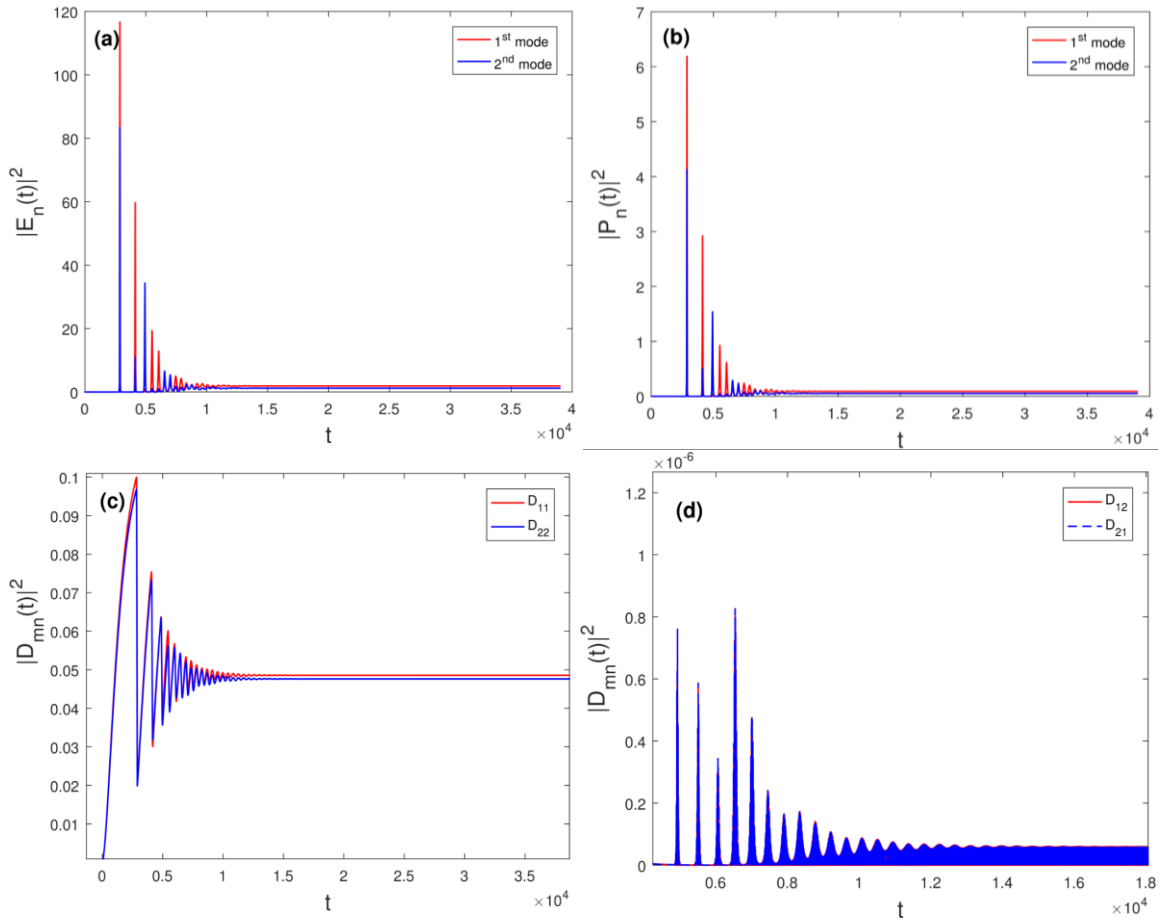

Figure 24- Time dynamics of the square magnitude, of electric field coefficients in (a), of induced polarization coefficients in (b), of the diagonal inversion coefficients in (c) and of the off-diagonal inversion coefficients in (d). The applied pump value is D_0=0.337.

In fig. (25) it's shown the Fourier spectra[3] for pump values $D_0 = 0.233$ in (a) and $D_0 = 0.337$ in (b), while in fig. (26) are presented the intensity of each coefficient of the electric field and the corresponding lasing frequencies for different pump values:

[3] The width of the Fourier spectra has numerical origin and is related to the time window which we choose, in order to truncate the oscillating electric field coefficients in time, as a result it doesn't have a physical origin. As we mention, in chapter 1, we can't make a linewidth computation with semiclassical laser theory if we don't introduce the quantum noise.

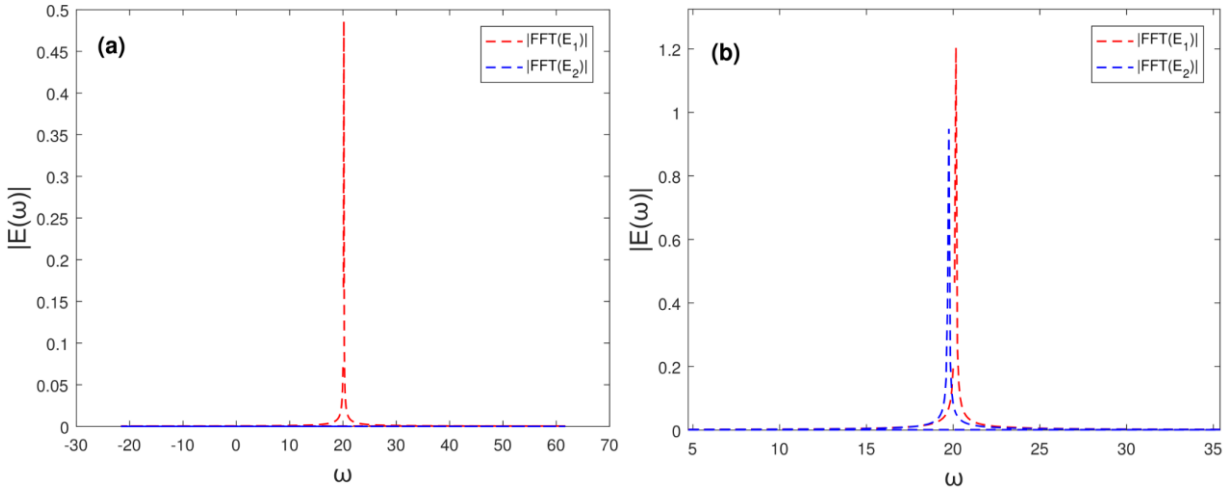

Figure 25- Fourier spectra of the electric field coefficients for $D_0 = 0.233$ in (a) and for $D_0 = 0.337$ in (b).

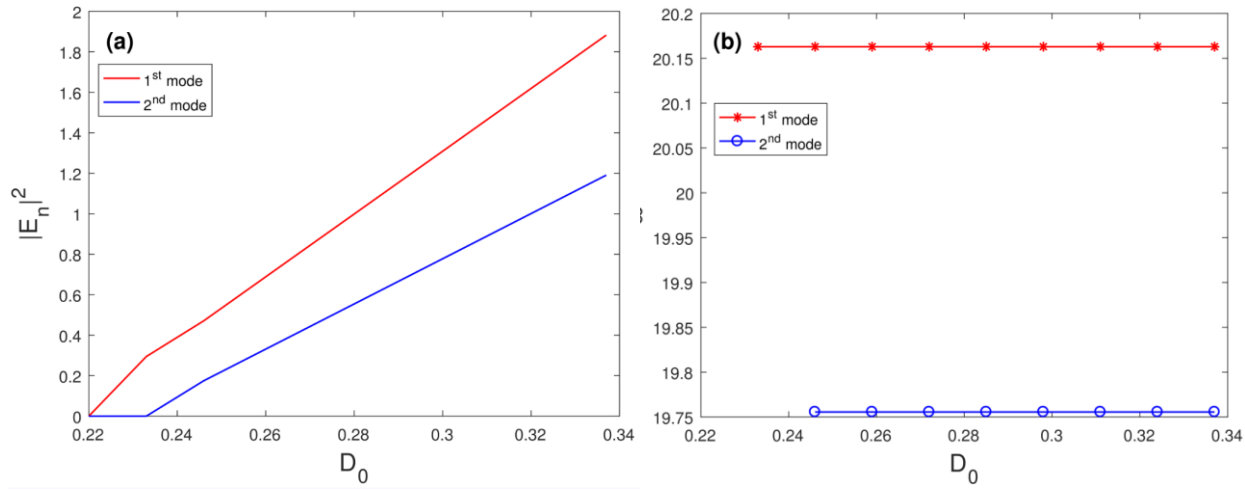

Figure 26- (a) Square magnitude of the electric field coefficients as a function of the applied gain (b) Lasing frequencies as a function of the applied gain.

As one can see from fig. (26), this laser system operates in a single frequency domain, only in the small pump interval $\boldsymbol{D_0 = [0.220, 0.233]}$, where the single laser frequency corresponds to the first CF-state. The increase of the pump value in both cavities up to the value $\boldsymbol{D_2^{(th)} = 0.233}$ (which is the second mode's threshold) gives rise to the appearance of one additional lasing frequency, which corresponds, to the second CF-state which we consider.

6.1-2. Non-uniform pump

When the system of the two coupled cavities operates in a PT-like phase, i.e. when gain is applied only to one cavity, we expect the existence of a single frequency phase, for a pump interval larger than the corresponding one, for the case of uniform pumping. The numerical solution of Maxwell-Bloch equations for the non-uniform pumping regime, gives the time dynamics of system's observables as shown in fig. (27) for the pump value $D_0 = 0.543$. The two CF-states, which considered in this regime, are the first two (which are referred in section 5.3), as we also used in the regime of uniform pumping (section 6.1.1).

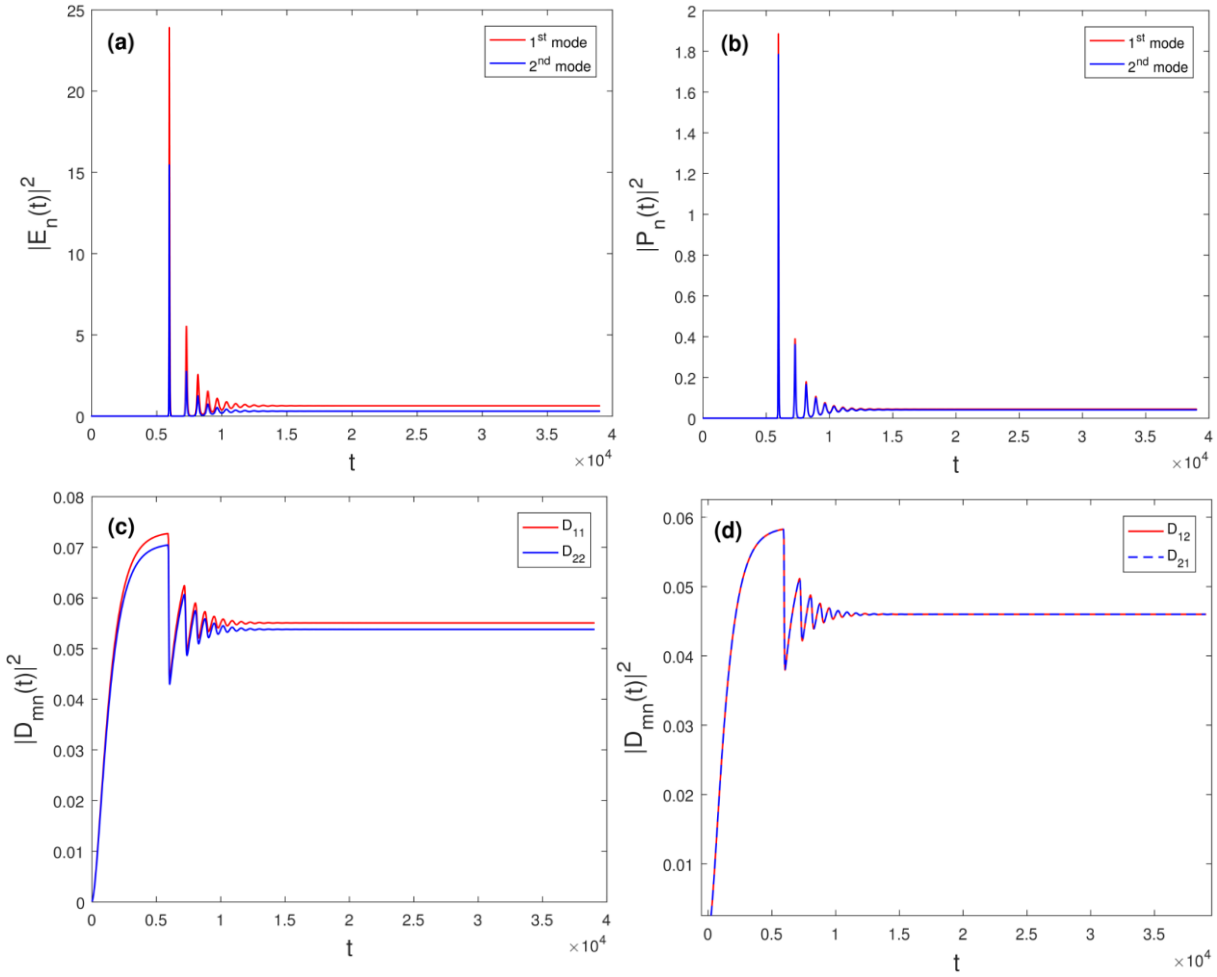

Figure 27- Time dynamics of the square magnitude, of electric field coefficients in (a), of induced polarization coefficients in (b), of the diagonal inversion coefficients in (c) and of the off-diagonal inversion coefficients in (d). The applied pump value in one cavity is $D_0 = 0.543$.

Modal intensities as well as the lasing frequencies for several pump values, in one cavity are shown in fig. (28). As one can see we observe the presence of two distinct curves (Modal intensity vs Pump) with the same lasing threshold, $\boldsymbol{D_{1,2}^{(th)} = 0.478}$ and with the same lasing frequency, $\bar{\omega} = \bar{\omega}_{\alpha} = 20$ (fig. (28.b)) for each pump value.

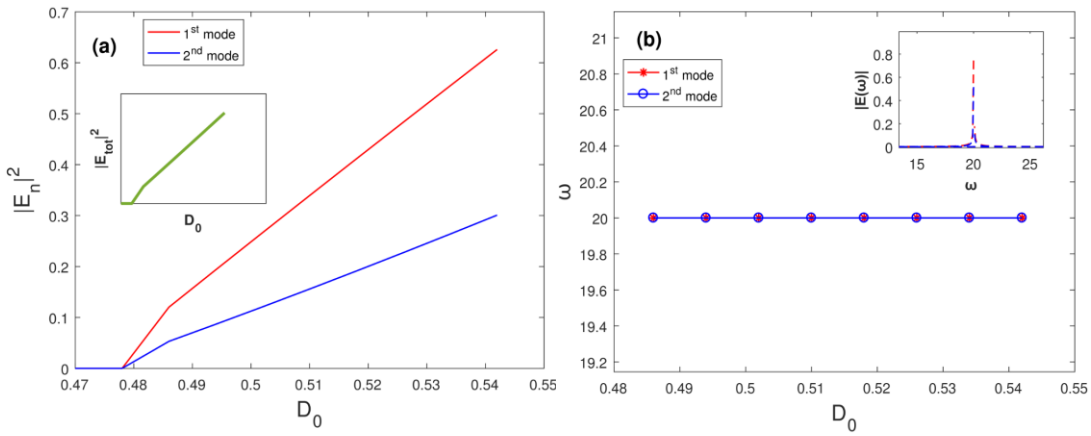

Figure 28- (a) Square magnitude of electric field coefficients as a function of the applied gain in one cavity. In the inset is shown the total intensity of both modes. (b) Lasing frequency as function of the applied gain. In the inset is shown the Fourier spectrum of both modes for the pump value $D_0 = 0.543$.

In the inset of fig. (28.a) is depicted the total intensity which corresponds to the dominant lasing frequency. Total intensity is calculated, as $|E_{tot}|^2 = |E_1 + E_2|^2$, while in the inset of fig. (28.b) is shown the Fourier spectrum for the pump value, $\mathrm{D}_0 = 0.543$.

6.2- Two mode lasing (Case Ib)

The results presented below, are obtained by solving numerically the Maxwell-Bloch equations with the parameters shown in table 7.

Table 7- Parameter values used in the numerical simulation.

$\bar{\gamma}_\perp$	$\bar{\gamma}_\parallel$	$\bar{\omega}_a$	Cavities refractive index	Intracavity refractive index
10	10^{-3}	20	3+0.001i	1.2

From the linear SALT analysis described in section 5.2, for the case of homogeneous pump in both cavities, arises that the modes with the lowest threshold are they with CF frequencies, $\boldsymbol{\omega_2 \cong 19.639 - 0.251i}$ and $\boldsymbol{\omega_3 \cong 21.814 - 0.225i}$ while for the case of non-uniform pump the first lasing modes are they with CF-frequencies: $\boldsymbol{\omega_3 \cong 21.814 - 0.225i}$ and $\boldsymbol{\omega_5 \cong 22.349 - 0.219i}$.

6.2-1 Uniform pumping

As a first step of our analysis we study the time dynamics for the system's observables, as depicted in fig. (29) for pump value D_0=0.236 in both cavities (regime of the fig. (23.a)):

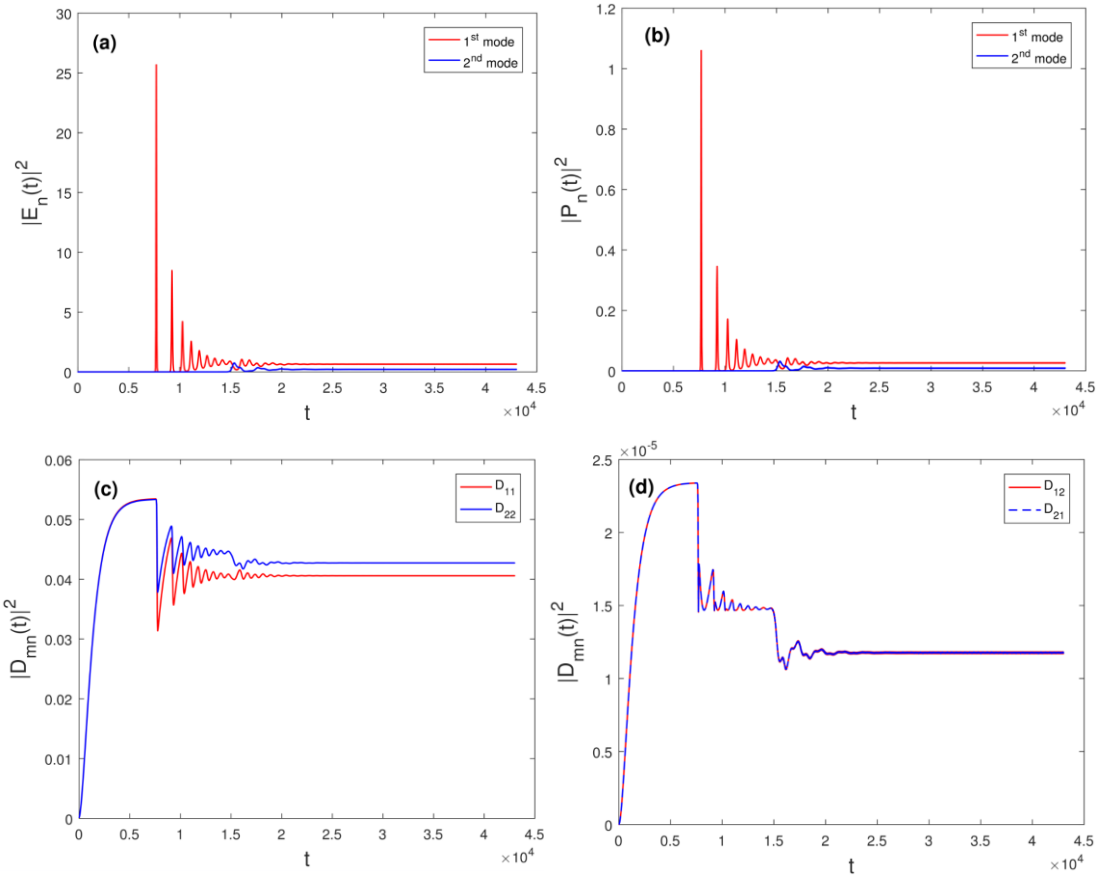

Figure 29- Time dynamics of the square magnitude, of electric field coefficients in (a), of induced polarization coefficients in (b), of the diagonal inversion coefficients in (c) and of the off-diagonal inversion coefficients in (d). The applied pump value in both cavities is D_0=0.236.

The time dynamics of the observables depicted on the above figures, reach a steady state after a long time. For different pump values, we obtain the numerical solution of MB equations and we get the steady state values of modal intensities and the corresponding lasing frequencies, as a function of the applied gain in both cavities, as shown in fig. (30). It is important to note that the slope changes, which are observed in fig. (30. a), are due to the fact that we get the mean values for the magnitude of the electric field coefficients because due to the parameter we use they don't reach a steady state but they make small oscillations.

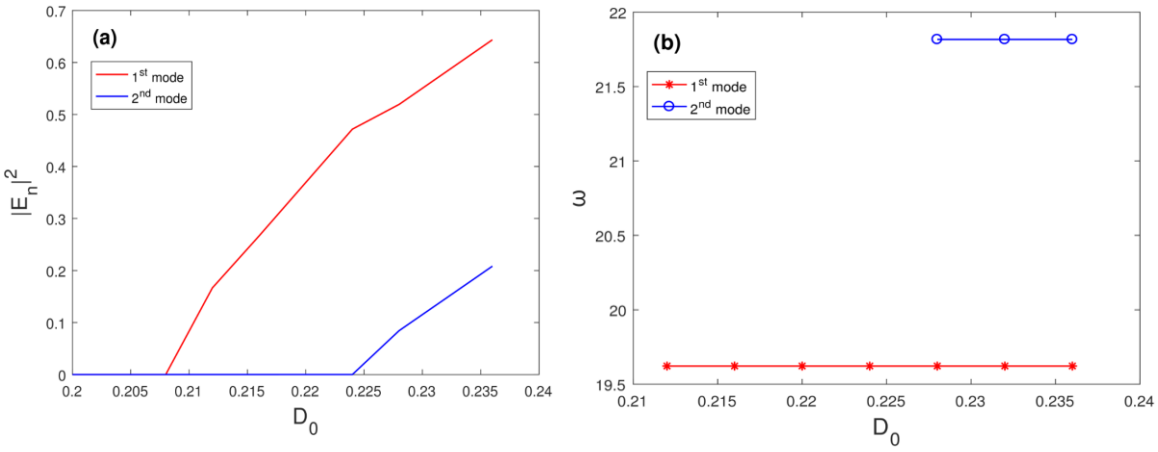

Figure 30- (a) Characteristic curves of the square magnitude of the electric field coefficients and (b) modal frequencies as a function of the applied gain to both cavities

In the regime, of homogeneous pump in both cavities, the system operates in a single frequency regime for pump values in the interval, $\mathbf{D_0 \in [0.208, 0.224]}$, i.e. when the applied gain is between the two lasing thresholds. For pump values smaller than D_0 =0.224, the observed lasing frequency is $\bar{\omega}_2 = \mathbf{19.620}$ (second CF-state). The increase of the pump up to the value $D_3^{(th)} = 0.224$ (lasing threshold for the third CF-state), leads to the appearance of the second lasing mode, with its lasing frequency to be, $\bar{\omega}_3 = \mathbf{21.81}$ (third CF-state).

On fig. (31) we can see the Fourier spectra of the electric field coefficients for the pump values D_0=0.216 in (a) and for D_0=0.236 in (b). The presence of two distinct frequencies is observed in the Fourier spectrum when the applied gain is greater of both lasing thresholds. Each peak corresponds to the respective CF-state. One additional result which comes from fig. (31) is that no mixing of CF states occurs in the corresponding electric fields when we pump uniformly the system of two cavities[4].

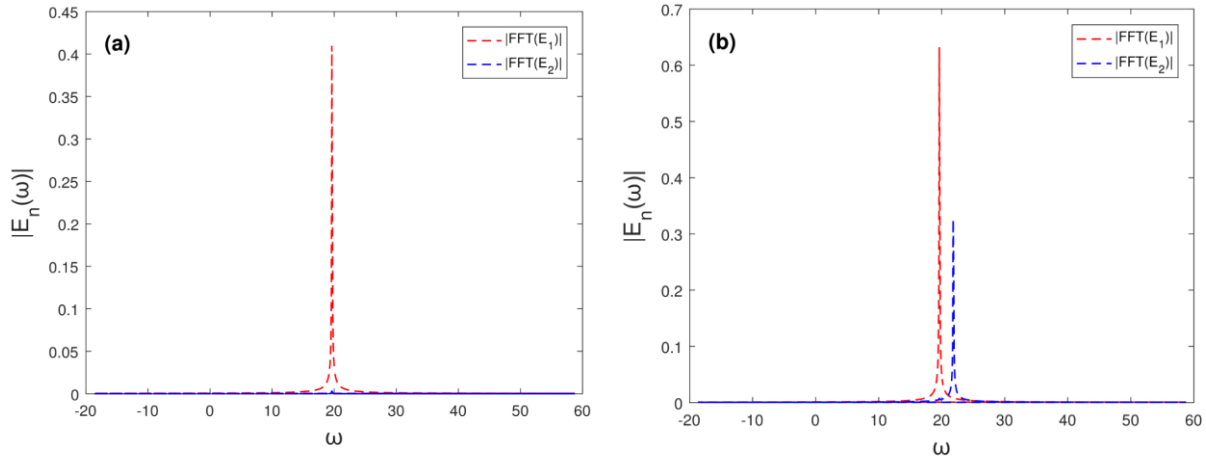

Figure 31- Fourier spectrum of the electric field coefficients, for: (a) D_0=0.216 and for (b) D_0=0.236.

[4] One should not be create the impression that CF-states mixing is only associated with the heterogeneous pump distribution, in the cavities. Each mode is in general a superposition of CF states independently of the pump distribution.

6.2-2 Non-uniform pump

If we apply gain only to cavity a while the cavity b remains unpumped (regime of the fig. (23. B)) the system operates in a PT-like phase. For the pump value D_0=0.395, we obtain the time dynamics, as depicted in fig. (32), as well as the square magnitude of the electric field coefficients and the corresponding lasing frequencies for several pump values in fig (33).

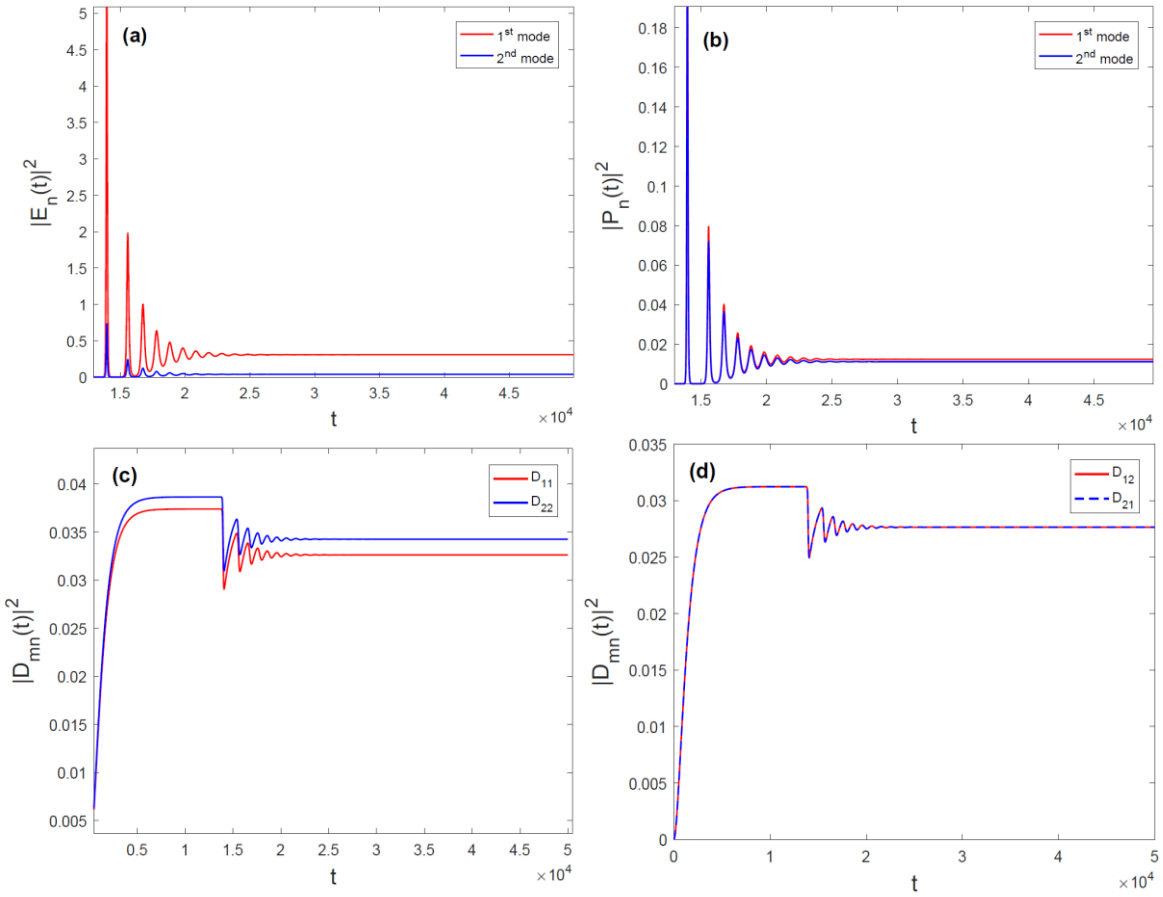

Figure 32- Time dynamics of modal intensities in (a) of induced polarizations due to modal fields in (b) of time dynamics of diagonal matrix elements of the inversion in (c) and the off-diagonal inversion elements in (d). The applied gain in one cavity is D_0=0.395.

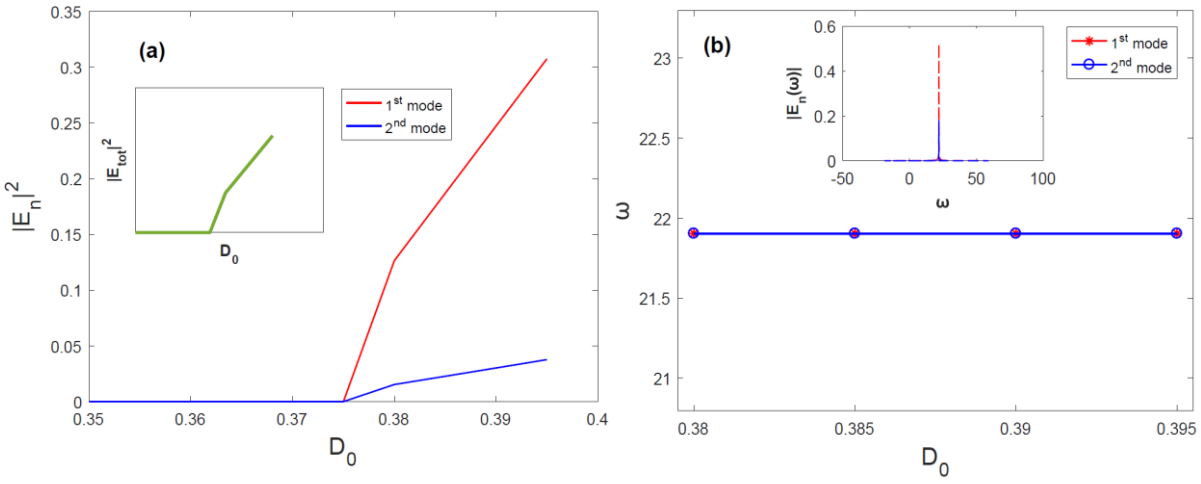

Figure 33- (a) Square magnitude of the electric field coefficients as a function of the applied gain in one cavity. In the inset is shown the total intensity of the lasing CF-state. (b) Lasing frequencies as a function of the applied gain in one cavity, in the inset is shown the Fourier spectrum for D_0=0.395, and its shown the presence of a single frequency.

As described in fig. (33), the laser system exhibits single frequency operation for the values of the applied gain in one cavity, we consider in our simulation. In the inset of the fig. (33.a) is shown the total intensity which is calculated as $|E_{tot}|^2 = |E_3 + E_5|^2$, with E_3, E_5 to be the electric field coefficients which corresponds to the third and the fifth CF-states respectively while in the inset of fig. (33. b) is shown the Fourier spectrum for the pump value, $\mathrm{D}_0 = 0.395$. The observed lasing frequency in the phase of single frequency operation is $\boldsymbol{\bar{\omega}_3 = 21.904}$, which corresponds to the third CF-state.

Chapter 7 -Four-mode lasing in ridge cavities

In this section, we consider the same system as before, but we take into account four CF-states (instead of two in the previous chapter). The selection of these four modes among all others, based on the linear SALT analysis, as it was presented in chapter 5. Similar to the analysis of chapter 6, the simulations of this system were based on Maxwell- Bloch equations.

Regarding the distribution of the gain in these cavities, we'll examine both cases represented in fig. (34) as also me make in the chapter above. The first case deals with, the pumping of both cavities while the second one, refers to the regime of pumping only one of them.

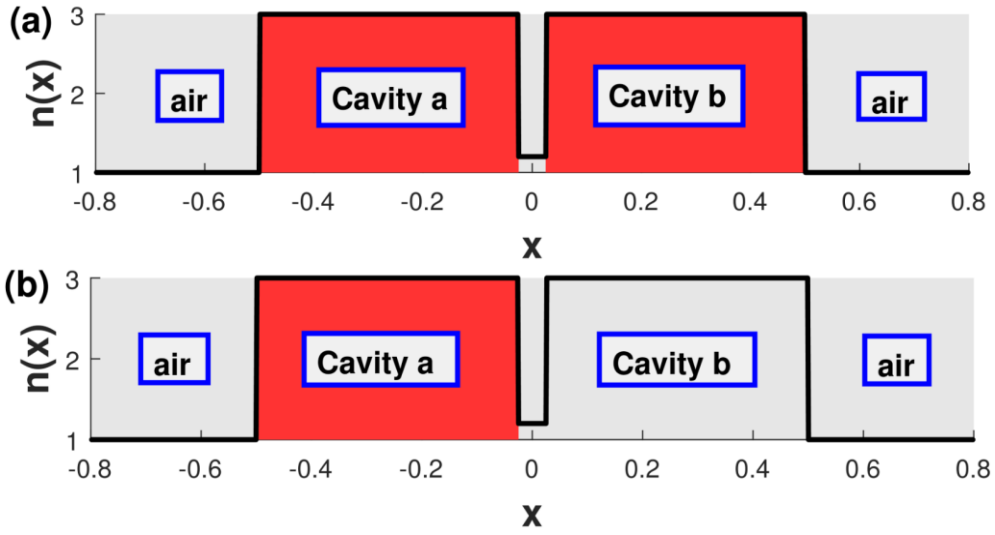

Figure 34- Pump distribution in the two cavities. The pumped regions are shown with red color. (a) Pump both cavities, (b) Pump only cavity a.

The parameters, we use in our simulation are as depicted in tables 6,7 on the above chapter.

7.1- Four-mode lasing (Case Ia)

The frequencies of the first four modes corresponds to the first four CF-states, as they calculated from the finite difference solver, with CF-boundary conditions are shown in table 2.

7.1-1 Uniform pump distribution

In fig. (35), we can see the temporal behavior of the square magnitude of electric field coefficients, the polarization coefficients and the diagonal inversion matrix elements, for the regime of pumping homogeneously both cavities (fig. 34. a) with pump value D_0=0.490. As we can see, after a long time, all the observables reach a steady state.

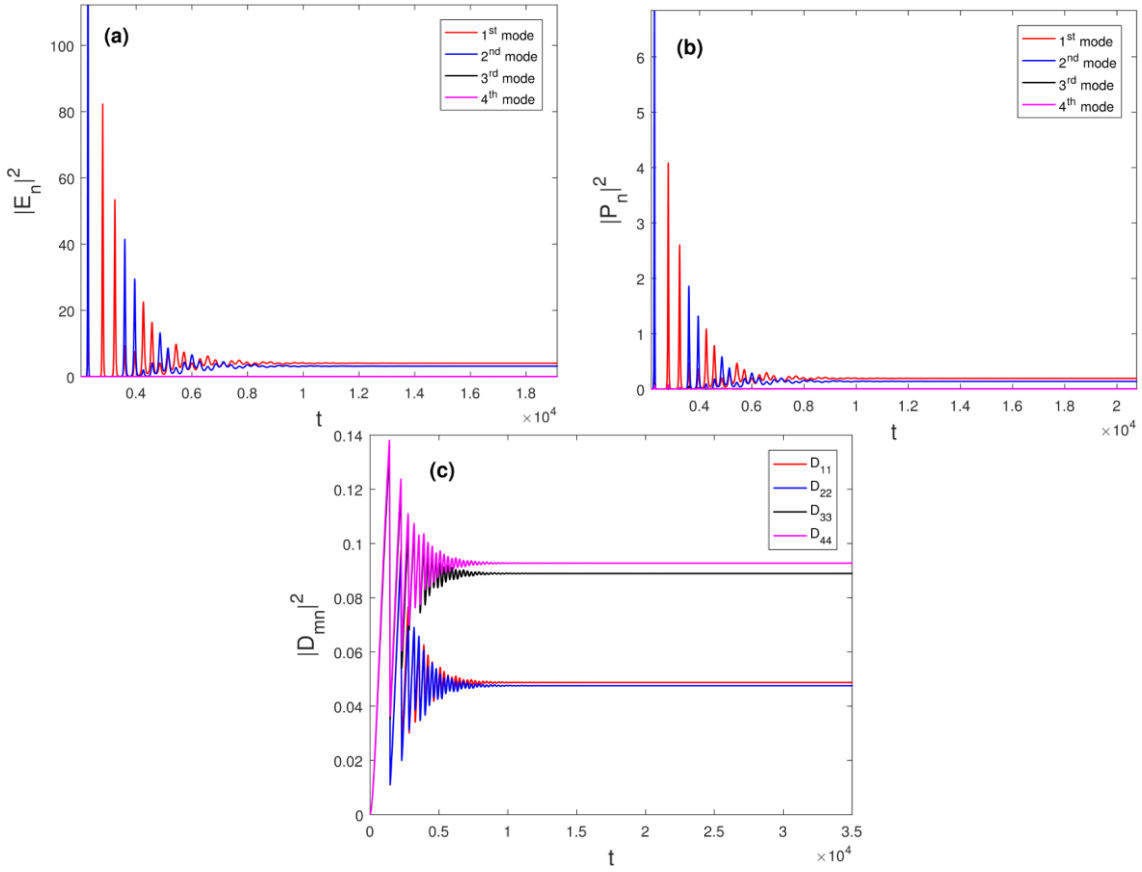

Figure 35- Time dynamics of the square magnitude of the electric field coefficients in (a) of the induced polarizations in (b) and for the diagonal inversion density elements. The applied pump value in both cavities in D_0=0.491.

The Fourier spectra of the electric field coefficients for D_0=0.236 and for D_0=0.491 are shown in fig. (36). For the first pump value, we observe the presence of only one frequency, while this pump value is lower than the second lasing threshold. For the second pump value which is higher of both thresholds pump values, in the Fourier spectrum there exist two distinct frequencies.

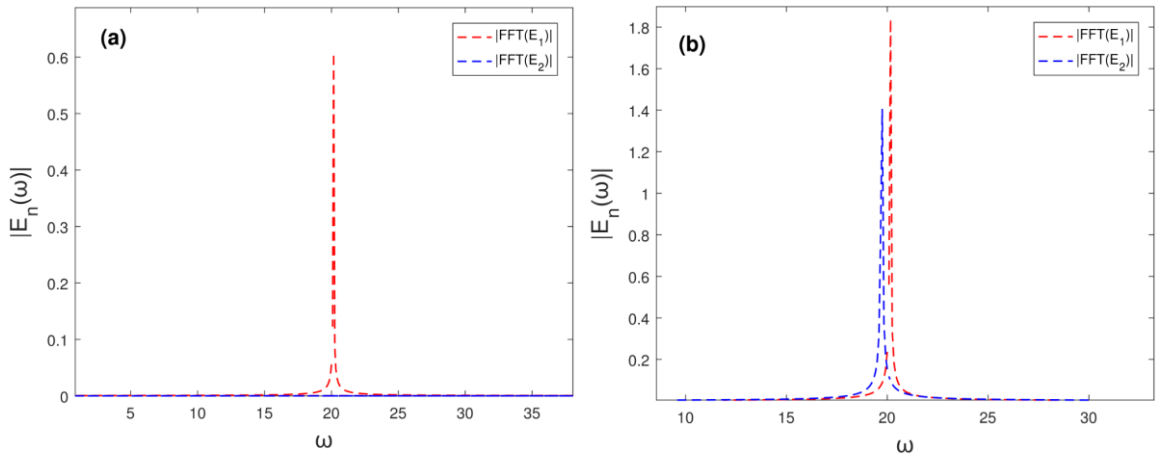

Figure 36- Fourier spectrum of the electric field coefficients, for D_0=0.236 in (a) and for D_0=0.491 in (b).

The square magnitude of the electric field coefficients and the corresponding lasing frequencies for several pump values are presented in fig. (37). With dashed lines in the inset of fig. (37. a), are depicted

the square magnitude of the electric field coefficients for the modes we consider in chapter 6, when we examine the two-mode lasing, for the same gain curve. Furthermore, for the pump interval we consider only two modes lase.

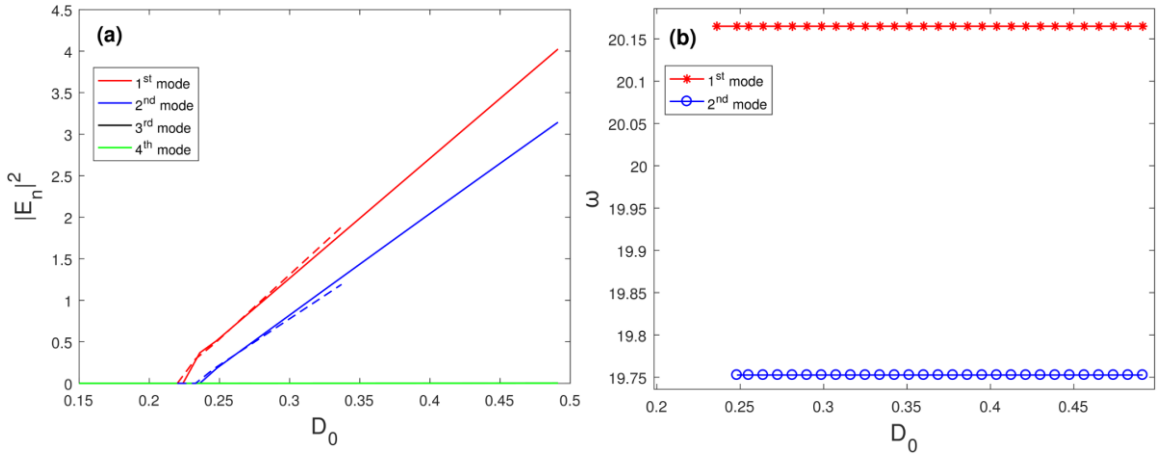

Figure 37- Square magnitude of the electric field coefficients as a function of the applied gain in (a) and lasing frequencies as a function of the applied gain in (b). In (a) the dashed lines are the results obtained for two-mode lasing.

The single frequency operation is observed in the pump interval, $\boldsymbol{D_0 = [0.220, 0.233]}$, i.e. between the two lasing thresholds.

7.1-2 Non-uniform pump

For the case of the non-uniform pump distribution in the cavities system we make the same analysis as before. The temporal behavior of system's observables for $\boldsymbol{D_0 = 0.691}$ is shown in fig. (38):

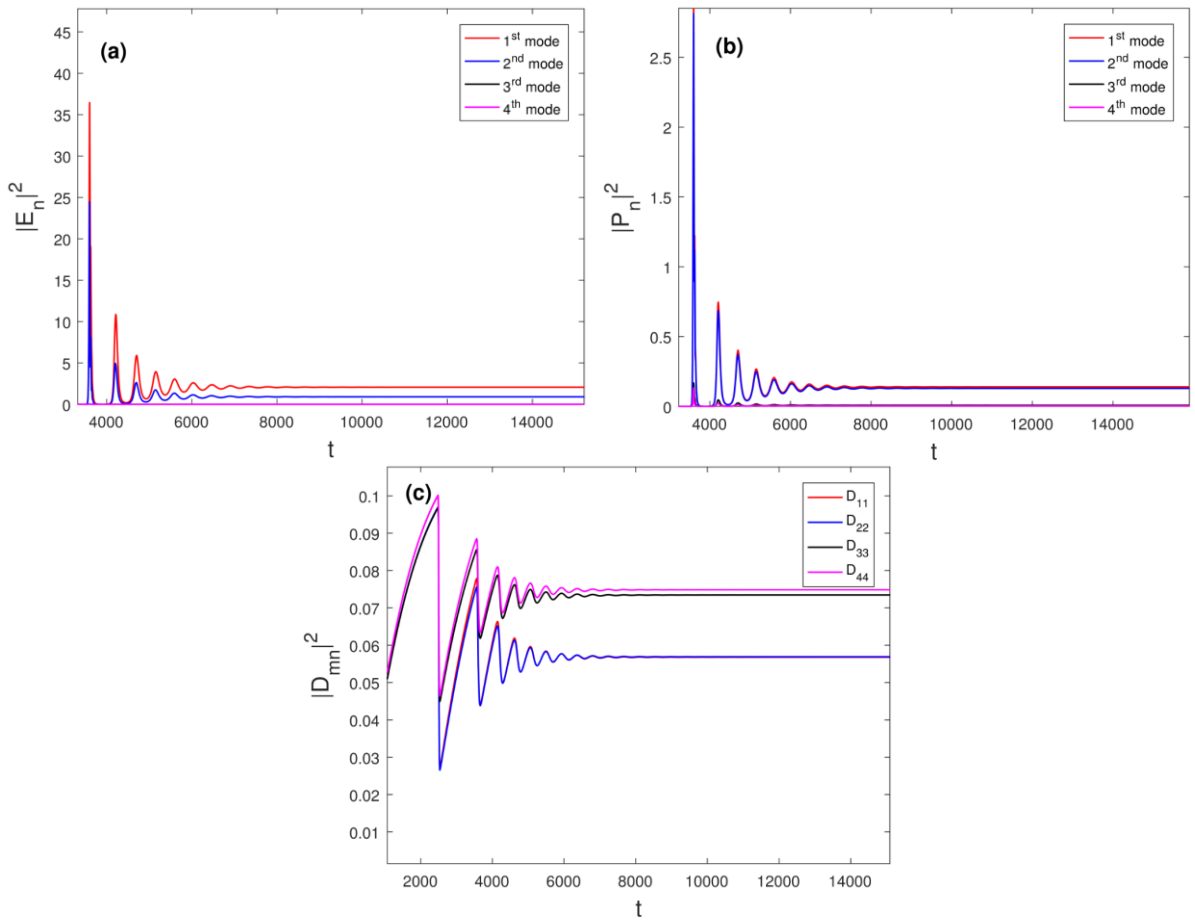

Figure 38- Time dynamics of (a) the square magnitude of the electric field coefficients (b) Polarization coefficients (c) Diagonal matrix elements of the inversion. The simulation which give us these plots, became for D_0=0.691.

The square magnitude of the electric field coefficients and the corresponding lasing frequencies as a function of the applied gain are shown in fig. (39). Furthermore, in the inset of fig. (39.a) is shown the total intensity in the dominant lasing frequency, $\bar{\omega} = \bar{\omega}_{\alpha} = \mathbf{20}$, which is defined as: $|E_{tot}|^2 = |E_1 + E_2|^2$, with E_1, E_2 to be the electric field coefficients which corresponds to the first and the second CF-state respectively. The lasing frequency in the single frequency phase as calculated for the cases of two and four-mode lasing is absolutely the same. In the inset of fig. (39. b) is shown the Fourier spectrum of the electric field coefficients for the applied pump value, D_0=0.691 in the one cavity.

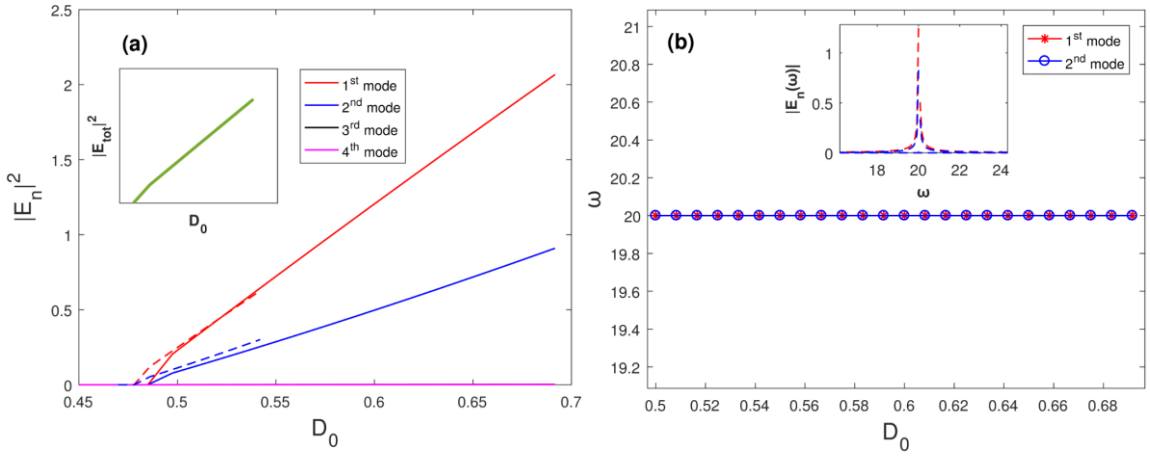

Figure 39- (a) Square magnitude of the electric field coefficients as a function of the applied gain. In the inset is shown the total intensity in the dominant lasing frequency. (b) Modes frequency as a function of the applied gain, for the regime of non-uniform pumping. In the inset is shown the Fourier spectrum of modal fields for the pump value D_0=0.691. In (a) the dashed lines are the results obtained for two-mode lasing.

Similar to the two-mode lasing describing in the section 6.1.2, only the first CF-state contributes to the mode's profile, while both modal fields are expressed as a function only for this CF-state. More specifically, for the pump value D_0=0.691, the mode's profile (fig. 40) is defined from the expression:

$$\Psi_1(x) = \sum_n a_n^{(\mu)} \varphi_n(x, \bar{\omega}_a) = a_1^{(1)}\varphi_1(x, \bar{\omega}_a) + a_2^{(1)}\varphi_2(x, \bar{\omega}_a) + a_3^{(1)}\varphi_3(x, \bar{\omega}_a) + a_4^{(1)}\varphi_4(x, \bar{\omega}_a)$$

with the expansion coefficients are given from the Fourier spectra of the electric field coefficients.

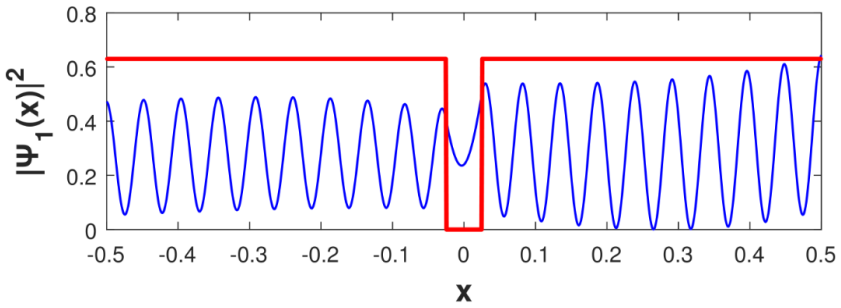

Figure 40- Lasing mode's profile for D_0=0.691, with blue, while with red are represented the two cavities.

We can calculate the intensity of the lasing mode in each cavity as, $I_{a,b}^{(\mu)} = \int |\Psi_\mu(x)|^2 dx \,/ L_{cav}$, where the integral is calculated in each cavity of length L_{cav}, the index μ refers to the lasing mode and the indices a,b are mentioned to the active and the passive cavity respectively. For the specific pump value referred above, we get that, $I_a^{(1)} = 0.278$ and $I_b^{(1)} = 0.295$, therefore the intensity ratio $I_a^{(1)}/I_b^{(1)} = 0.942$. The fact that the intensity ratio is very close to unity verifies that the system lases in the PT-phase, so in both cavities we have approximately the same intensity. This result corresponds to the lasing in the PT- phase as examined in chapter 4 for the two ring coupled cavities.

7.2- Lorentzian gain curve with (Case Ib)

We'll follow the same procedure, with that of the previous section, with the frequencies of the first four CF- modes presented in table 2.

7.2-1. Uniform pump

When the cavities are pumped uniformly, as shown in fig. (34. a), the time dynamics of system's observables, for the applied pump D_0=0.360 is depicted in fig. (41):

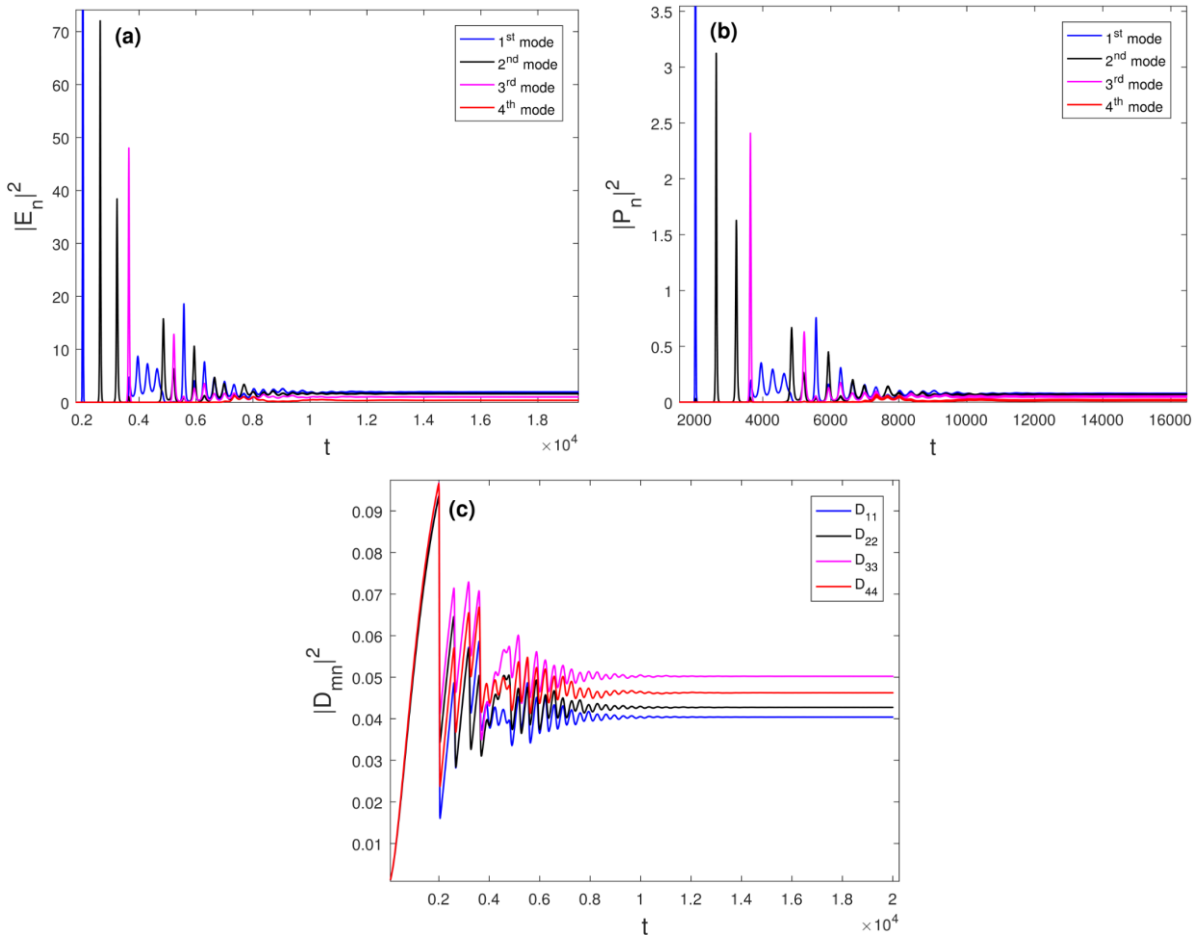

Figure 41- Time dynamics of the (a) square magnitude of the electric field coefficients (b) induced polarization coefficients and (c) diagonal inversion elements. The applied pump value in bot cavities is D_0=0.360.

For several pump values, in fig. (43) are presented the square magnitude of the electric field coefficients as well as the corresponding lasing frequencies. In fig. (43. a) it is clear the very good agreement between the modal intensities of the first two modes as they calculated for the cases of two-mode lasing and the four-mode lasing. This shows the method's consistency and convergence. In addition, in fig. (42) are presented the Fourier spectra for four different pump values:

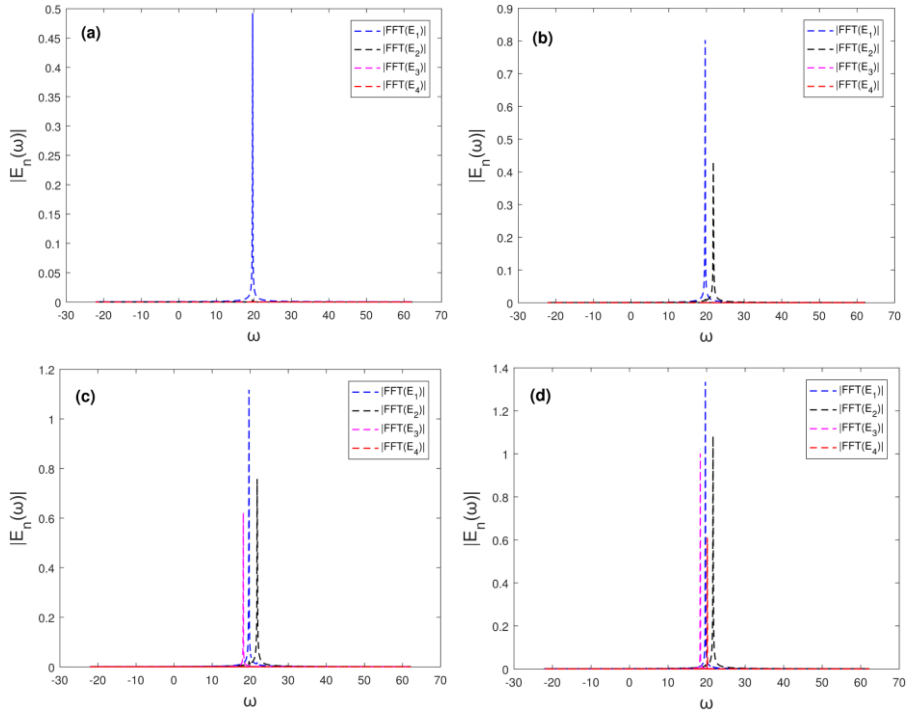

Figure 42-Fourier spectra of the electric field coefficients for (a) D_0=0.217 (b) D_0=0.243 (c) D_0=0.243 (d) D_0=0.360.

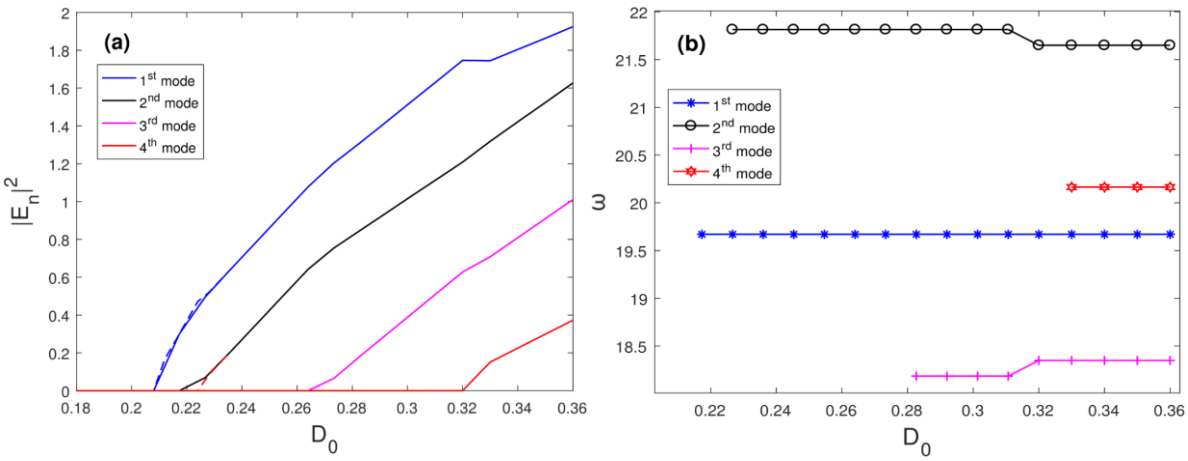

Figure 43- (a) Square magnitude of the electric field coefficients as a function of the applied gain in both cavities. With dashed lines are shown the intensities of the first two modes, as they calculated for the case of two-mode lasing. (b) Lasing frequencies as a function of the applied gain. In (a) the dashed lines are the results obtained for two-mode lasing.

We refer the 1st, the 2nd, the 3rd and the 4th modes regarding to the order in which they lase and they corresponds to the 2nd, the 3rd, the 4th and the 1st CF-states respectively. In this pumping regime, single frequency operation is observed, only in a small pump interval: $\mathbf{D_0} \in$ **[0.208, 0.217]**, with the lasing frequency to be, $\bar{\omega}_2 = 19.621$, which corresponds to the second CF-state of the open resonator. Further increase in the pump value gives rise to the appearance of additional lasing frequencies. Just after the second lasing threshold $D_3^{(th)} = 0.217$, the second lasing frequency is appeared, $\bar{\omega}_3 = 21.814$, which correspond to the third CF-state. When the applied pump reaches the third lasing threshold, $D_4^{(th)} = 0.264$, appears the third lasing frequency, $\bar{\omega}_4 = 18.185$ which corresponds to the forth CF-state. Finally, when the pump value takes values greater than the fourth lasing threshold,

$D_1^{(th)} = 0.320$ appears the fourth lasing frequency, $\bar{\omega}_1 = 20.165$ which corresponds to the first CF-state.

7.2-2. Non-uniform pump

When pump is applied on only one cavity, we obtain the time dynamics of square magnitude of the electric field coefficients, the polarization coefficients and the diagonal inversion elements for D_0=0.487, as shown in fig. (44):

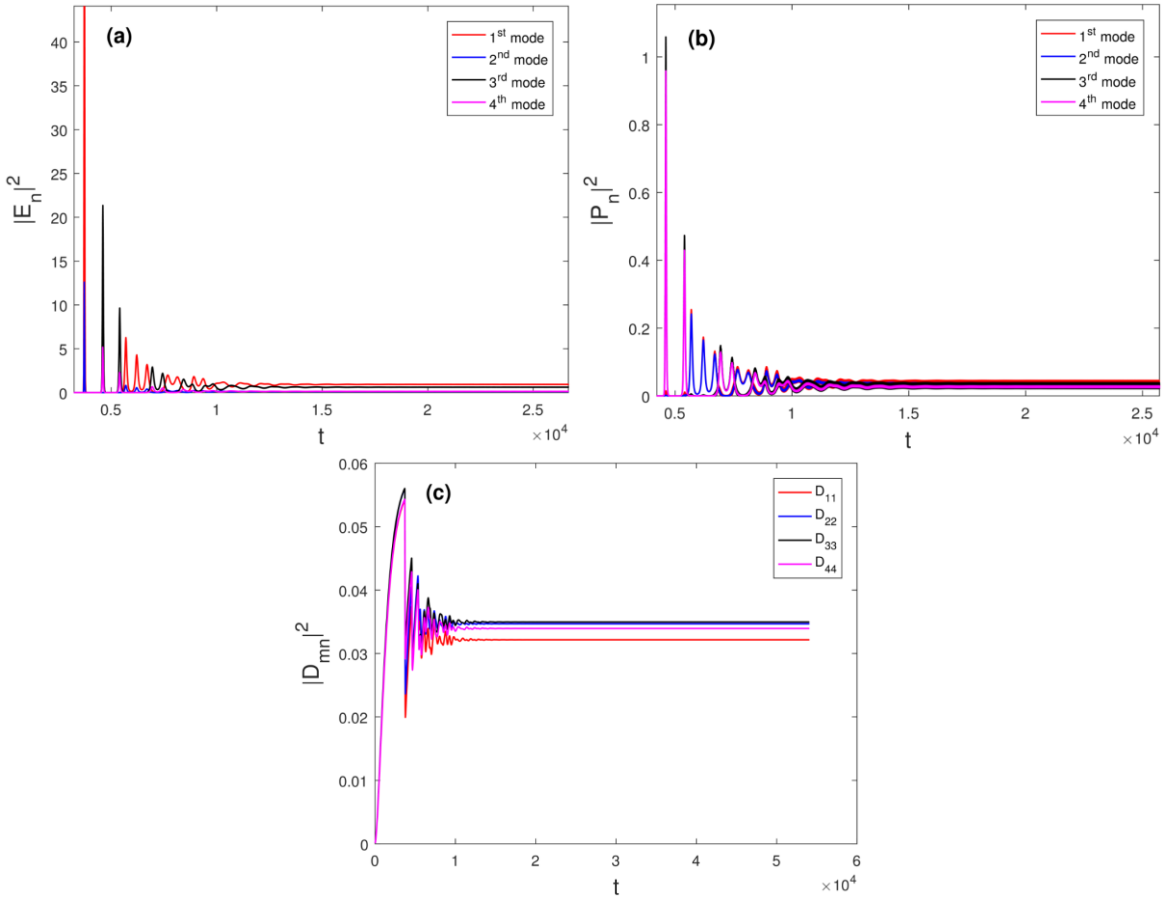

Figure 44- Time dynamics of the (a) Square magnitude of the electric field coefficients (b) polarization coefficients and (c) diagonal inversion elements. The applied pump value is, D_0=0.487.

The first two modes (CF-states) has the same lasing thresholds, $D_3^{(th)} = D_5^{(th)} = 0.370$ (fig. (45. a)), and they correspond to the third and the fifth CF-state respectively. Single frequency operation with $\bar{\omega}_3 = 21.936$, is observed for the pump values, $D_0 \in$ **[0.370, 0.396]** and this frequency corresponds to the third CF-state. The pump interval in which the system operates in a single frequency phase is greater than the corresponding one for the case of uniform pumping by **189%**. In addition, the lasing frequency in the single frequency phase, differs from the corresponding one for the case of two-mode lasing by **0.146%**. The third and fourth lasing modes, which corresponds to the fourth and the sixth CF-states have the same lasing thresholds ($D_4^{(th)} = D_6^{(th)}$). For the pump values up to this threshold, $D_4^{(th)} = D_6^{(th)} = 0.396$ we observe the appearance of the second lasing frequency, $\bar{\omega}_4 = 18.066$ which corresponds to the fourth CF-state, as shown in fig. (45.c). In the fig. (43.c) are depicted the total intensities which corresponds to the lasing frequencies referred above for several pump values. They

are calculated as, $|E_{n,tot}|^2 = |E_i + E_j|^2$, with E_i, E_j to be the electric field coefficients which corresponds to the third and the fifth CF-states for the 1st lasing mode and to the 4th and 6th CF-states for the 2nd lasing mode respectively.

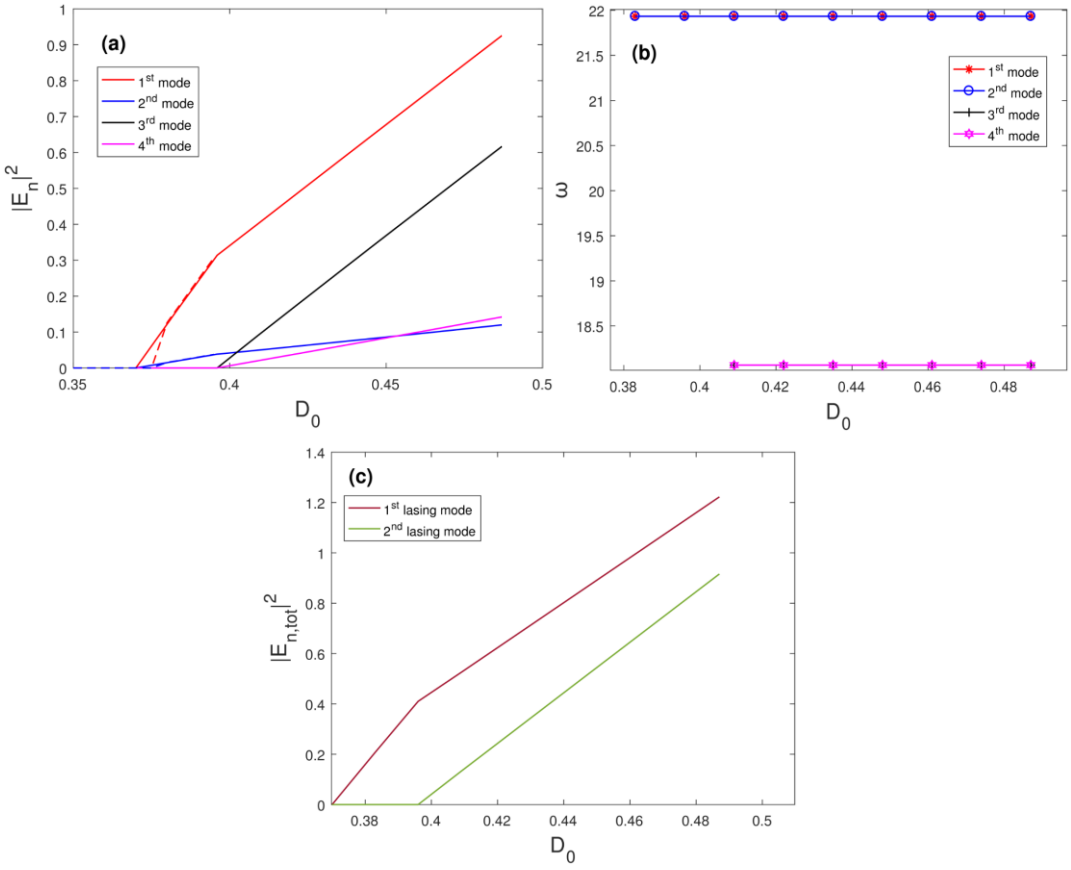

Figure 45- (a) Square magnitude of the electric field coefficients as a function of the applied gain (b) lasing frequencies as a function of the applied gain. (c) total intensities of the two lasing modes as a function of the applied gain. In (a) the dashed lines are the results obtained for two-mode lasing.

The Fourier spectra for the pump values, D_0=0.396 and D_0=0.487 are shown in fig. (46):

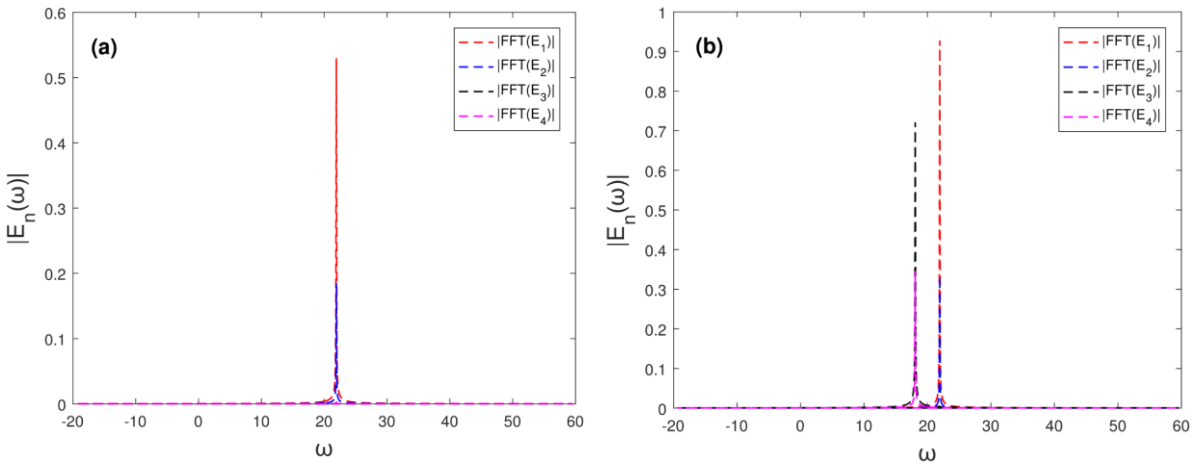

Figure 46- Fourier spectrum of the electric field coefficients for pump values: (a) D_0=0.396, (b) D_0=0.487.

For the pump value D_0=0.396, in which we have singe frequency operation the mode's profile (fig. (47)) is defined from the expression:

$$\Psi_1(r) = \sum_n a_n^{(\mu)} \varphi_n(x, \bar{\omega}_a) = a_3^{(3)}\varphi_3(x, \bar{\omega}_a) + a_5^{(3)}\varphi_5(x, \bar{\omega}_a) + a_4^{(3)}\varphi_4(x, \bar{\omega}_a) + a_6^{(3)}\varphi_6(x, \bar{\omega}_a)$$

with the expansion coefficients given from the Fourier spectra of the electric field coefficients.

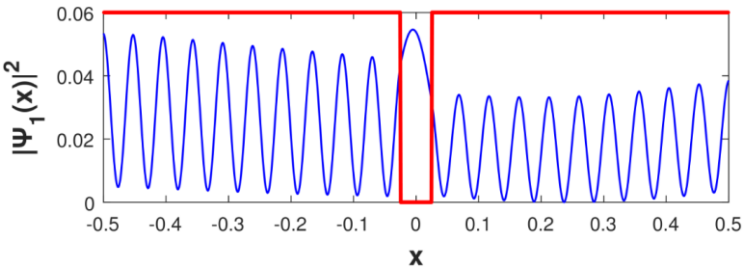

Figure 47- First lasing mode's profile for D_0=0.396, with blue, while with red are represented the two cavities.

We can calculate the intensity of the lasing mode in each cavity as, $I_{a,b}^{(\mu)} = \int |\Psi_\mu(x)|^2 dx / L_{cav}$, where the integral is calculated in each cavity of length L_{cav}, the index μ refers to the lasing mode and the indices a,b are mentioned to the active and the passive cavity respectively. For the specific pump value referred above, we get that, $I_a^{(1)} = 0.026$ and $I_b^{(1)} = 0.018$, therefore the intensity ratio $I_a^{(1)}/I_b^{(1)} = 1.468$. The fact that the intensity ratio is enough greater to unity verify that the system lases in the broken PT- phase, so the intensity in the active cavity (a) is greater than the intensity in the passive one (b). This result corresponds to the lasing in the broken PT- phase as examined in chapter 4 for the two ring coupled cavities.

Chapter 8 - Six mode lasing in ridge cavities

For the case of the homogeneous broadened Lorentzian gain curve with $\bar{\gamma}_\perp = 10$ (Case Ib), we want to examine which CF-states are lasing in the regime of the non-uniform pumping. These modes, are different from the first four CF-states as we'll see below. The reason for this is because the non-uniform pumping enhances the mixing of the CF-states, therefore we have to consider more than the first four CF-states. In the sections 8.1 and 8.2 we'll examine the uniform and nonuniform pumping regimes, respectively, for cavities at a distance d/L=0.025 (Case Ib), while in section 8.3 we present the numerical simulations for two coupled cavities at a distance d/L=0.1 and with refractive index n=3+0.008i, referred as Case II.

8.1- Uniform pump- Case Ib

When both cavities are pumped uniformly, we get the time dynamics for the square magnitude of the electric field coefficients, the polarization coefficients and the diagonal inversion elements when the applied pump is D_0=0.386 as shown in fig. (48):

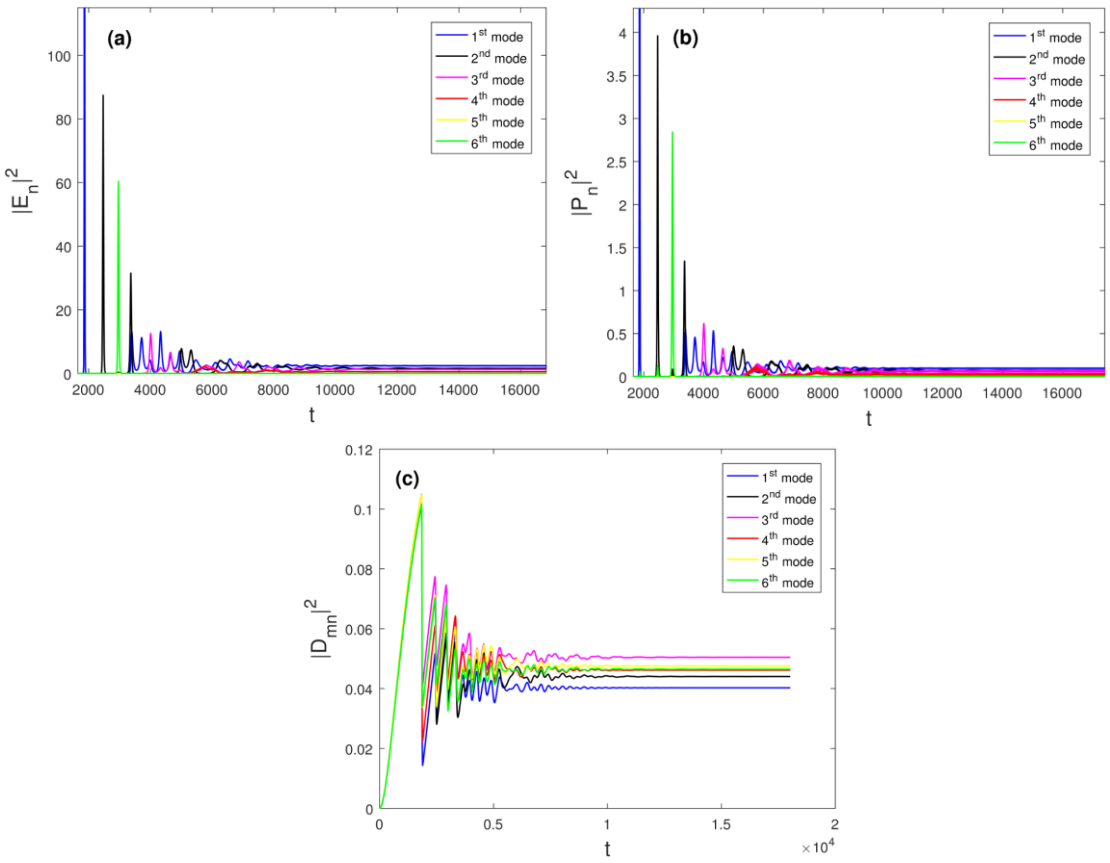

Figure 48- Time dynamics of the (a) Square magnitude of the electric field coefficients (c) polarization coefficients (d) diagonal inversion elements. The applied pump value is D_0=0.386.

The square magnitude of the electric field coefficients as well as the corresponding lasing frequencies for several pump values are depicted in fig. (49):

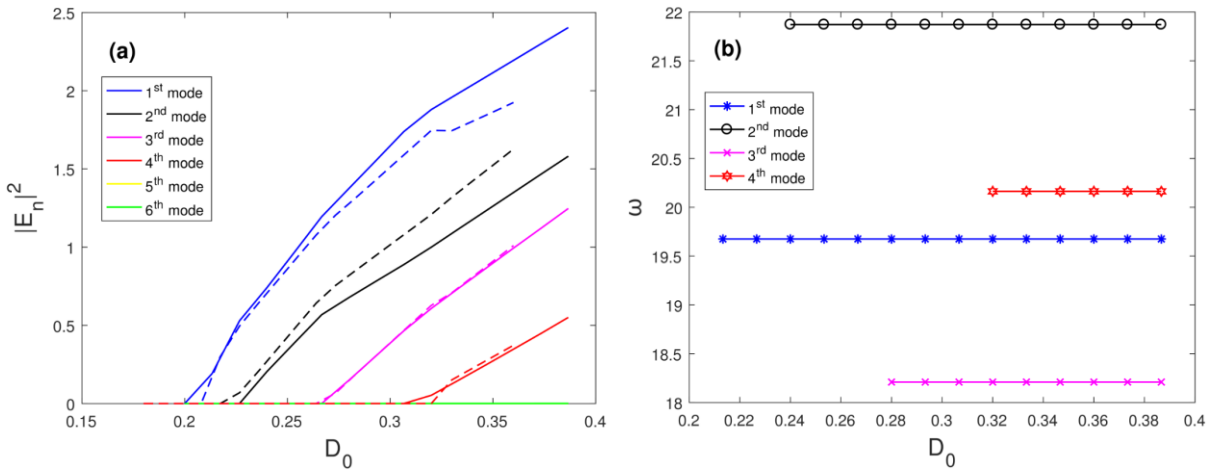

Figure 49- (a) Square magnitude of the electric field coefficients as a function of the applied gain. With dashed lines are shown the square magnitude of the electric field coefficients as they calculated in chapter 7 for the four-mode lasing (b) lasing frequencies as a function of the applied gain.

As mode 1, we refer the first lasing mode and it's corresponds to the second CF-state, with the same manner we have defined all other lasing modes in fig. (49). The second lasing mode corresponds to the third CF-state, the third lasing mode corresponds to the fourth CF-state and the fourth lasing mode corresponds to the first CF-state. With dashed lines in fig. (49. a) are shown the square magnitude of the electric field coefficients as they calculated in chapter 7, for the case of the four-mode lasing. As one can see for the 3rd and the 4th mode we get very good agreement between the four and six mode lasing, while for the first two modes the convergence it isn't very good, maybe because the 5th and the 6th modes affects the first two even while there are not appears to lase, since the corresponding electric field coefficients have values of the order of 10^{-3} for the pump values presented on the above figure. Nevertheless, the lasing thresholds are close enough.

Single mode operation exists, only between the first two lasing threshold, i.e. in the pump interval, $\boldsymbol{D_0 = [0.200, 0.226]}$. The lasing frequency in the single frequency domain, is $\boldsymbol{\bar{\omega}_2 = 19.674}$, which corresponds to the second CF-frequency. The increase of the pump value up to the second lasing threshold, $D_3^{th} = 0.226$ has as a consequence the appearance a second lasing frequency, $\bar{\omega}_3 = 21.872$ which corresponds to the third CF-state. Furthermore, when the pump overcomes the value, $D_4^{th} = 0.266$ the third lasing frequency makes its appearance, $\bar{\omega}_4 = 18.209$ and corresponds to the fourth CF-state. Finally, for pump values up to the fourth lasing threshold, $D_1^{th} = 0.306$ we observe, the presence of the fourth lasing frequency, $\bar{\omega}_1 = 20.163$ which corresponds to the first CF-state.

8.2- Non-uniform pump- Case Ib

For the case of the non-uniform pumping, we get the time dynamics of the system's observables for the pump value, D_0=0.585 as shown in fig. (50):

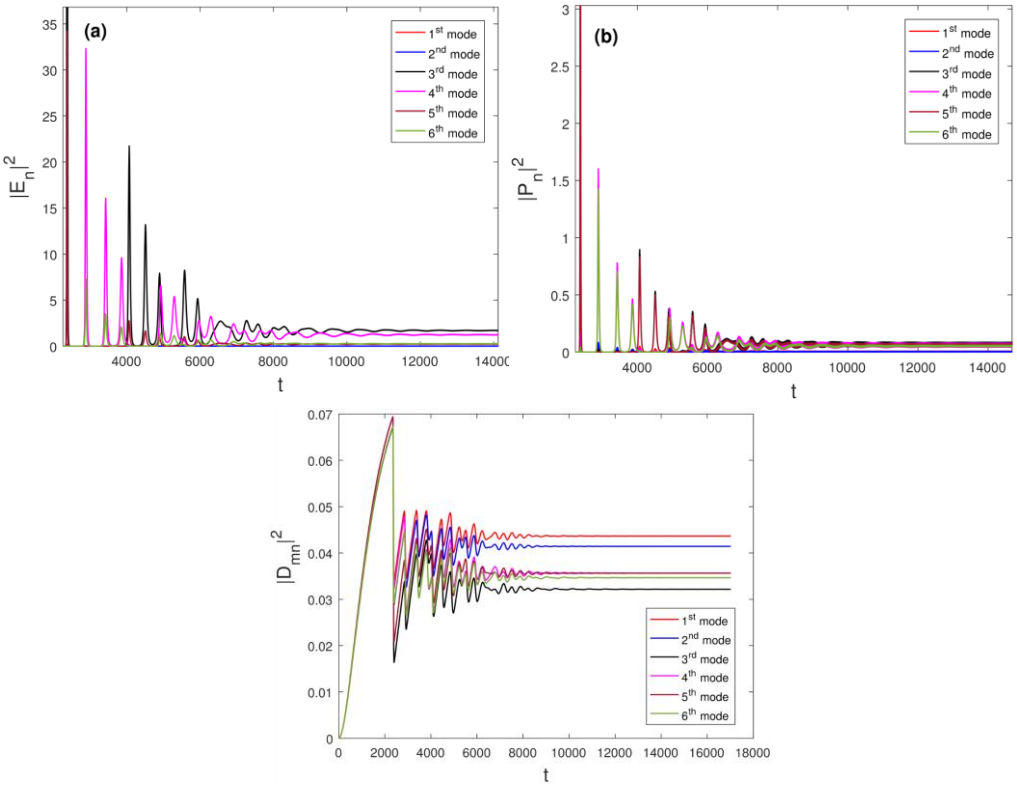

Figure 50- Time dynamics of the (a) Square magnitude of the electric field coefficients (c) polarization coefficients (d) diagonal inversion elements. The applied pump value is D_0=0.585.

The square magnitude of the electric field coefficients, the corresponding lasing frequencies as well as the total intensity of the first two lasing modes for several pump values, are shown in fig. (51):

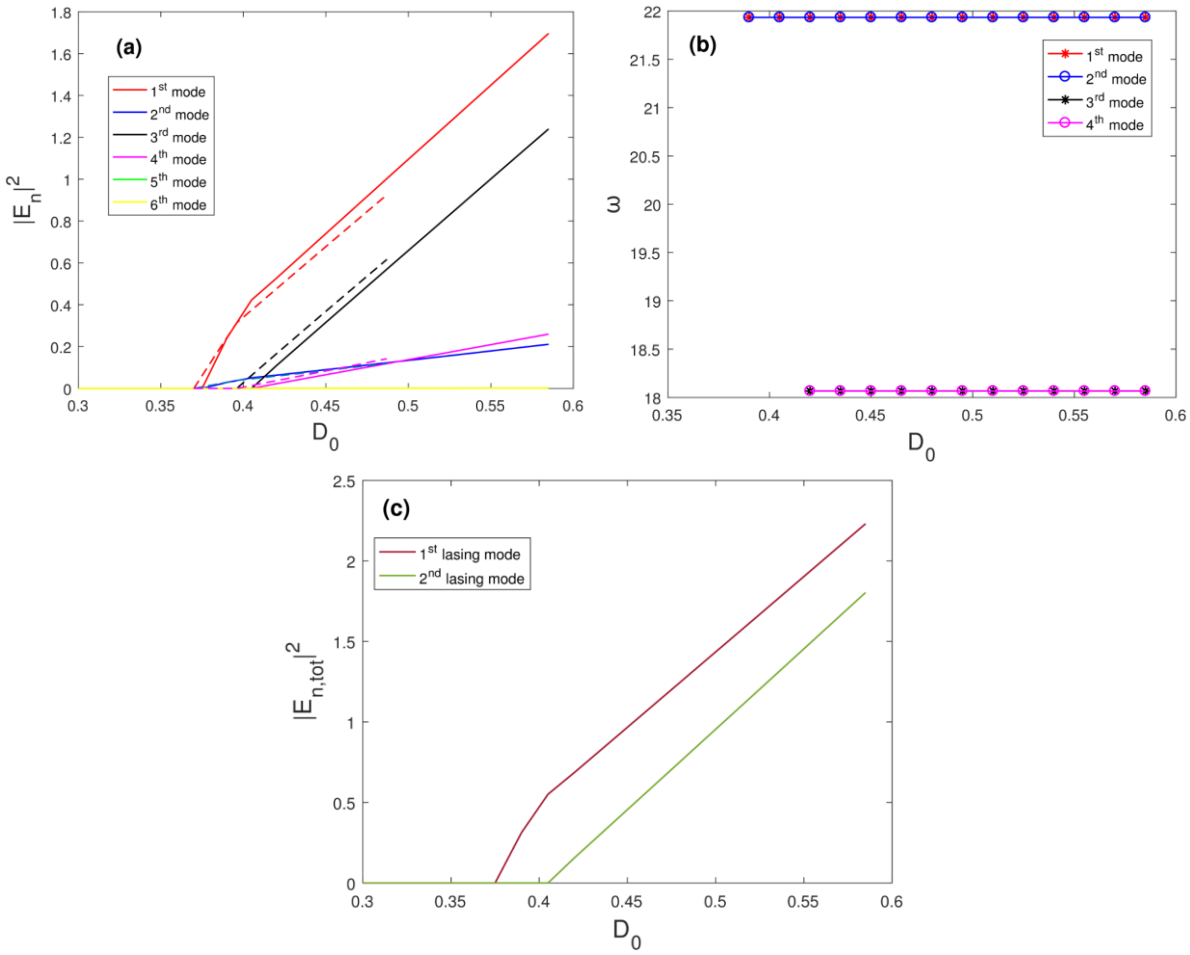

Figure 51 - (a) Square magnitude of the electric field coefficients as a function of the applied gain (b) lasing frequencies as a function of the applied gain (c) total intensity in each lasing frequency as a function of the applied gain.

The lasing threshold of the third and fifth CF-states are, $D_{3,5}^{th} = 0.375$ while the fourth and sixth CF-states lase at, $D_{4,6}^{th} = 0.405$. The system exhibits single mode operation for the pump interval, $\boldsymbol{D_0} \in [\mathbf{0.375}, \mathbf{0.405}]$, and the corresponding lasing frequency is $\bar{\omega}_3 = 21.933$.This frequency corresponds to the third CF-state. The pump interval in which the system operates in a single frequency phase is greater than the corresponding one in the case of uniform pumping by **115%**. In addition, the lasing frequency in the single frequency phase, differs from the corresponding one for the case of four-mode lasing by **0.014%**. The increase of the pump up to the value $D_{4,6}^{th}$, give rise to the appearance of one additional lasing frequency, which corresponds to the fourth CF-state, $\bar{\omega}_4 = 18.066$. The corresponding Fourier spectra for the pump values, D_0=0.390 and D_0=0.585 are shown in fig. (52):

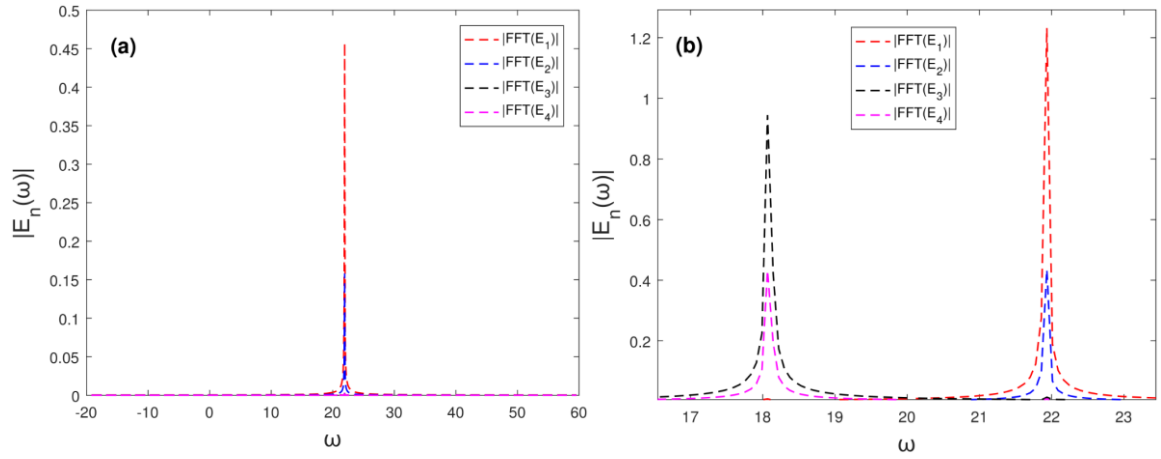

Figure 52- Fourier spectra of the electric field coefficients for: (a) D_0=0.390 and (b) D_0=0.385.

8.3- Non-uniform pump- Case II

Since we have verified the convergence of our computational method of the description of multimode laser effects, we will examine one additional regime, which corresponds to increased intracavity distance. As one can understand, the coupling between the modes in a system of two cavities depends on the distance between them. Therefore, if we want to make the laser system lase in the broken PT-phase we must increase the intracavity distance, which has as a following the decrease of the modes coupling. This regime was also examined in chapter 4, where we make the description of the discrete cavities model. So, we'll consider the normalized distance between cavities to be d/L=0.1 and their refractive index to be n=3+0.008i **(Case II)**. The CF-frequencies of the first six modes closest to the gain curve's center are presented in table 3 and their spatial profiles are shown in fig. (22). Also, the linear lasing thresholds of these modes are presented in table 5.

Therefore, when the system of cavities is pumped nonuniformly, we obtain the time dynamics for the pump value, D_0=0.490 as presented in fig. (53):

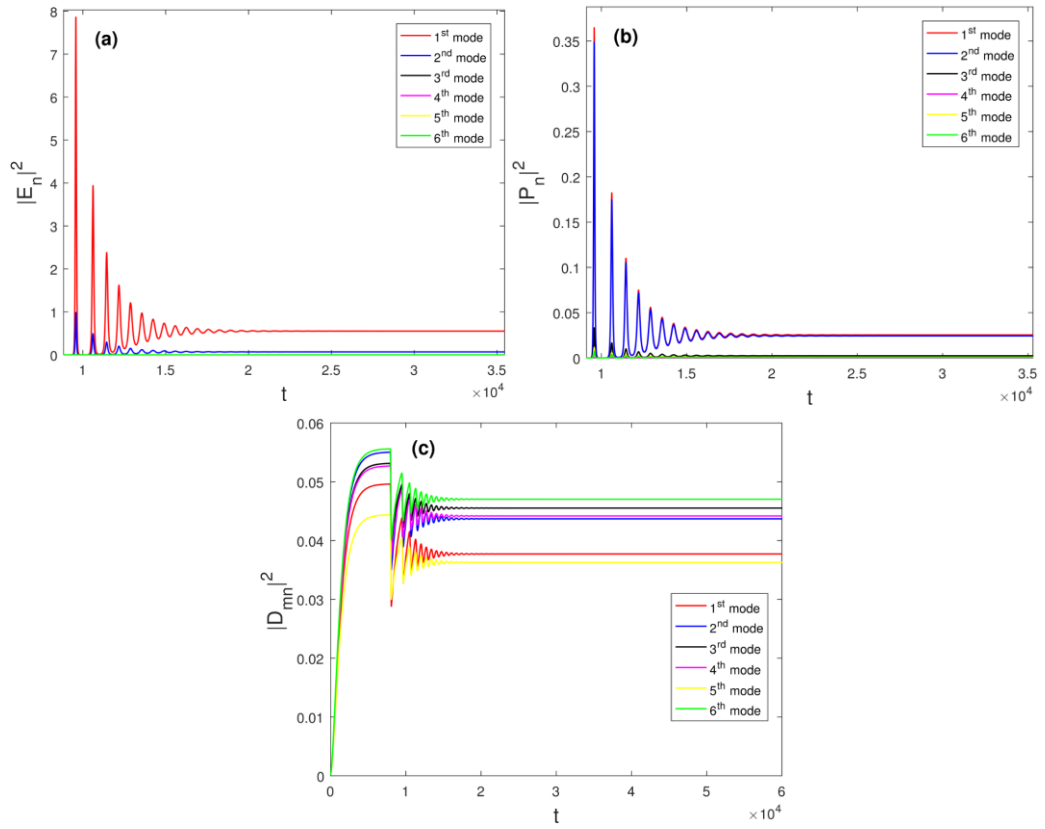

Figure 53- Time dynamics of the (a) square magnitude of the electric field coefficients (b) polarization coefficients (c) diagonal inversion elements, for the pump value D_0=0.490.

For different pump values we obtain the square magnitude of the electric field coefficients and the corresponding lasing frequencies as presented in fig. (54):

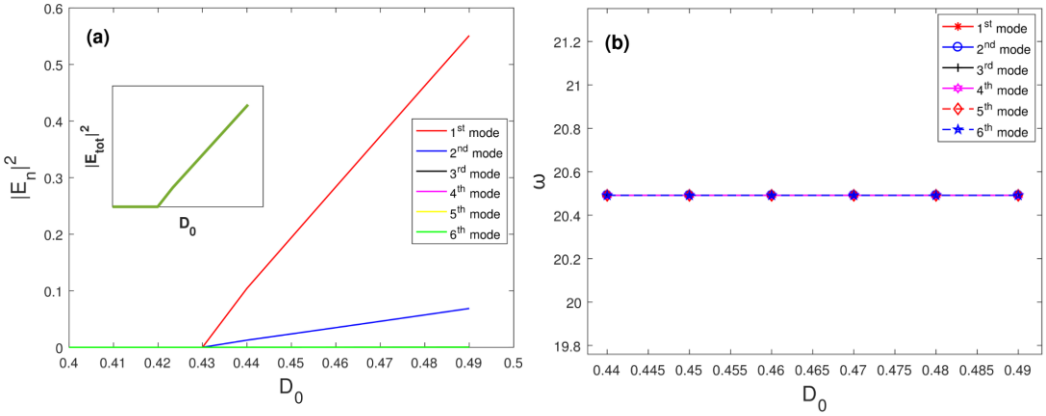

Figure 54- (a) Square magnitude of the electric field coefficients as a function of the applied gain in one cavity. In the inset is shown the total intensity of all modes, in the single frequency presented in (b). (b) Lasing frequency for different pump values.

The numbering of the modes on the above figures corresponds to the CF-states from the first to the 6th respectively. As we can see in the Fourier spectrum shown in the fig. (55) all the modes are expressed in terms of the first CF-state. In the inset of fig. (54. a) is depicted the total intensity which corresponds

to the lasing frequency referred above. This was calculated as, $|E_{tot}|^2 = |E_1 + E_2|^2$, with E_1, E_2 to be the electric field coefficients which corresponds to the first and the second CF-states respectively.

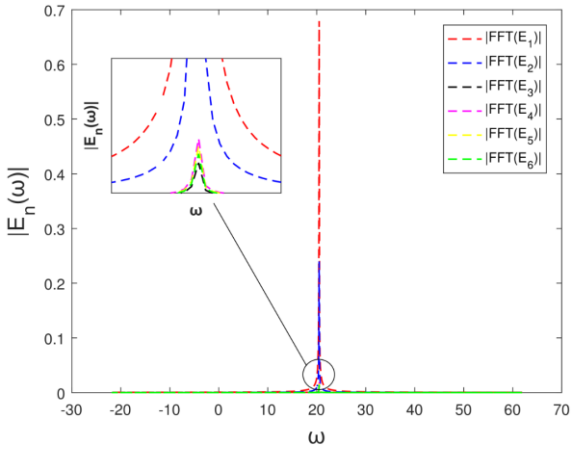

Figure 55- Fourier spectra of the electric field coefficients for D_0=0.490.

In addition, we can calculate the intensity of the lasing mode in each cavity as, $I_{a,b}^{(\mu)} = \int |\Psi_\mu(x)|^2 dx / L_{cav}$, where the integral is calculated in each cavity of length L_{cav}, the index μ refers to the lasing mode and the indices a, b are mentioned to the active and the passive cavity respectively. Therefore, for each pump value we obtain the mode's intensity in each cavity, and in fig. (56) are shown the ratio I_a/I_b as a function of the applied pump:

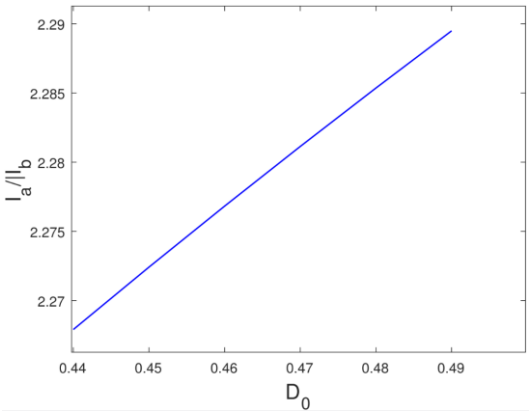

Figure 56- Intensity ratio, I_a/I_b for different pump values.

The intensity in the active cavity is approximately twice times the intensity in the passive one for each pump value. Therefore, we can claim that for the specific set of parameters, the system lase in the broken PT- phase. For the pump value D_0=0.490, in which we have singe frequency operation the mode's profile (fig. (57)) is defined from the expression:

$$\Psi_1(r) = \sum_n a_n^{(\mu)} \varphi_n(x, \bar{\omega}_a)$$
$$= a_1^{(1)}\varphi_1(x, \bar{\omega}_a) + a_2^{(1)}\varphi_2(x, \bar{\omega}_a) + a_3^{(1)}\varphi_3(x, \bar{\omega}_a) + a_4^{(1)}\varphi_4(x, \bar{\omega}_a) + a_5^{(1)}\varphi_5(x, \bar{\omega}_a)$$
$$+ a_6^{(1)}\varphi_6(x, \bar{\omega}_a)$$

with the expansion coefficients are given from the Fourier spectrum of the electric field coefficients.

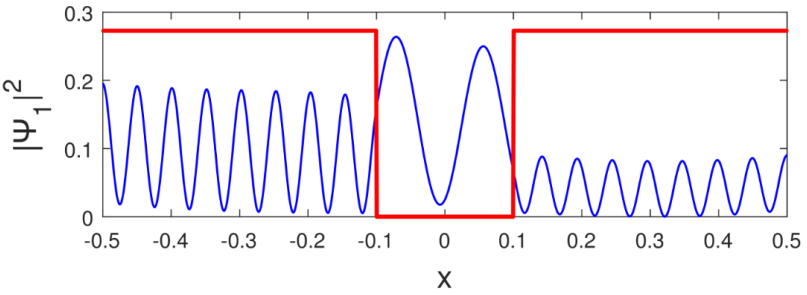

Figure 57- Lasing mode's profile for D_0=0.490, with blue, while with red are represented the two cavities

Chapter 9 – Conclusions and open questions

In this thesis we have presented the application of the semiclassical laser theory on the system of coupled cavities.

First of all, we discussed about single mode coupled ring cavities and we examined the system both linearly and nonlinearly (for the case of class A laser). This system has shown to present exceptional points, therefore a transition from the PT-symmetric phase to the broken PT-phase is observed upon varying the gain which is applied in one cavity. The order in which the transition occurs, was shown to change when we investigate the system nonlinearly.

Secondly, we studied a system of two-coupled ridge cavities for the cases of a Lorentzian gain curve with width $\bar{\gamma}_\perp = 1$ and $\bar{\gamma}_\perp = 10$, for the cases of uniform and nonuniform pumping. The treatment of this system was done by consider successively two, four and six open cavity modes (CF-states). The modal expansion method's consistency and convergence were verified. In addition, the pump interval in which single mode operation is observed appears to be much greater for the case of nonuniform pumping as compared to the case of uniform pumping. For the case of a Lorentzian gain curve with $\bar{\gamma}_\perp = 1$, the system lase in the PT-phase while when the coupling between two cavities became smaller and the loss in the passive cavity (cavity without gain) became greater the system lase in the broken PT-phase. This behavior is similar with the case of coupled ring cavities. On the other hand, for the case of a Lorentzian gain curve with $\bar{\gamma}_\perp = 10$, the system lase in the broken PT-phase for the parameter values which were used.

As a further study, we would like to extend our method in two spatial dimensions in order to compare the theoretical with the experimental results, obtain for the case of coupled ring cavities presented in [35]. So far, we haven't considered the noise due to spontaneous emission. Within the framework of the semiclassical laser theory, a Langevin type of stochastic noise can be integrated in the Maxwell-Bloch equations in order to incorporate the effect of the spontaneous emission in the laser dynamics. So, the computation of the laser linewidth can be numerically calculated.

Appendix A- Bi-orthogonality conditions

The biorthogonality condition, of the modes arises from the Helmholtz one dimensional eigenvalue problem. Let the eigenfunctions be $\varphi_m(x)$, $\varphi_n(x)$ with different eigenvalues k_m, k_n respectively, which satisfy the following equations:

$$\varphi_m'' + k_m^2 \varepsilon(x)\varphi_m = 0 \quad (\boldsymbol{A.1})$$

$$\varphi_n'' + k_n^2 \varepsilon(x)\varphi_n = 0 \quad (\boldsymbol{A.2})$$

In this thesis, we are dealing with two different kinds of boundary conditions, at the edges of the interval $x \in [-l, l]$. First of all, the periodic boundary conditions (ring cavities) are,

$$\varphi_{m,n}(l) = \varphi_{m,n}(-l) \text{ and } \varphi'_{m,n}(l) = \varphi'_{m,n}(-l).$$

and then with CF-boundary conditions (ridge cavities) which are,

$$\varphi'_{m,n}(\pm l) = \pm ik\varphi_{m,n}(\pm l).$$

We begin by multiplying equation (A.1) with $\varphi_n(x)$ and equation (A.2) with $\varphi_m(x)$ and by taking the integral along the cavity,

$$\int_{-l}^{l} \varphi_n \varphi_m'' dx + k_m^2 \int_{-l}^{l} \varepsilon(x)\varphi_n\varphi_m dx = 0 \ (\boldsymbol{A.3})$$

$$\int_{-l}^{l} \varphi_m \varphi_n'' dx + k_n^2 \int_{-l}^{l} \varepsilon(x)\varphi_m\varphi_n dx = 0 \ (\boldsymbol{A.4})$$

If we subtract from (A.3) the (A.4),

$$\int_{-l}^{l} [\varphi_n\varphi_m'' - \varphi_m\varphi_n'']dx + (k_m^2 - k_n^2)\int_{-l}^{l} \varepsilon(x)\varphi_n\varphi_m dx = 0 \quad (\boldsymbol{A.5})$$

For the first integral, we have:

- $\int_{-l}^{l}[\varphi_n\varphi_m'' - \varphi_m\varphi_n'']dx = [\varphi_n\varphi_m']_{-l}^{l} - \int_{-l}^{l}\varphi_n'\varphi_m' dx - [\varphi_m\varphi_n']_{-l}^{l} + \int_{-l}^{l}\varphi_n'\varphi_m' dx = \varphi_n(l)\varphi_m'(l) - \varphi_n(-l)\varphi_m'(-l) - \varphi_m(l)\varphi_n'(l) + \varphi_m(-l)\varphi_n'(-l)$

And this integral is equal to zero if we consider both the periodic boundary conditions and the open boundary conditions (CF-states),

So, equation (A.5), gives:

$$\int_{-l}^{l} \varepsilon(x)\varphi_n(x)\varphi_m(x)dx = 0 \ (\boldsymbol{A.6})$$

Equation (A.6) is the so called biorthogonality condition, and we use it in Chapter 2 for the derivation of Maxwell-Bloch laser equations.

Appendix B- Finite difference method

In order to obtain the eigenvalues and eigenmodes of one-dimensional cavities, we have to solve the complex Helmholtz differential equation (the non-Hermiticity stems from the complex refractive index in the cavity region and the boundary conditions):

$$\varphi_m''(x) + n^2(x)k_m^2\varphi_m(x) = 0 \quad (\boldsymbol{B.1})$$

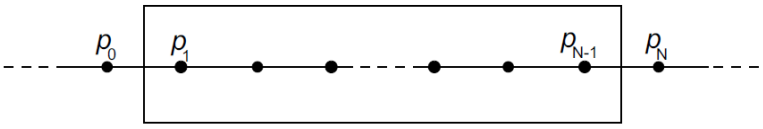

Figure 58- Space discretization [13].

In the discretization method N equally spaced grid points are placed in the cavity. The distance between them is named Δ. The first point, which belongs inside the cavity region is p_1 and the last one is p_{N-1}. The two points p_0 and p_N outside the cavity are $\frac{\Delta}{2}$, away from the edges of the cavity.

By making the approximation,

$$\frac{d\varphi_n}{dx} \cong \frac{\varphi_n - \varphi_{n-1}}{\Delta} \cong \frac{\varphi_{n+1} - \varphi_n}{\Delta}$$

the second derivative becomes,

$$\frac{d^2\varphi_n}{dx^2} = \frac{\varphi_{n+1} + \varphi_{n-1} - 2\varphi_n}{\Delta^2}$$

where the index n describes the n^{th} grid point. Consequently, the discretized Helmholtz equation, takes the form,

$$\frac{\varphi_{n+1} + \varphi_{n-1} - 2\varphi_n}{\Delta^2} = -n_n^2 k_m^2 \varphi_n \quad (\boldsymbol{B.2})$$

For n=1, the equation (B.2) takes the form, $\frac{\varphi_2+\varphi_0-2\varphi_1}{\Delta^2} = -n_1^2 k_m^2 \varphi_1$ and for n=N, $\frac{\varphi_{N+1}+\varphi_{N-1}-2\varphi_N}{\Delta^2} = -n_N^2 k_m^2 \varphi_N$. In similar manner we can construct a system of N equations, which constitute a generalized eigenvalue problem, written in matrix form as,

$$\begin{pmatrix} -2/\Delta^2 & 1/\Delta^2 & 0 & \cdots & \dots \\ 1/\Delta^2 & -2/\Delta^2 & 1/\Delta^2 & 0 & \cdots \\ \cdots & \cdots & \cdots & \cdots & \cdots \\ 0 & \cdots & 1/\Delta^2 & -2/\Delta^2 & 1/\Delta^2 \\ \dots & 0 & 0 & 1/\Delta^2 & -2/\Delta^2 \end{pmatrix} \begin{pmatrix} \varphi_1 \\ \varphi_2 \\ \cdots \\ \varphi_{N-1} \\ \varphi_N \end{pmatrix} = -k_m^2 \begin{pmatrix} n_1^2 & & & & \\ & n_2^2 & & \cdots & \\ & & & & \\ & & & n_{N-1}^2 & \\ & & & & n_N^2 \end{pmatrix} \begin{pmatrix} \varphi_1 \\ \varphi_2 \\ \cdots \\ \varphi_{N-1} \\ \varphi_N \end{pmatrix} \quad (\boldsymbol{B.3})$$

where, $(\varphi_1 \quad \varphi_2 \quad \cdots \quad \varphi_{N-1} \quad \varphi_N)$ is the eigenvector, and k_m^2 are the corresponding eigenvalues.

The eigenvalue problem (B.3) can then be solved for each set of boundary conditions we want.

Appendix C- Runge-Kutta method

The system of equations, which we solve in this thesis, are numerically solved with fourth order Runge-Kutta integration algorithm.

Runge-Kutta method, was developed around 1900 by the German mathematicians C. Runge and M.W. Kutta. It's a numerical algorithm for the approximate solution of ordinary differential equations, via implicit and explicit iterations by using temporal discretization [32]. Before we proceed to the derivation of the formulas used in Runge-Kutta algorithm, needs to be mention the Taylor's theorem in one variable.

Consider, an one variable function g(x), as well as its derivatives of order n which are continuous in the domain D. Let, $x_0 \in D$, a point around which we will make the expansion of this function. So, we can write,

$$g(x) \cong P_n(x)$$

where for n=2,

$$P_2(x) = g(x_0) + (x - x_0)\frac{dg}{dx}|_{x_0} + \frac{(x - x_0)^2}{2}\frac{d^2g}{dx^2}|_{x_0} \quad (\boldsymbol{C.1})$$

The family of Runge-Kutta methods, consist of several order approximation algorithms, with the most common in use to be the fourth order one, which is generally referred as "**RK4**". We set an initial value problem which consists, of several coupled ordinary differential equations referred as y_i,

$$\dot{y}_i = f_i(t, y_i(t)), \qquad y_i(t_0) = y_{i,0} \quad (\boldsymbol{C.2})$$

y_i's, are functions (scalar or vector) of time t. The dot represents the time derivative. First of all, we make a temporal discretization, through which we begin from a time t_0, and with a small step h, we cover the time interval in which we want to solve the system of differential equations. The method we develop, has an explicit form, because we want to calculate the functions values at time $t_0 + h$ knowing the functions value at t_0. From formula (1) we obtain the expansion of a function y, around t_0,

$$y(t) = y(t_0) + y'(t_0)(t - t_0) + y''(t_0)\frac{(t - t_0)^2}{2} + O(h^3) \quad (\boldsymbol{C.3})$$

where $O(h^3)$, includes the higher order terms.

The first step of RK4 includes the approximation of function's slopes at $t = t_0$, knowing the initial values, $y_1(t_0) = y_0^{(1)}, y_2(t_0) = y_0^{(2)}, \dots, y_{N-1}(t_0) = y_0^{(N-1)}, y_N(t_0) = y_0^{(N)}$,

$$k_i^{(1)} = f_i(t, y_i) \quad (\boldsymbol{C.4})$$

Then we move on to the second step in which we use the above calculated slopes, to find the functions values at an intermediate point, $t = \frac{h}{2}$. By holding the first two terms from expression (C.3), we have,

$$y_i\left(t_0 + \frac{h}{2}\right) = y_i(t_0) + k_i^{(1)}\frac{h}{2} \quad (\boldsymbol{C.5})$$

Inserting equations (C.5), into (C.2), we take slopes, at time $t = \frac{h}{2}$, so we have,

$$k_i^{(2)} = f_i(t_0 + \frac{h}{2}\,, y_i(t_0) + k_i^{(1)}\frac{h}{2}) \quad (\boldsymbol{C.6})$$

In addition, we make use of slopes given by (C.6), and we calculate from scratch the functions values at $t = \frac{h}{2}$. This is, the third step of the algorithm.

$$y_i\left(t_0 + \frac{h}{2}\right) = y_i(t_0) + k_i^{(1)}\frac{h}{2} \quad (\boldsymbol{C.7})$$

by the substitution of (C.7) into (C.2), we take a better approximation, of the slopes,

$$k_i^{(3)} = f_i(t_0 + \frac{h}{2}\,, y_i(t_0) + k_i^{(2)}\frac{h}{2}) \quad (\boldsymbol{C.8})$$

The fourth and last step, is to approximate the functions at time t=h. From, relation (C.3) we take,

$$y_i(t_0 + h) = y_i(t_0) + k_i^{(3)}h \quad (\boldsymbol{C.9})$$

Ultimately, the substitution of (C.9) into (C.2), gives the slopes,

$$k_i^{(4)} = f_i(t_0 + h\,, y_i(t_0) + k_i^{(3)}h) \quad (\boldsymbol{C.10})$$

The final approximation, of functions values at t=h is given by the weighted average of the form,

$$y_i(t_0 + h) = y_i(t_0) + \frac{1}{6}\left(k_i^{(1)} + 2k_i^{(2)} + 2k_i^{(3)} + k_i^{(4)}\right) \quad (\boldsymbol{C.11})$$

Fourth order Runge-Kutta numerical method, has a local truncation error $O(h^4)$ (the error introduced in each successive stage of the iterated algorithm) [33].

Appendix D- Two dimensional Runge-Kutta method

For the multimode lasing, we applied a Runge-Kutta integration algorithm, which solves N^2+2N nonlinear, coupled ordinary differential equations, where N is the mode's number. For these purposes, were crucial to rearrange the $(N \times N)$, D_{mn} inversion matrix into a vector with $2N$ elements by using the command "reshape" of MATLAB. Finally, we want to have a column vector containing N^2+2N elements. The first $2N$ components are the inversion matrix elements, the next N elements are the modal fields and the final N elements are the corresponding polarizations. The reshape command works as follows:

If we consider a (2×2) matrix: $A = \begin{bmatrix} a_{11} & a_{12} \\ a_{21} & a_{22} \end{bmatrix} \Rightarrow B = reshape(A, 1,4)$. This command creates a (1×4) matrix B, containing the elements of A as:

$$B = [a_{11}\ a_{12}\ a_{21}\ a_{22}]$$

Therefore, for the case of N-modes, the inversion operator has the general form:

$$D_{N\times N} = \begin{bmatrix} D_{11} & D_{12} & \cdots & D_{1N} \\ D_{21} & D_{22} & \cdots & D_{2N} \\ \vdots & \vdots & \cdots & \vdots \\ D_{N1} & D_{N2} & \cdots & D_{NN} \end{bmatrix}$$

by applying the reshape command in the transpose-D matrix, we get:

$$\text{reshape}(\mathrm{D}, 1, N \cdot N)$$
$$= [\, D_{11}\, D_{12}\, \cdots\, D_{1N} \mid D_{21}\, D_{22}\, \cdots\, D_{2N} \mid D_{31}\, D_{32}\, \cdots\, D_{3N} \mid \cdots\ \cdots\ \cdots \mid D_{N1}\, D_{N2}\, \cdots\, D_{NN}\,]$$

We can clearly see that the rule that connects, the D_{nm} elements of the D $(N \times N)$ matrix, to the corresponding $\widetilde{D}$ element of the 1-D array is the following:

$$\boldsymbol{D_{nm} \rightarrow \widetilde{D}[\,(n-1)N + m\,]\ where\ n, m = 1, 2, \ldots, N}$$

Finally, if we consider far from D-elements and the modal fields and the polarizations, we get the vector:

$$\boldsymbol{g = [\, D_{11}\, D_{12}\, \cdots\, D_{1N} \mid D_{21}\, D_{22}\, \cdots\, D_{2N} \mid D_{31}\, D_{32}\, \cdots\, D_{3N} \mid \cdots\ \cdots\ \cdots \mid D_{N1}\, D_{N2}\, \cdots\, D_{NN} \mid}$$
$$\boldsymbol{e_1\, e_2\, \cdots\, e_N \mid p_1\, p_2\, \cdots\, p_N]}$$

This **g** vector we use in the Runge-Kutta algorithm for many modes. As one can see the first N^2 vector elements are related to the inversion, the next N elements concerns the electric field of each mode and the final N are the polarizations induced from each mode.

References

[1] H. Haken, Light (North Holland, Amsterdam, 1986), Vol. II.

[2] K. Shimoda, Introduction to laser physics (Berlin Heidelberg GmbH 1984), Vol. 44

[3] A. E. Siegman. Lasers. University Sience Books, Mill Valley, California, USA, 1986.

[4] https://www.orc.soton.ac.uk/how-fibre-lasers-work

[5] S. Qian, J. B. Snow, H. Tzeng, and R. K. Chang. Lasing droplets: Highlighting the liquid-air interface by laser emission. Science, 231, 486 (1986).

[6] A. Mekis, J. U. Nöckel, G. Chen, A. D. Stone, and R. K. Chang. Ray chaos and Q spoiling in lasing droplets. Phys. Rev. Lett., 75, 2682 (1995).

[7] S. Chang, R. K. Chang, A. D. Stone, and J. U. Nöckel. Observation of emission from chaotic lasing modes in deformed microspheres: displacement by the stable-orbit modes. Journal of the Optical Society of America B, 17, 11 (2000).

[8] J. Wiersig and M. Hentshcel. Combining directional light output and ultralow loss in deformed microdisks. Phys. Rev. Lett., 100, 033901 (2008).

[9] J. U. Nöckel and A. D. Stone. Ray and wave chaos in asymmetric resonant optical cavities. Nature, 385, 45 (1997).

[10] H. E. Türeci, H. G. L. Schwefel, P. Jacquod, and A. D. Stone. Modes of wave-chaotic dielectric resonators. Prog. Opt., 75, 138 (2005).

[11] H. E. Türeci, A. D. Stone, and B. Collier. Self-consistent multimode lasing theory for complex or random lasing media. Phys. Rev. A, 74, 043822 (2006).

[12] Christine Y. Wang, L. Diehl, A. Gordon, C. Jirauschek, F. X. Kartner, A. Belyanin, D. Bour, S. Corzine, G. Hofler, M. Troccoli, J. Faist, and Federico Capasso. Coherent instabilities in a semiconductor laser with fast gain recovery. Phys. Rev. A, 75, 031802 (2007).

[13] Li Ge, PhD thesis (Steady-state Ab Initio Laser Theory and its Applications in Random and Complex Media), Yale university (2010).

[14] M. Sargent, M. O. Scully, and W. E. Lamb. Laser Physics. Addison-Wesley, Reading, MA, 1974.

[15] J. Andreasen and H. Cao. Finite-difference time-domain formulation of stochastic noise in macroscopic atomic systems. J. Lightwave Technol., 27, 4530 (2009).

[16] Carl M. Bender and Stefan Boettcher. Real spectra in non-Hermitian Hamiltonians having PT-symmetry. Phys. Rev. Lett., 80, 5243 (1998).

[17] Liang Feng, Ramy El-Ganainy and Li Ge. Non- Hermitian photonics based on parity-time symmetry. Nature Physics, 12, 752 (2017).

[18] El-Ganainy, R., Makris, K. G., Christodoulides, D. N. & Musslimani, Z. H. Theory of coupled optical PT-symmetric structures. Opt. Lett., 32, 2632 (2007).

[19] Makris, K. G., El-Ganainy, R., Christodoulides, D. N. & Musslimani, Z. H. Beam dynamics in PT symmetric optical lattices. Phys. Rev. Lett. 100, 103904 (2008).

[20] Musslimani, Z. H., Makris, K. G., El-Ganainy, R. & Christodoulides, D. N. Optical solitons in PT periodic potentials. Phys. Rev. Lett. 100, 030402 (2008).

[21] A. Guo, G. J. Salamo, D. Duchesne, R. Morandotti, M. Volatier-Ravat, V. Aimez, G. A. Siviloglou, and D. N. Christodoulides. Observation of PT-symmetry breaking in complex optical potentials. Phys. Rev. Lett. 103, 093902 (2009).

[22] Rüter, C. E., Konstantinos G. Makris, Ramy El-Ganainy, Demetrios N. Christodoulides, Mordechai Segev and Detlef Kip. Observation of parity–time symmetry in optics. Nat. Phys., 6, 192, (2010).

[23] Ruschhaupt, A., Delgado, F. & Muga, J. G. Physical realization of PT-symmetric potential scattering in a planar slab waveguide. J. Phys. Math. Gen., 38, 171 (2005).

[24] Klaiman, S., Günther, U. & Moiseyev, N. Visualization of branch points in PT-symmetric waveguides. Phys. Rev. Lett. 101, 080402 (2008).

[25] T. Kottos. Broken symmetry makes light work. Nat. Phy., 6, 166 (2010).

[26] Ramy El-Ganainy, Konstantinos G. Makris, Mercedeh Khajavikhan, Ziad H. Musslimani, Stefan Rotter and Demetrios N. Christodoulides. Non-Hermitian physics and PT symmetry. Nature Physics 14, 11, (2017).

[27] A A Zyablovsky, A P Vinogradov, A A Pukhov, A V Dorofeenko, A A Lisyansky. PT-symmetry in optics. Physics-Uspekhi, 57, 1063 (2014).

[28] Zihe Gao, Stewart T. M. Fryslie, Bradley J. Thompson, P. Scott Carney, and Kent D. Choquette. Parity-time symmetry in coherently coupled vertical cavity laser arrays. Optica, 4, 323 (2017).

[29] W D Heiss. Exceptional points of non-Hermitian operators. J. Phys. A: Math. Gen, 37, 2455, (2004).

[30] Absar U. Hassan, Hossein Hodaei, Mohammad-Ali Miri, Mercedeh Khajavikhan, and Demetrios N. Christodoulides. Nonlinear reversal of the PT -symmetric phase transition in a system of coupled semiconductor microring resonators. PHYSICAL REVIEW A, 92, 063807 (2015).

[31] O.Malik, K. G. Makris and H. E. Türeci. Spectral method for efficient computation of time-dependent phenomena in complex lasers. PHYSICAL REVIEW A 92, 063829 (2015).

[32] https://en.wikipedia.org/wiki/Runge–Kutta_methods

[33] Richard L. Burden, J. Douglas Faires, Numerical Analysis, BROOKS/COLE.

[34] Alaxey V. Kavokin, Geremy J. Baumberg, Guillaume Malpuech, Fabrice P. Laussy, Microcavities, Second edition, Oxford Science Publications.

[35] Hossein Hodaei et. al. Design Considerations for Single-Mode Microring Lasers Using Parity-Time-Symmetry. IEEE JOURNAL, 22, No. 5 (2016).

[36] Hong Fu and H. Haken. Multifrequency operations in a short-cavity standing wave laser. PHYSICAL REVIEW A 43, 2446 (1991).